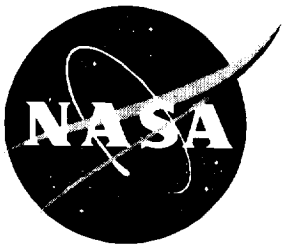

NASA Contractor Report 4630

Development of the CSI Phase-3 Evolutionary Model Testbed

M. J. Gronet, D. A. Davis, and M. K. Tan
Lockheed Missiles & Space Company, Inc. • Sunnyvale, California

National Aeronautics and Space Administration
Langley Research Center • Hampton, Virginia 23681-0001

Prepared for Langley Research Center
under Contract NAS1-19241

October 1994

Table of Contents

List of Acronyms

AEC-Able	AEC-Able Engineering Company, Inc.
CEM	CSI Evolutionary Model
CEM1	Phase-1 CSI Evolutionary Model
CEM2	Phase-2 CSI Evolutionary Model
CEM3	Phase-3 CSI Evolutionary Model
CERES1	EOS AM-1 science instrument
c.g.	center-of-gravity
CSA	CSA Engineering, Inc.
CSI	Controls-Structures Integration
DOF	Degrees-of-Freedom
DMSP	Defense Meteorological Satellite Program
EOS	Earth Observing System
FEM	Finite Element Method
FRF	Frequency Response Function
HGA	High Gain Antenna
GN&C	Guidance, Navigation, and Control
JADE	Jitter Attenuation and Dynamics Experiment
LMSC	Lockheed Missiles & Space Company, Inc.
LaRC	Langley Research Center
MISR	EOS AM-1 science instrument
MODIS	EOS AM-1 science instrument
MOPITT	EOS AM-1 science instrument
MSC	MacNeal-Schwendler Corporation
NASA	National Aeronautics & Space Administration
NOAA	National Oceanic and Atmospheric Administration
PM	Propulsion Module
ROM	Reduced Order Model
rms	root-mean-square
RWA	Reaction Wheel Assembly
SA	Solar Array
SDRC	Structural Dynamics Research Corporation, Inc.
SWIR	Short Wavelength Infrared part of EOS AM-1 ASTER science instrument
TAM	Test-Analysis Model
TIR	Thermal Infrared part of EOS AM-1 ASTER science instrument
TR	Tape Recorder
VNIR	Visible and Near Infrared part of EOS AM-1 ASTER science instrument
XO	Cross-Orthogonality

List of Symbols

Variables

C	Viscous Damping Coefficient
EA	Axial Rigidity
EI	Bending Rigidity
g	gravity
GA	Shear Rigidity
GJ	Torsional Rigidity
I	Mass Moment of Inertia
K	Stiffness
K_b	Bending Mode Gain Factor
L	Length
M	Mass
r	moment arm length
T	Torque
x	Deflection
ε	Strain
λ	Scale Factor
ϕ	Mode Shape
θ	Angular Rotation
ω	Frequency
ζ	Modal Damping

Subscripts

b	bending
EA	Axial Rigidity
EI	Bending Rigidity
GA	Shear Rigidity
GJ	Torsional Rigidity
L	Length
m	mass
t	time
x	deflection

Acknowledgements

The successful completion of this task is a result of the cooperative effort of a number of people. The authors wish to acknowledge the consultation and support of Jim Thorne, John Nelson, Jim Desimpel, Jack Rodden, and Bruce Simpson of the Lockheed Missiles & Space Company, Inc. in the areas of design, controls and dynamics. We also acknowledge the contributions of Bob Crawford, Ray Garza, and Dave Gross of the AEC-Able Engineering Company, Inc. in fabricating the original CEM Phase-2 mast and the additional diagonal struts. The help that Tom Venator of NASA/GSFC and James Reed of Swales & Associates, Inc. provided in obtaining the EOS AM-1 modal data is sincerely appreciated. Finally, the support and direction of the technical monitor, Ken Elliott, as well as Jerry Newsom, Keith Belvin, Mike Gilbert, John Teter, and Rudeen Smith-Taylor of NASA/LaRC is gratefully acknowledged.

1.0 EXECUTIVE SUMMARY

As a part of a program of ongoing research and technology development activities in the Controls-Structures Integration (CSI) technology area, the NASA Langley Research Center (NASA/LaRC) initiated the design and fabrication of the CSI Evolutionary Model (CEM) in 1990 to provide a testbed for the development, implementation, and validation of CSI technology and associated hardware and software. Since that time, the CEM has evolved from the Phase-0 through the Phase-1 and Phase-2 configurations (designated CEM1 and CEM2) in support of integrated CSI design, pointing, jitter, disturbance rejection, isolation, and distributed control experiments. The CEM has also been used in the development of associated ground test techniques, including advanced zero-g suspension systems, actuators, sensors, and precision pointing optical scoring systems.

This report describes the configuration and structural development effort for the evolution of the CEM2 testbed into the new CEM Phase-3 (CEM3) configuration performed under Contract NAS1-19241 to NASA/LaRC. This evolutionary step responds to the need to develop and test CSI technologies associated with typical planned earth science and remote sensing platforms, such as the eight-satellite Earth Observing System (EOS), Defense Meteorological Satellite Program/National Oceanic and Atmospheric Administration (DMSP/NOAA) weather satellites, LandSat, and others. The EOS spacecraft series is of particular interest in that the CEM3 testbed will be used to support system identification and CSI technology development experiments that may fly on the EOS AM-1 spacecraft, as part of the Jitter Attenuation and Dynamics Experiment (JADE).

1.1 BACKGROUND AND APPROACH

The primary objective of the CEM3 testbed development is to reconfigure the components of the existing CEM2 testbed (Figure 1-1) in order to simulate the overall on-orbit dynamic behavior of a typical earth science and remote sensing platform, namely the EOS AM-1 spacecraft (Figure 1-2). Key elements of the objective outlined by NASA/LaRC include approximating the overall geometry of the EOS AM-1 spacecraft and simulating the low-frequency solar array (SA) and high gain antenna (HGA) appendage dynamic interaction. Like the CEM2 testbed, the CEM3 design is to be erectable, allowing for the changeout of testbed components associated with different CSI experiments. It will also be suspended from cables attached to suspension devices for the simulation of the free-free zero-g spacecraft environment.

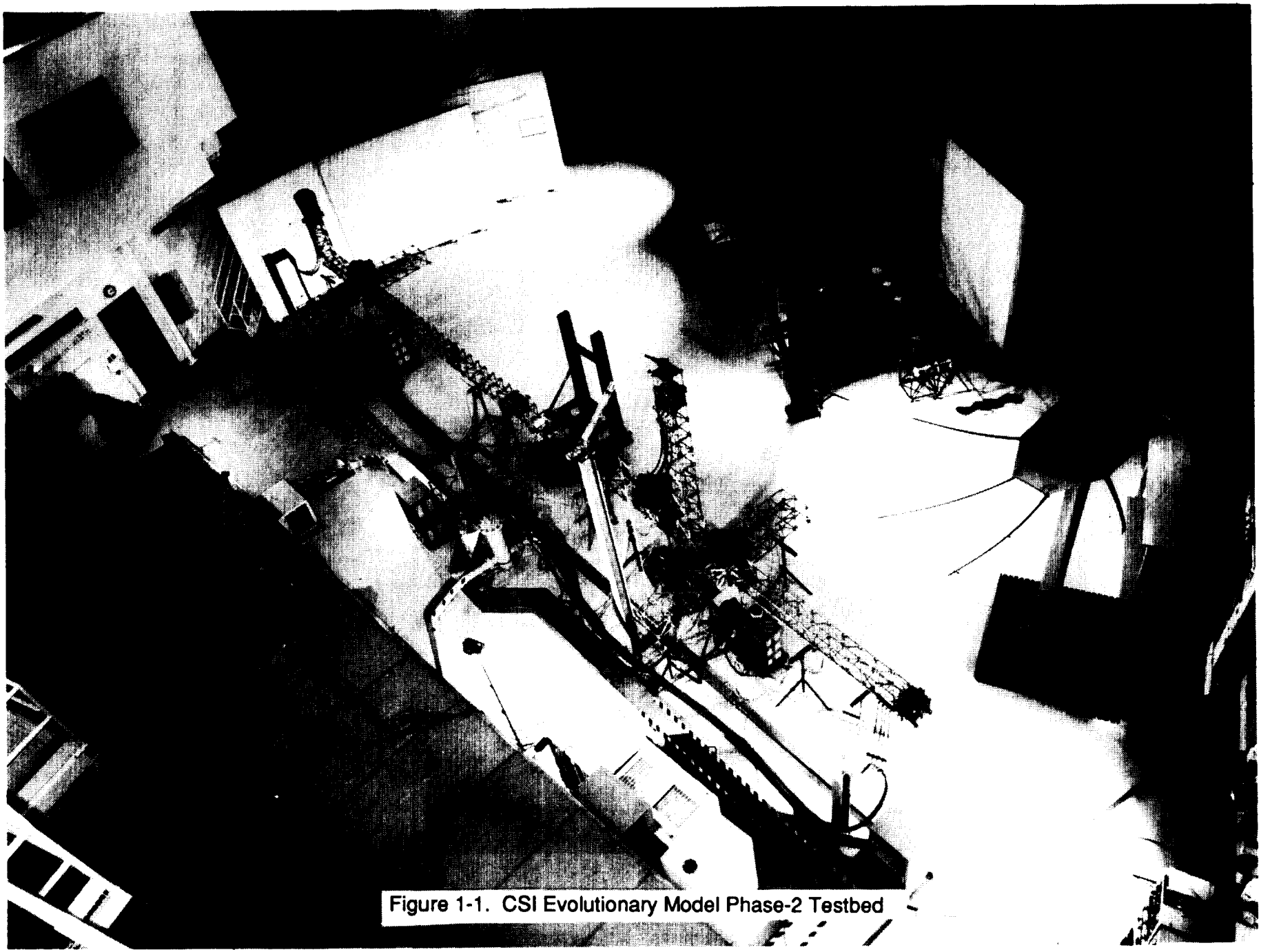

Figure 1-1. CSI Evolutionary Model Phase-2 Testbed

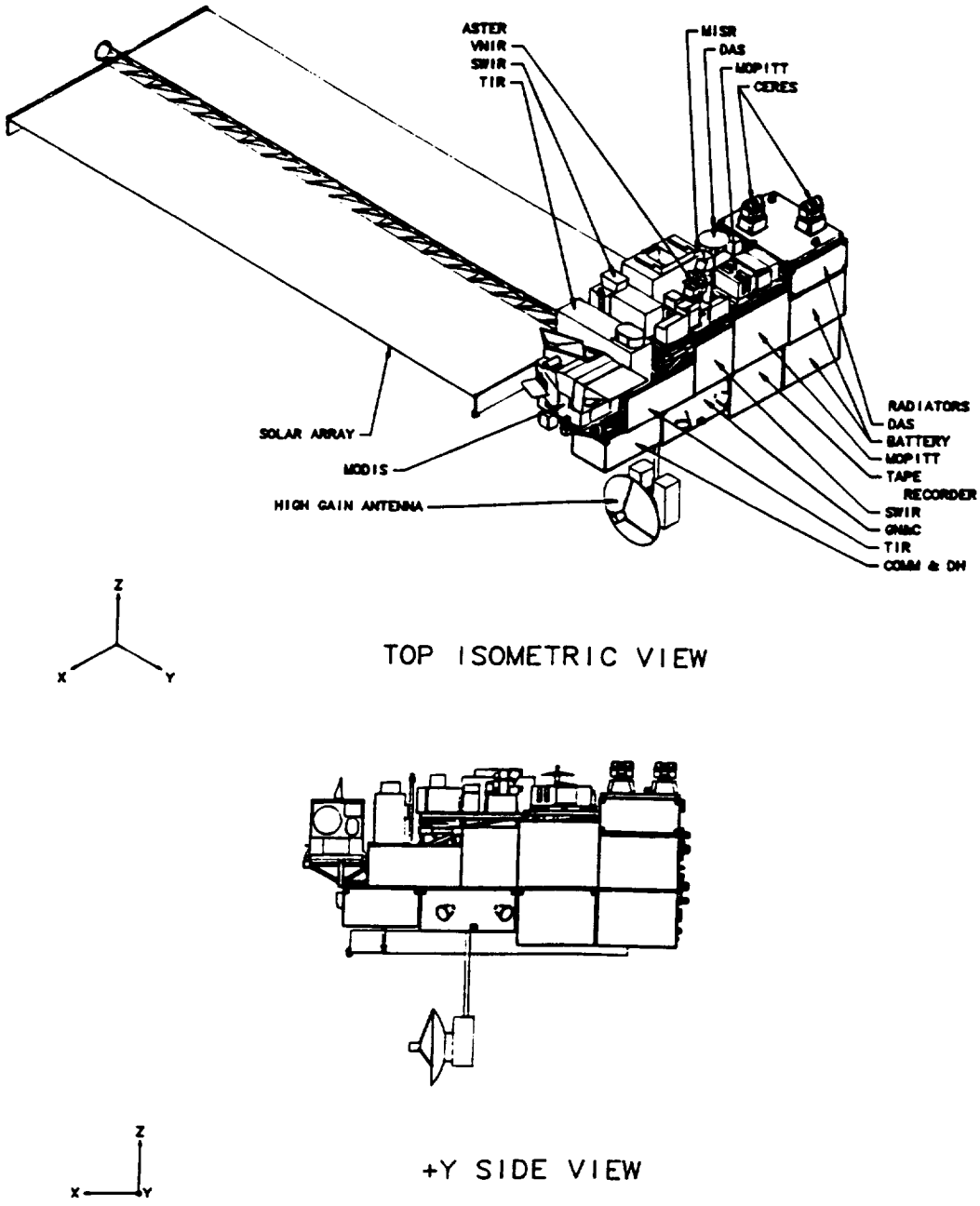

Figure 1-2. EOS AM-1 On-Orbit Configuration (Isometric and Side Views)

The following guidelines were provided by NASA/LaRC for the accomplishment of the CEM3 design objectives:

(a) Use the existing CEM2 hardware - develop a minimum of new hardware at minimal cost.
(b) Use existing suspension system hardware which is capable of supporting up to 2,000 pounds in the Building 1293A test facility.
(c) Approximate the overall size, shape, and dynamics of the EOS AM-1 spacecraft to as near full-scale as practicable.
(d) Use existing finite element models and EOS AM-1 data provided by NASA.
(e) Assemble the testbed for suspension in Building 1293A within five months.

The existing CEM2 testbed hardware consisted of approximately 1,900 aluminum truss struts assembled in 10-inch bays, a 15-foot deployable solar array mast and tip weight, three 2-axis gimbaled instrument simulators, and associated control sensors (inertial reference units) and actuators (gas-jet thrusters). Reconfiguring this hardware provides a new ground testbed at minimal cost.

The baseline EOS AM-1 spacecraft weighs nearly 10,500 pounds at end-of-life (Figure 1-2). The bus structure is composed of a graphite/epoxy truss that is approximately 21 feet long and 6 feet wide. Five science instruments and a full complement of spacecraft subsystem boxes are supported on graphite/epoxy sandwich panels attached to the truss. Two large, flexible appendages are attached to the bus: a 29.3-foot solar array and an 8.3-foot high gain antenna. These appendages have four important modes in the 0.3 - 0.7 Hz range, corresponding to the first bending modes of both appendages about each bending axes. Further information on the baseline EOS AM-1 spacecraft is provided in Section 2.1.

The approach to meeting the CEM3 testbed objectives required a highly iterative analysis, design, and development process. Apart from the limitations associated with using the existing CEM2 components, the most difficult challenges included (1) simulating the low-frequency appendage interaction in the 1-g laboratory environment, (2) achieving a testbed weight within the 2,000 pound capability of the suspension system, and (3) designing the scaled SA and HGA appendages to meet the appendage dynamic interaction requirements.

The approach to simulating the SA and HGA appendage dynamic interaction is based on matching the fundamental parameters in the open-loop structural frequency response functions (FRF's) which relate responses at the spacecraft sensors due to torque inputs from the actuators. The key parameters are the spacecraft inertias, the

appendage modal frequencies, damping values, and structural gains (K_b's); and the frequency of the first spacecraft bus system mode. The design goal was to match the open-loop FRF's of the suspended CEM3 testbed with those of the EOS AM-1 spacecraft, as discussed in Section 2.2.

To meet the objective of simulating the overall dynamic characteristics of EOS AM-1 with a testbed weighing less than 2,000 pounds, new versions of the multiple scaling method were specifically developed for the CEM3 testbed (Section 2.3). Using 1/10:1 multiple scaling, design parameters such as mass (M & I) and stiffness (EI, GJ, EA, & GA) scale as 1/10 of full-scale, while geometry and frequency scale as unity. The result is a scaled CEM3 testbed having the same overall size and structural frequencies as predicted for the full-scale EOS AM-1 spacecraft, but at only 1/10 of the weight.

The scaling of the SA and HGA appendages posed a difficult dilemma. Analyses indicate that given the fixed bending rigidity (EI) and short length of the existing 15-foot CEM2 mast, it is impossible to satisfy both the K_b and frequency requirements using the baseline multiple scaling method. Barring the construction of a proper 30-foot array simulator (which is a possible option constrained by funding), it was decided to use a variant of the 1/10:1 multiple scaling method which doubles the frequency of the appendages relative to the full-scale EOS AM-1 spacecraft. Until a properly scaled, 30-foot solar array simulator can be developed, this approach serves as a useful compromise, allowing the competing objectives of the CEM3 testbed to be met using the existing CEM2 testbed hardware and suspension system. A summary of the key scaled EOS AM-1 parameters for the CEM3 testbed design is provided in Section 2.4.

1.2 TESTBED DESIGN AND DEVELOPMENT

The CEM3 testbed consists of a spacecraft bus structure, two flexible appendages, gimbaled instrument simulators, and dummy masses to simulate both science instruments and spacecraft subsystems. The testbed is oriented so that the payloads on the +Z side face the optical scoring systems on the laboratory floor (Figure 1-3). Reconfiguration of the CEM2 testbed was accomplished using existing hardware, with the exception of a new HGA simulator and some additional 14-inch diagonal bracing struts. Existing CEM2 suspension devices are also used to suspend the spacecraft from long cables to simulate the free-free on-orbit environment.

As discussed in Section 3.1.1, the key design drivers for the primary structure design were (1) matching the spacecraft geometry, (2) matching the 23 Hz first bus system

Figure 1-3. CSI Evolutionary Model Phase-3 Testbed

mode, and (3) supporting the attached payloads and equipment at the proper center-of-gravity (c.g.) locations in order to match the overall spacecraft inertia properties. The existing quantity of CEM2 struts also strongly influenced the configuration design. In summary, the resulting CEM3 primary structure matches the overall dimensions of the EOS AM-1 spacecraft (Figure 1-4).

Eighty-eight new "stock tube" diagonals were added to the CEM3 design in order to increase the testbed torsional stiffness to meet the 23 Hz frequency requirement. These diagonals are based on the existing CEM2 strut design, using a "stock" size for the inner and outer diameter of the strut tube. The added diagonals are located in the plane of the open bays of truss between the bulkheads (Figure 1-4). These new diagonal struts were tested in tension and compression to characterize their stiffness, as discussed in Section 3.1.2.

As discussed in Section 3.2, the EOS AM-1 "payloads" (science instruments and subsystem equipment) are simulated on the CEM3 testbed using discrete rigid masses. The rigid masses simulating the MISR, SWIR, and VNIR science instruments are attached to the three CEM2 2-axis pointing gimbals. Because the CEM3 primary structure and appendage designs are driven by other variables, the weight and placement of the attached payloads served as the only unconstrained testbed variables that could be adjusted to match the overall spacecraft inertias and c.g. Even the payload weight variables are somewhat constrained because of the "out-of-scale" 90-pound weight of the 2-axis gimbals. Nonetheless, a spreadsheet and optimization program were developed and used to provide a good match of the mass properties.

The design of the SA and HGA appendages was driven by the need to meet the associated frequency and K_b requirements (Section 3.3). Though the existing CEM2 deployable mast is about half the desired length, the EOS AM-1 solar array was simulated by attaching a 40-pound weight to the tip of the mast. This resulted in matching the frequency and K_b goals for the first two bending modes. For the HGA, a new design was developed to meet the scaled requirements for the geometry, weight, frequencies, and K_b's. Modal tests of both the SA and HGA were conducted to characterize their dynamics and update the Finite Element Method (FEM) models. The results are discussed in Sections 3.3.2 and 3.3.4, respectively.

Five existing CEM2 suspension devices are used to support the CEM3 testbed and simulate free-free on-orbit boundary conditions. The advanced suspension devices provide vertical isolation, while long cables provide horizontal isolation. Four devices are attached to the primary structure and one to the tip of the solar array

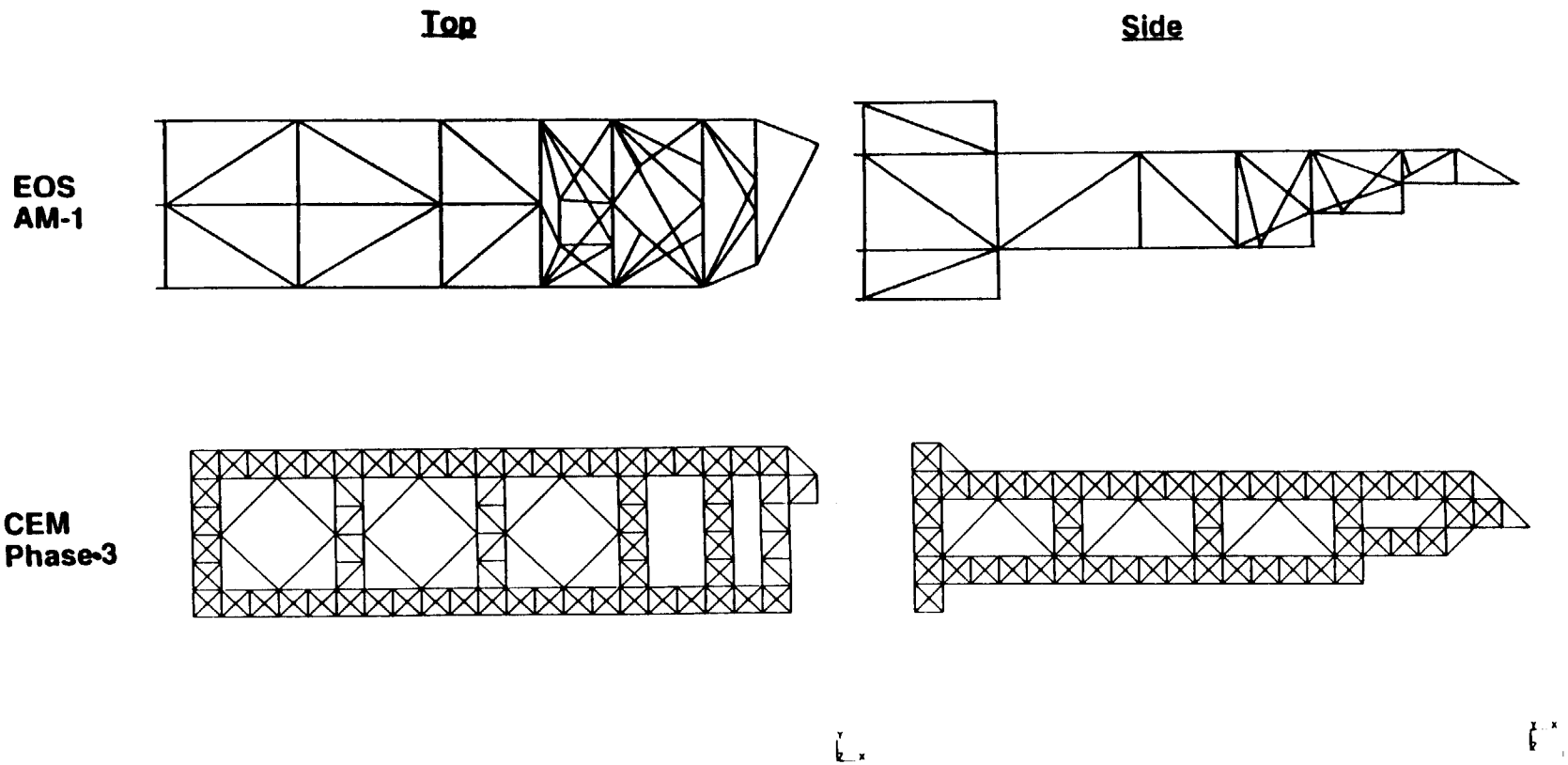

Figure 1-4. CEM3 vs. EOS Primary Structure Comparison

simulator. Each device supports a load of less than 500 pounds. Analyses were conducted to locate cable attachment points which provide both positive CEM3 structural load margins and rigid-body suspension modes below 0.2 Hz. In addition, the stiffness gains of the suspension devices were tuned to minimize the suspension interaction. Further information on the suspension system is provided in Section 3.4.

1.3 CEM3 and EOS AM-1 COMPARISON SUMMARY

The fidelity of the CEM3 testbed in terms of simulating the EOS AM-1 spacecraft was evaluated by comparing the suspended CEM3 geometry, mass property, dynamics, and appendage interaction FEM results with the corresponding scaled EOS AM-1 spacecraft FEM results (Tables 1-1 and 1-2). The most important parameters are shaded in gray. The CEM3 FEM model used to generate these results reflects the CEM3 configuration at the time of delivery to NASA/LaRC. It also includes updated component FEM models incorporating the results of the stock tube diagonal, solar array simulator and HGA simulator hardware characterization tests.

The results in Table 1-1 show good agreement for the overall geometry of the bus and the high gain antenna. Because of the requirement to use the existing CEM2 mast, the CEM3 solar array simulator is approximately half of the length desired for the testbed. This difficulty was overcome by using a different scaling method for the appendage design which preserved the important appendage dynamic interaction characteristics.

The total weight of the CEM3 testbed meets the requirement to be below 2,000 pounds, but exceeds the EOS AM-1 target value by 36%. This was a result of using existing aluminum CEM2 struts to simulate the stiffness and frequency characteristics of the graphite/epoxy composite EOS AM-1 primary structure. Fortunately, this has no effect on the pointing performance of the testbed, which involves mainly the diagonal inertias. The results for the center-of-gravity show good agreement for the Y and Z c.g. locations. The X c.g. difference of 14 inches is acceptable, a result of the fact that the aft end of the CEM3 structure was shortened due to the limited supply of CEM2 struts.

For the purposes of simulating the on-orbit dynamics of the EOS AM-1 spacecraft, the most important mass properties are the diagonal inertias. Comparison of the diagonal inertias indicates excellent agreement between the CEM3 testbed and the scaled EOS AM-1 spacecraft values. In contrast, the cross products of inertia show poor agreement, largely due to the use of the existing CEM2 2-axis gimbals. This is an entirely acceptable compromise however, as in both the EOS AM-1 spacecraft and

Table 1-1. CEM3 Comparison with EOS AM-1 Spacecraft

PROPERTY		EOS AM-1 Full Scale	EOS AM-1 Scaled - (A)	CEM3
BUS GEOMETRY (In)	L	256	256	220
	W	68	68	60
	H	78	78	80
APPENDAGE GEOMETRY (in)	SA L	351	351	180
	HGA L	100	100	100
MASS PROPERTIES (lbf, in, lbf-in^2)	Total Weight	10,500	1,050	1,425
	X-CG	157.3	157.3	171.86
	Y-CG	-3.1	-3.1	-6.37
	Z-CG	-8.2	-8.2	-0.04
	Ixx	4.35E+07	4.35E+06	4.39E+06
	Iyy	6.73E+07	6.73E+06	6.84E+06
	Izz	8.14E+07	8.14E+06	8.10E+06
	Ixy	-1.23E+06	-1.23E+05	-1.82E+04
	Ixz	1.63E+06	1.63E+05	4.18E+05
	Iyz	3.37E+06	3.37E+05	8.04E+04
1st System Freq (Hz)	Bus	23	23	24
	Payload	35	35	22

Table 1-2. CEM3 Comparison with EOS AM-1 Appendage Dynamics

Appendage Modes		EOS AM-1 Full Scale	EOS AM-1 Scaled - (C)	CEM3
SA Yaw	Freq (Hz)	0.295	0.590	0.716
	Kb	0.33	0.33	0.35
SA Roll	Freq (Hz)	0.380	0.760	0.815
	Kb	0.61	0.61	0.81
HGA Pitch	Freq (Hz)	0.501	1.002	1.258
	Kb	0.07	0.07	0.07
HGA Roll	Freq (Hz)	0.660	1.320	1.517
	Kb	0.61	0.61	0.73

the CEM3 testbed the cross products of inertia are very small compared to the diagonal inertias.

Table 1-1 also shows that the first system mode frequency of the bus is well-matched, though the first payload mode is not. The latter is an artifact of the requirement to use the existing CEM2 2-axis gimbal design.

Table 1-2 shows that the important overall character of the appendage dynamic interaction (in terms of frequency spacing, coupling, and modal gain) has been preserved, as further evidenced in the open-loop structural FRF's shown in Figures 1-5 through 1-7. A constant modal damping value of 0.5% was used for both the CEM3 and EOS AM-1 FRF's. In the region below 1 Hz, the CEM3 roll (Figure 1-5), pitch (Figure 1-6), and yaw (Figure 1-7) FRF's display the same basic characteristics as the scaled EOS AM-1 FRF's, with two exceptions. First, each CEM3 testbed FRF has a peak associated with a low-frequency suspension mode, as predicted in Section 2.2. Inspection of the CEM3 curves clearly shows that the suspension modes are uncoupled from the appendage modes. Second, as was intended with the approach described in Section 2.4 (using multiple scaling method C), there is approximately a factor of two difference between the EOS and CEM3 appendage frequencies, while the relative spacing and magnitude are preserved.

Overall, all of the parameters shaded in gray in Tables 1-1 and 1-2 show acceptable, if not good agreement, reflecting a testbed with good fidelity in the important parameters of interest. Considering the challenging constraints on the design effort, the dynamic comparison of the open-loop FRF's and the appendage frequencies and K_b's is surprisingly good. Further information on the testbed fidelity and associated analyses is provided in Section 4.0.

In conclusion, the CEM2 model hardware has been successfully reconfigured to provide a ground testbed representation of the low-frequency dynamic characteristics of the EOS AM-1 spacecraft. The effort was accomplished within the five-month schedule and at a very minimal cost in new hardware. The resulting CEM3 testbed is now available for use in experiments to develop CSI technology for jitter isolation and suppression and the enhancement of overall spacecraft pointing performance.

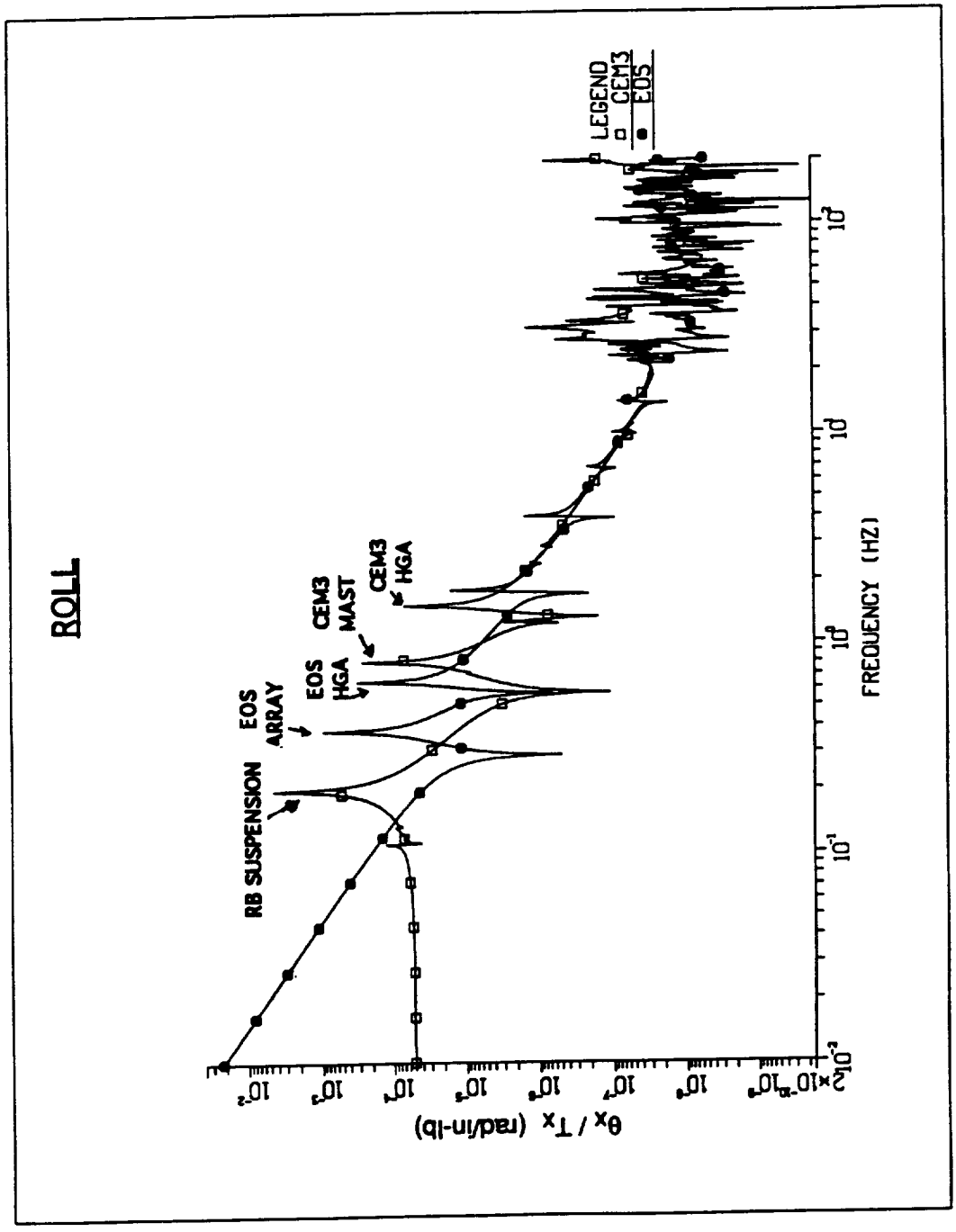

Figure 1-5. Frequency Response Function Comparison - Roll Axis

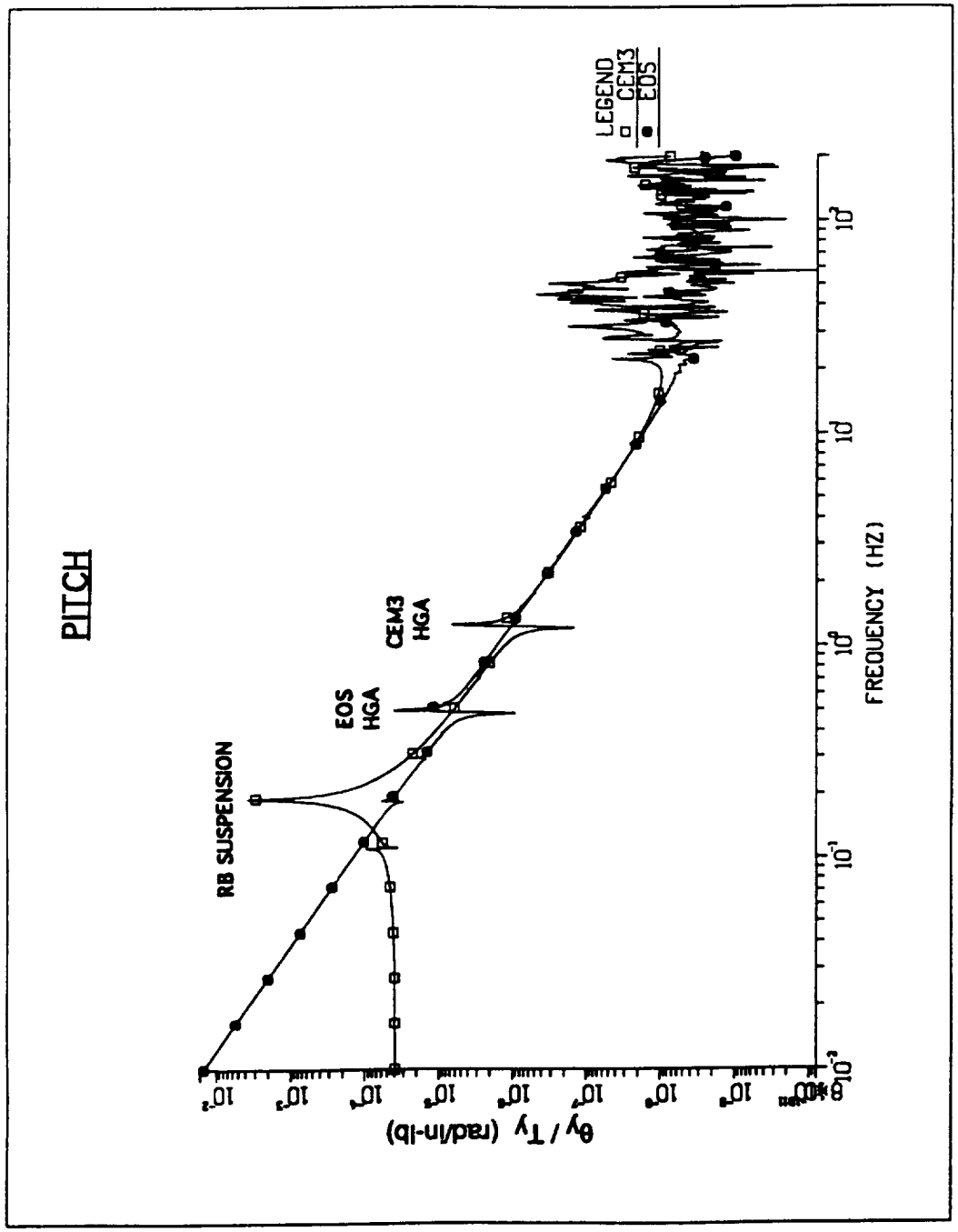

Figure 1-6. Frequency Response Function Comparison - Pitch Axis

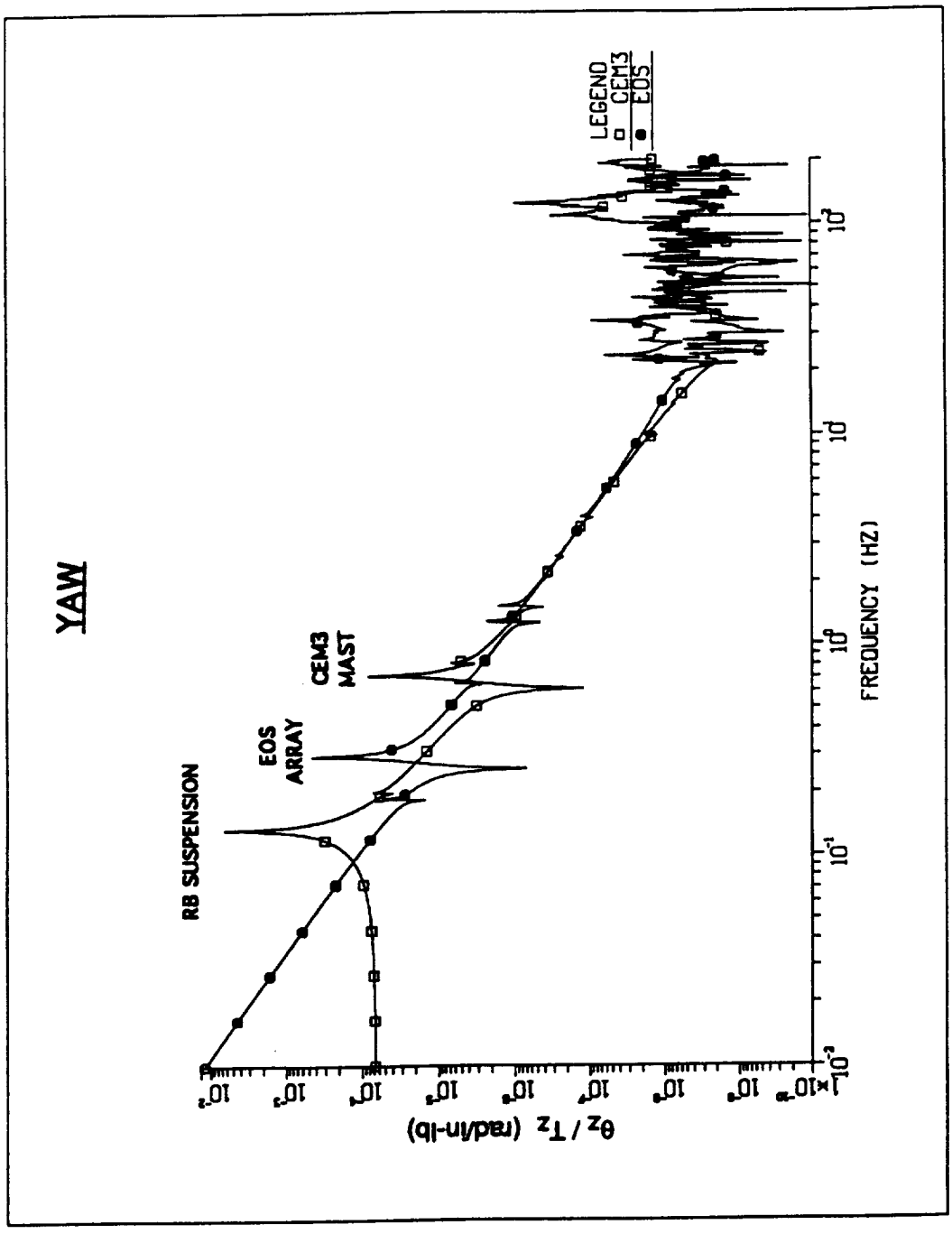

Figure 1-7. Frequency Response Function Comparison - Yaw Axis

2.0 BACKGROUND AND APPROACH

As a part of a program of ongoing research and technology development activities in the CSI technology area, NASA/LaRC initiated the design and fabrication of the CSI Evolutionary Model in 1990 to provide a testbed for the development, implementation, and validation of CSI technology and associated hardware and software[1,2,3]. Since that time, the CEM has evolved from the Phase-0 through the Phase-1 and Phase-2 configurations (designated CEM1 and CEM2) in support of integrated CSI design, pointing, jitter, disturbance rejection, isolation, and distributed control experiments[4]. The CEM has also been used in the development of associated ground test techniques, including advanced zero-g suspension systems, actuators, sensors, and precision pointing optical scoring systems[5].

This report describes the configuration and structural development effort for the evolution of the CEM2 testbed into the CEM3 configuration. This evolutionary step responds to the need to develop and test CSI technologies associated with typical planned earth science and remote sensing platforms, such as the eight-satellite EOS system, DMSP/NOAA weather satellites, LandSat, and others. The EOS spacecraft series is of particular interest in that the CEM3 testbed will be used to support system identification and CSI technology development experiments that may fly on the EOS AM-1 spacecraft, as part of the Jitter Attenuation and Dynamics Experiment[6].

The primary objective of the CEM3 testbed development is to reconfigure the components of the existing CEM2 testbed (Figure 1-1) in order to simulate the overall dynamic behavior of a typical earth science and remote sensing platform, namely the EOS AM-1 spacecraft (Figures 2-1a and 2-1b). In addition to this overall objective, several specific objectives for the CEM3 were outlined by NASA/LaRC:

(1) Approximate the overall size and shape of the EOS AM-1 spacecraft.
(2) Approximate the solar array and HGA flexible appendage dynamic interaction on the EOS AM-1 spacecraft.
(3) Simulate free-free on-orbit boundary conditions during CSI testing by suspending the testbed in the Building 1293A test facility.
(4) Allow for convenient removal and replacement of testbed components in in order to accommodate different passive and/or active structural members, GN&C equipment, and kinematic mounts.

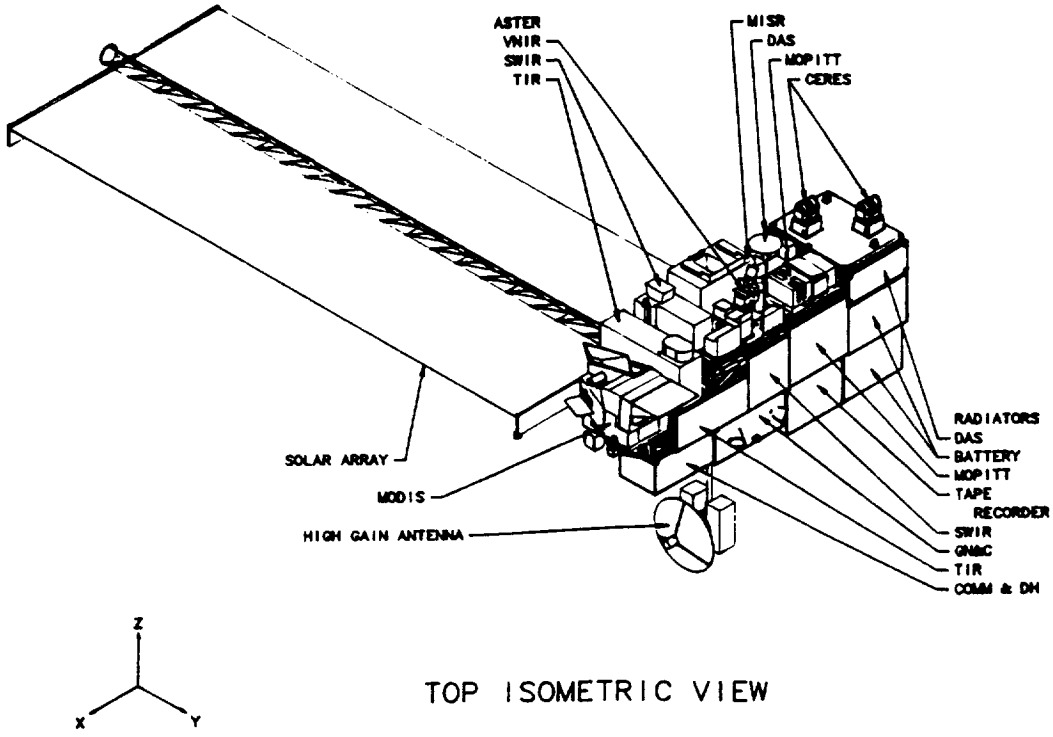

Figure 2-1a. EOS AM-1 On-Orbit Configuration (Isometric and Side Views)

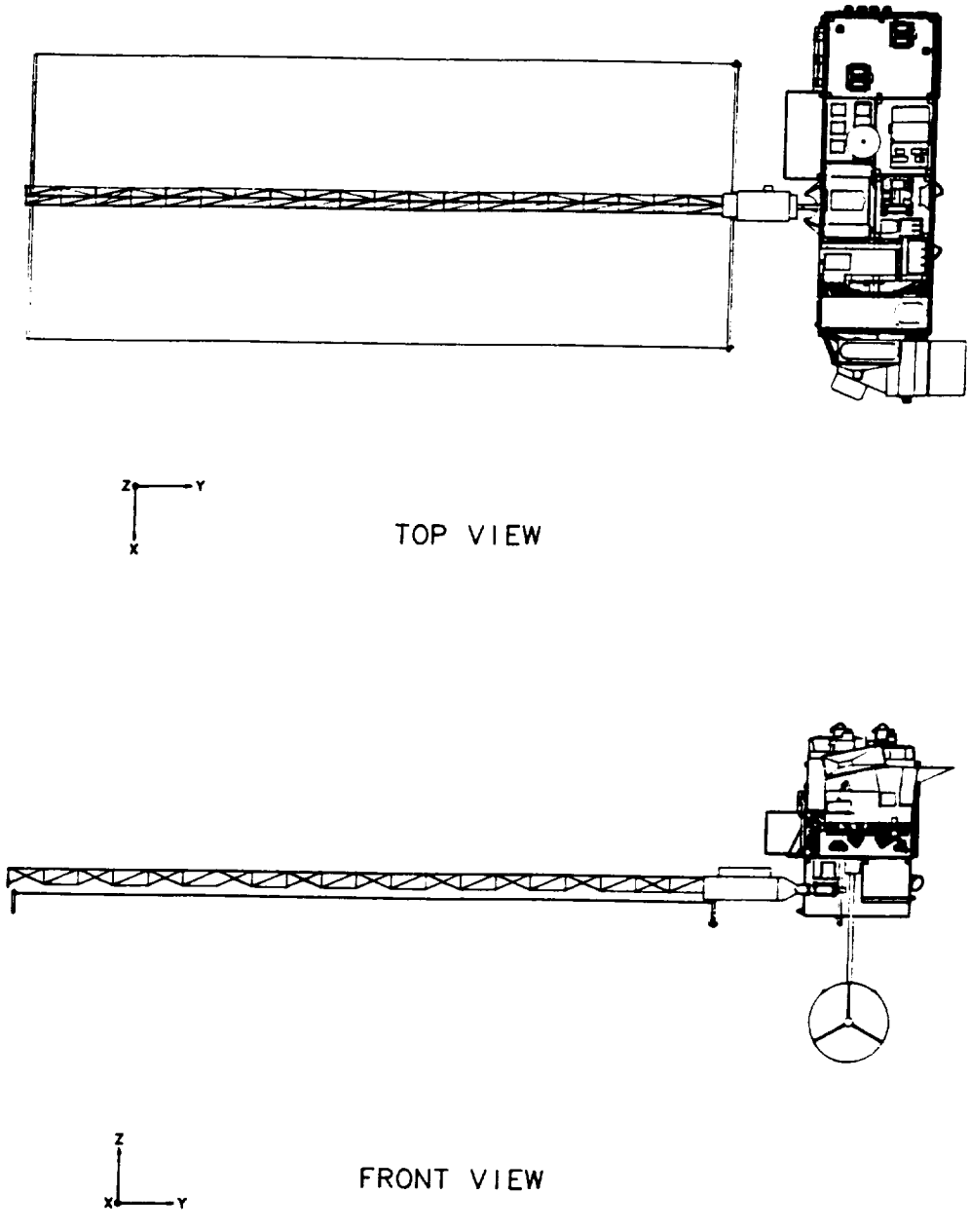

Figure 2-1b. EOS AM-1 On-Orbit Configuration (Front and Top Views)

The following guidelines were also provided for the accomplishment of the CEM3 objectives:

(a) Use the existing CEM2 hardware - develop a minimum of new hardware at minimal cost.
(b) Use existing suspension system hardware which is capable of supporting up to 2,000 pounds in the Building 1293A test facility.
(c) Approximate the overall size, shape, and dynamics of the EOS AM-1 spacecraft to as near full-scale as practicable.
(d) Use existing finite element models and EOS AM-1 data provided by NASA.
(e) Assemble the testbed for suspension in Building 1293A within five months.

Objective (4) is easily achieved in that the existing CEM2 testbed is composed of erectable struts and attached components using quick-connect joints. However, the remaining objectives and guidelines pose a difficult design challenge. In particular, objective (1) is challenging due to the constraint of using existing hardware imposed by guideline (a). The existing CEM2 components include approximately 1,900 aluminum truss struts assembled in 10-inch bays, a 15-foot deployable solar array mast and tip weight, three 2-axis gimbaled science instrument simulators, and associated control sensors (inertial reference units) and actuators (gas-jet thrusters). Objective (2) is challenging in terms of using the existing 15-foot deployable mast to simulate the dynamic interaction of the 30-foot EOS AM-1 array. A new simulator would have to be developed for the HGA, as no corresponding hardware exists. The approach to meeting objective (2) is further complicated by the need to simulate the free-free low-frequency appendage dynamics in 1-g, requiring adequate frequency separation between the suspension system and appendage modes. Finally, satisfying objective (3) and guideline (b) mandates that some sort of scaling method be used in the testbed design, as a full-scale EOS AM-1 spacecraft would weigh in excess of 10,000 lbs - five times the capability of the existing suspension system. Nonetheless, in order to provide the most realistic CSI simulations, it is desirable for the CEM3 testbed to be as near a full-scale model of the EOS AM-1 spacecraft as practicable.

The approach to meeting these challenging objectives required a highly iterative analysis, design, and development process. The following sections describe some of the fundamental analysis results which form the basis for the CEM3 development approach. Section 2.1 describes the physical and dynamic characteristics of the EOS AM-1 spacecraft. In Section 2.2, two-body models are used to develop a basic understanding of the flexible appendage dynamic interaction problem. The results of this analysis provide insight into the key parameters which must be simulated in the CEM3 testbed. These results are then generalized for the three-dimensional,

multiple-appendage case. The challenge of simulating the free-free dynamics of the EOS AM-1 spacecraft in the 1-g laboratory environment is also addressed. Section 2.3 describes the scale factor trades and a new variant of the multiple scaling method. This method permits simulation of full-scale dynamic behavior using a model with full-scale geometry, but only one-tenth the weight. Finally, Section 2.4 summarizes the CEM3 conceptual design approach based on the derived testbed requirements and the results of the analyses in Sections 2.2 and 2.3.

2.1 EOS AM-1 CONFIGURATION

The baseline EOS AM-1 spacecraft in its deployed configuration is shown in Figures 2-1a and 2-1b. The spacecraft is comprised of a rectangular main spacecraft body and two deployable flexible appendages - the solar array and high gain antenna. The main spacecraft body is comprised of truss primary structure, secondary structure, subsystem equipment boxes, and attached science instrument payloads. The truss primary structure when combined with kinematic payload mounts provides a dimensionally stable platform which minimizes the effects of thermal distortion and satisfies instrument alignment requirements.

The overall dimensions of the truss primary structure (without the payloads or appendages) are approximately 232 inches in length, 68 inches in width, and 78 inches in height (Figure 2-2). The addition of the MODIS payload to the front end of the spacecraft increases the overall length to approximately 256 inches. The deployed solar array is 351 inches in length with a blanket width of 196 inches, while the HGA is a slender boom with a cantilevered length of 100 inches. The truss structure, comprised of over 166 longerons, diagonals, and bulkheads, is constructed using high modulus graphite/epoxy tubes bonded to titanium fittings. This provides high stiffness and strength. The distances between bulkheads (bay lengths) are chosen to accommodate attached components. The EOS truss structure comprises 39% of the total 10,494 pound spacecraft weight. Accordingly, the attached components such as the appendages and science payloads account for the majority of the weight and in turn dominate the spacecraft inertia properties.

Two analytical models were used to define the physical properties and dynamic characteristics of the EOS AM-1 on-orbit configuration. Both models have a solar array angle of zero degrees. The first model was the NASA/LaRC Reduced Order Model (ROM) based on the Swales & Associates Version 3 EOS AM-1 On-Orbit Finite Element Model, dated 13 April 1993. This model was primarily used to define the physical properties of the spacecraft such as component weights and locations. In the

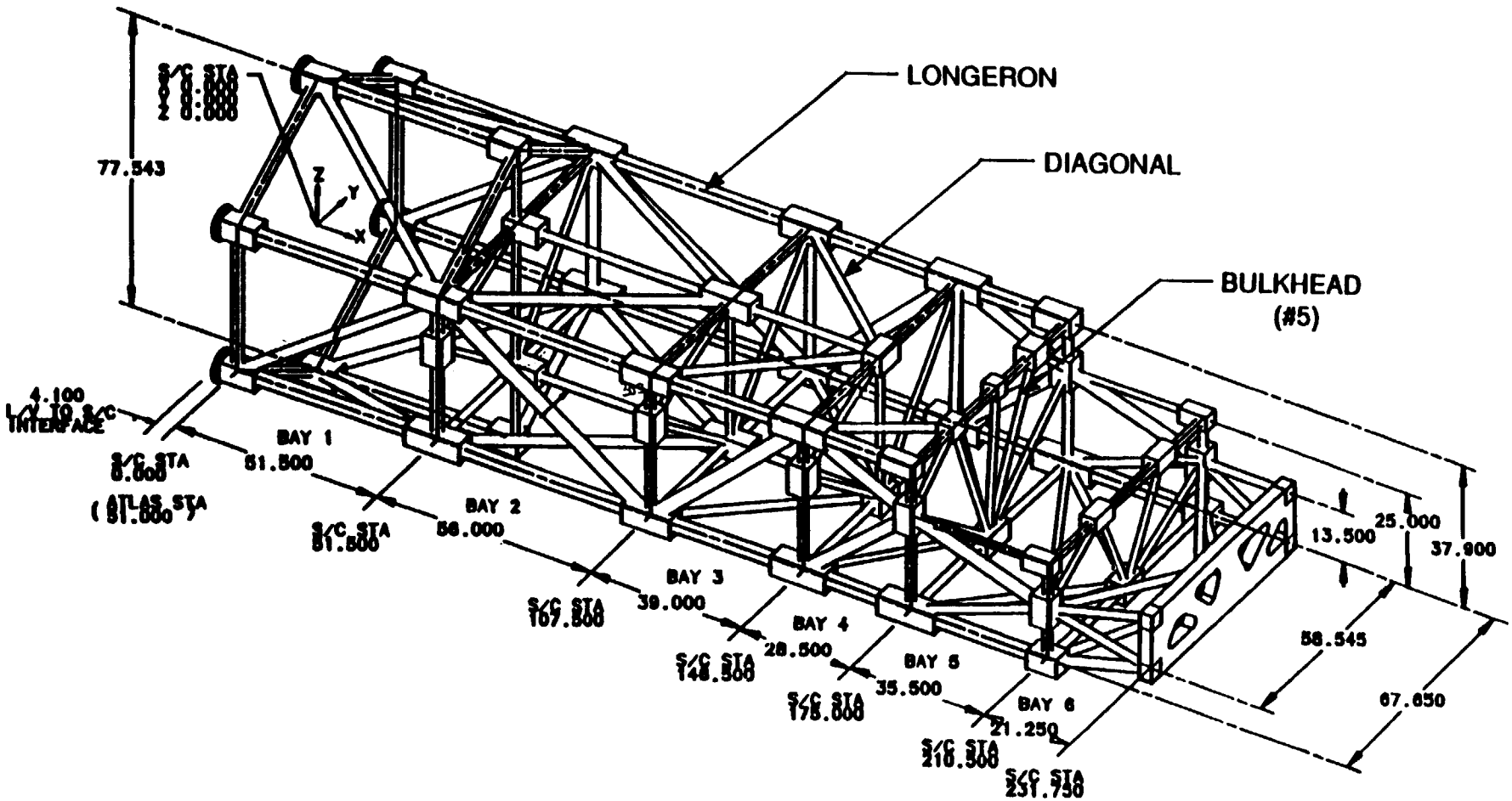

Figure 2-2. EOS AM-1 Bus Structure

ROM model, the instrument packages were reduced to equivalent lumped masses and shell elements were replaced with equivalent beam elements. These changes were necessary in order for NASA/LaRC to analyze the EOS spacecraft using their CSI Design code[4]. The ROM model was extremely useful in the CEM3 design effort since the EOS instrument packages are also modeled as mass simulators on the testbed.

The second model used was the EOS AM-1 On-Orbit Modal Model, Version 3b (dated 22 July 1993)[7], which contains spacecraft mass property, frequency, and mode shape data up to 200 Hz. The dynamic characteristics of the spacecraft, including frequency response functions and bending mode gains, were computed using the information contained in the modal model.

FRF's calculated using the on-orbit modal model indicate the important modes which characterize the appendage dynamic interaction with the spacecraft bus (Figures 2-3, 2-4, and 2-5). The FRF's were developed assuming that torques were generated at the location of the reaction wheels and responses were calculated at the location of the GN&C sensors. A critical damping ratio of 0.5% was used in the analysis. Altogether, there are four modes which characterize the open-loop dynamics below 1 Hz. These correspond to the first bending modes of the solar array and HGA in both the in-plane and out-of-plane directions. About the roll axis, there are solar array and HGA bending modes at 0.38 and 0.66 Hz, respectively. A third roll mode at 1.8 Hz has an order of magnitude lower response. About the pitch axis, the response is dominated by a HGA bending mode at 0.50 Hz. Similarly, about the yaw axis, the response is dominated by a solar array bending mode at 0.30 Hz. The first bus primary structural mode is a torsion mode about the roll axis, located at 23 Hz (Figure 2-3).

A summary of the EOS AM-1 geometry, mass property, and frequency characteristics is provided in Table 2-1.

2.2 SIMULATION OF FLEXIBLE APPENDAGE DYNAMIC INTERACTION

Intuitively, the approach to simulating the overall flexible appendage dynamic interaction is to design the CEM3 testbed to match the open-loop structural frequency response functions of the EOS AM-1 spacecraft. In this section, analyses are conducted to develop a basic understanding of flexible appendage dynamic interaction. Section 2.2.1 begins with a review of the flexible appendage interaction problem, using simple two-body models to illustrate the fundamental parameters

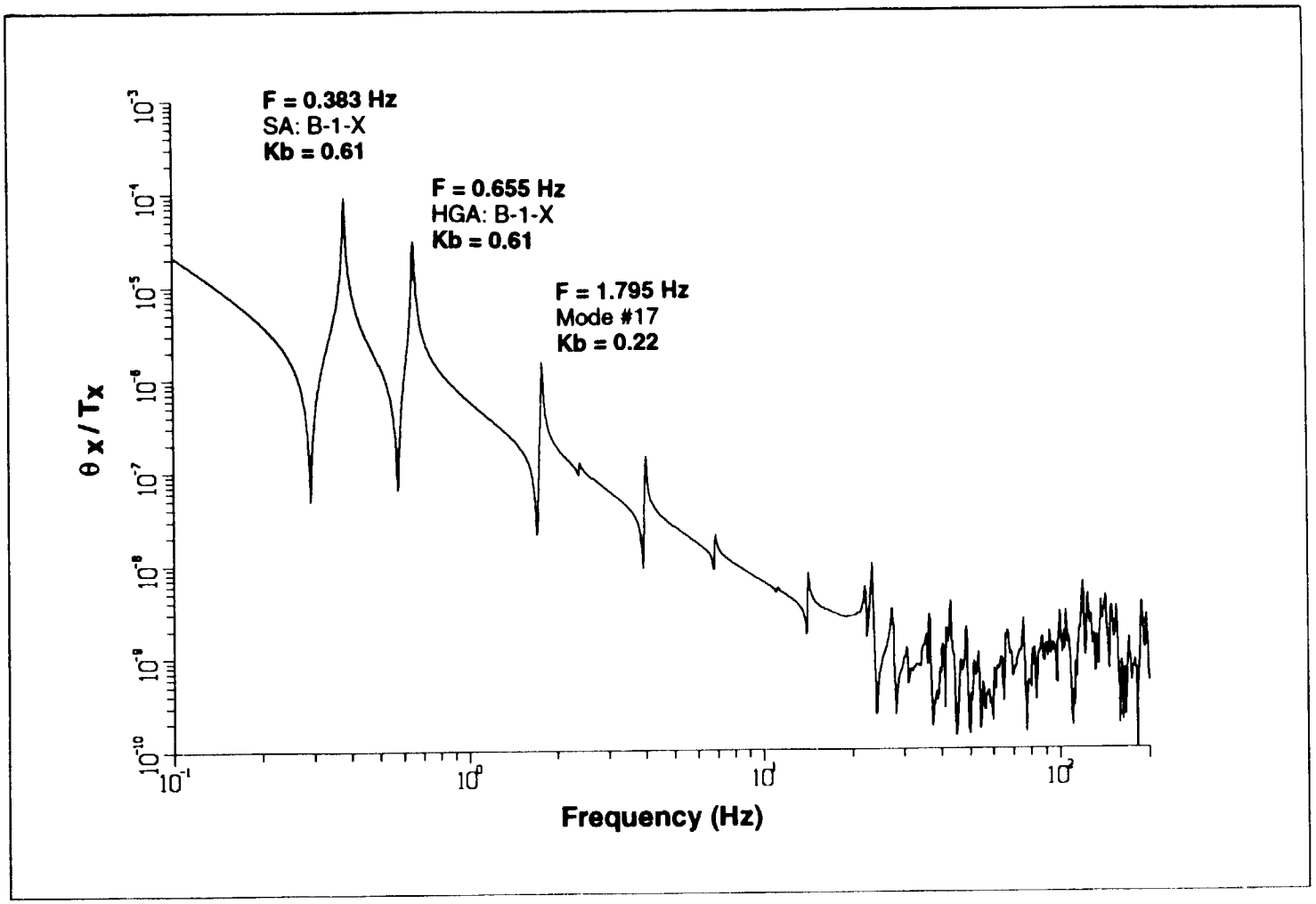

Figure 2-3. EOS AM-1 Free-Free Roll Transfer Function

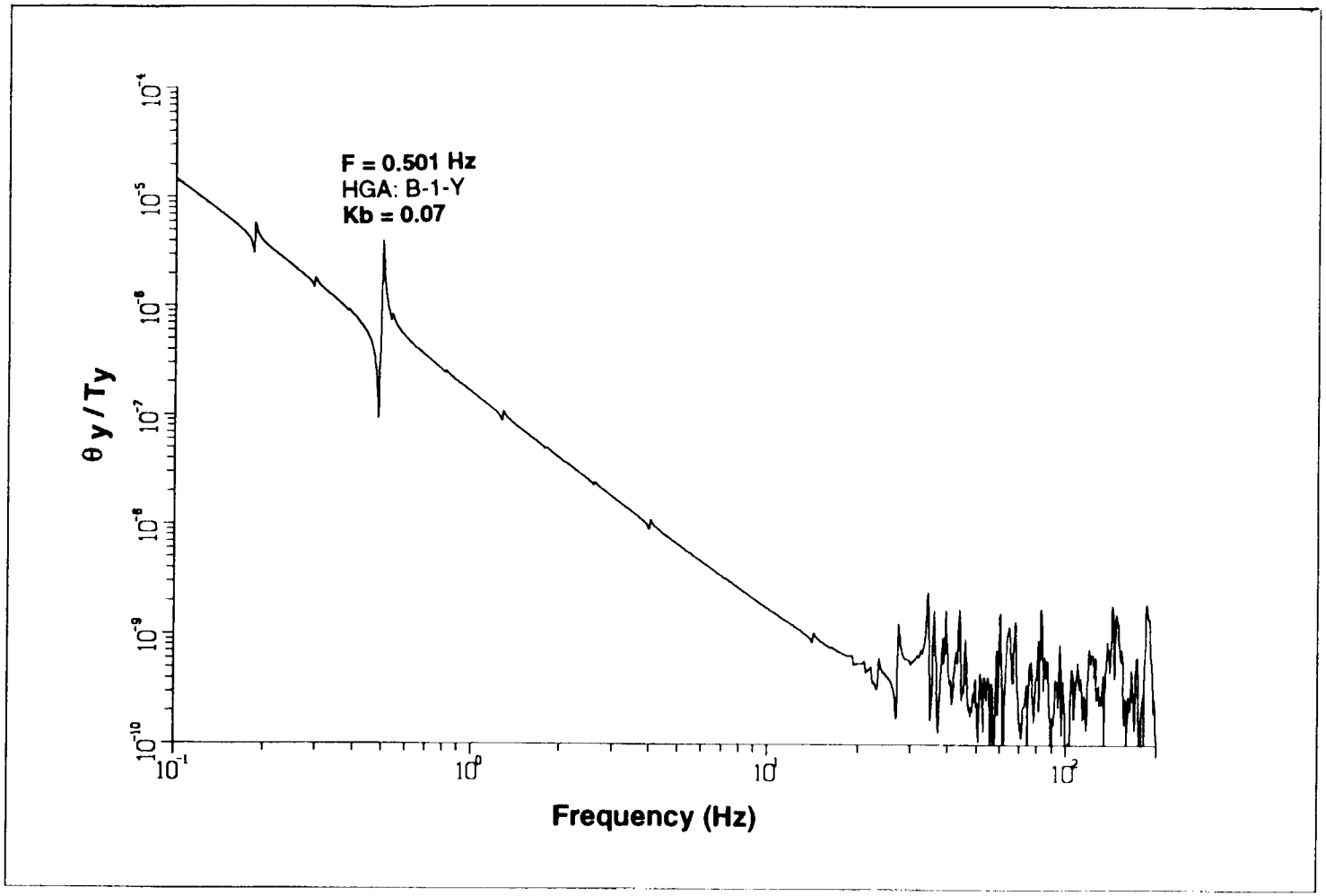

Figure 2-4. EOS AM-1 Free-Free Pitch Transfer Function

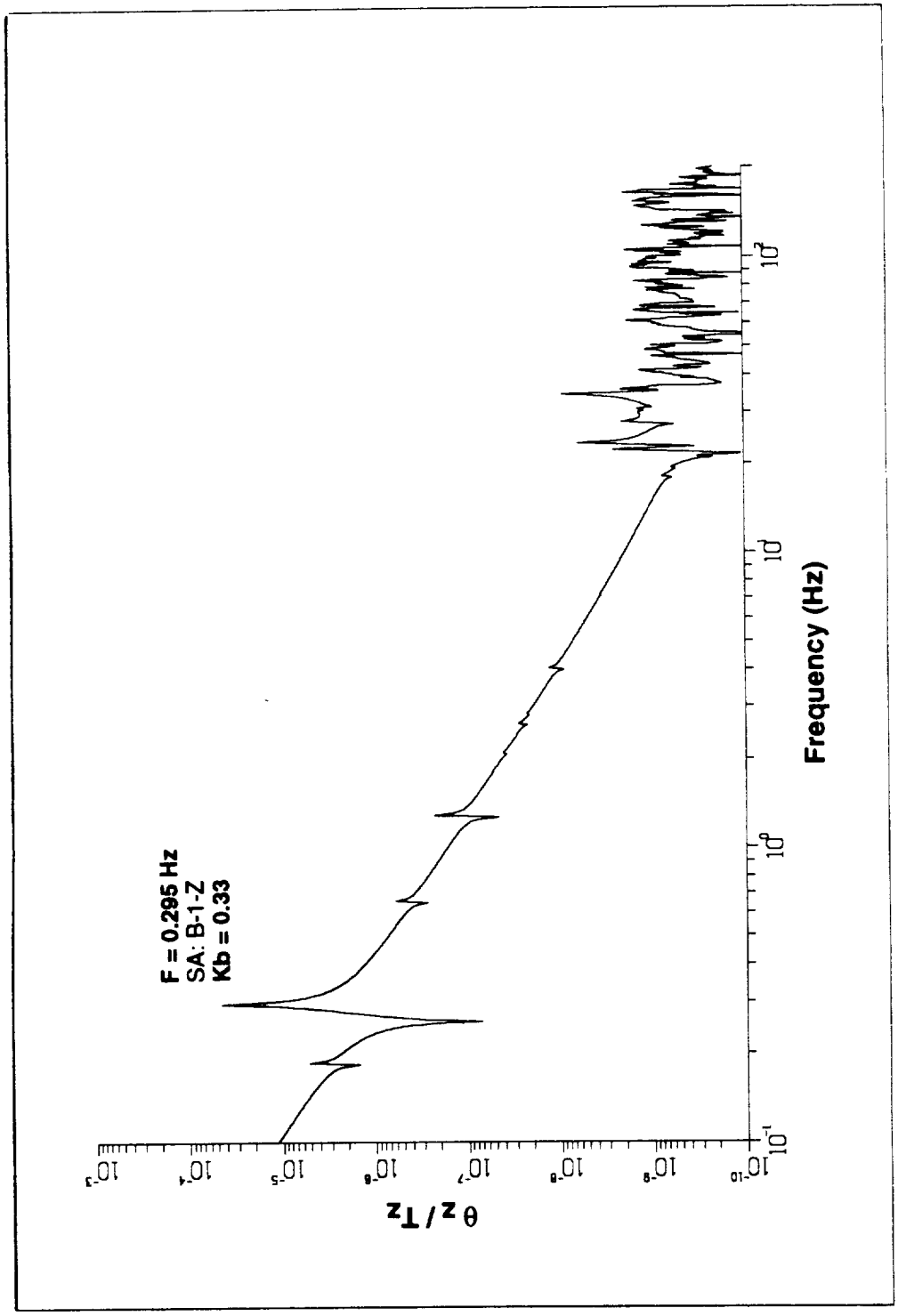

Figure 2-5. EOS AM-1 Free-Free Yaw Transfer Function

Table 2-1. Summary of EOS AM-1 On-Orbit Properties

PROPERTY		EOS AM-1 Full Scale
BUS GEOMETRY (In)	L	256
	W	68
	H	78
APPENDAGE GEOMETRY (In)	SA L	351
	HGA L	100
MASS PROPERTIES (lbf, In, lbf-In^2)	Total Weight	10,494
	Structure Wt.	4,094
	Payload Wt.	6,400
	X-CG	157.30
	Y-CG	-3.10
	Z-CG	-8.20
	Ixx	4.35E+07
	Iyy	6.73E+07
	Izz	8.14E+07
	Ixy	-1.23E+06
	Ixz	1.63E+06
	Iyz	3.37E+06
Key Modes	**Parameter**	**Value**
SA Yaw	Freq (Hz)	0.295
	Kb	0.33
SA Roll	Freq (Hz)	0.38
	Kb	0.61
HGA Pitch	Freq (Hz)	0.501
	Kb	0.07
HGA Roll	Freq (Hz)	0.66
	Kb	0.61
Bus System	Freq (Hz)	23
Payload	Freq (Hz)	35

which characterize the open-loop structural frequency response. In Section 2.2.2, these results are generalized for the three-dimensional, multiple-appendage case. Finally, the effects of an added suspension system on the flexible appendage simulation are addressed in Section 2.2.3.

2.2.1 Dynamics of Appendage Interaction

A simple two-body model and control block diagram illustrating the fundamental free-free dynamics of a spacecraft and a flexible appendage is described in Figure 2-6. For the sake of discussion, the flexible appendage is assumed to be a solar array. Actuators apply torques (T_1) to the rigid spacecraft bus (I_1) to change the spacecraft attitude (θ_1). The flexible solar array is represented by the spring-mass system with stiffness (K), damping (C), inertia (I_2), and attitude (θ_2). For this system, the modal frequency (ω_b), and modal damping (ζ_b) are defined by the equations shown in the figure. In addition, a parameter called the bending mode gain (K_b) is described.

The bending mode gain (K_b) is a measure of the severity of the flexible appendage interaction. For a torque input at resonance, it relates the amount of control actuator excitation energy that is expended in the flexible dynamics of the solar array relative to the amount expended in rigid-body pointing. For this simple two-body system with actuator and sensors collocated on the bus, the modal gain is simply a scalar reflecting the ratio of the flexible inertia to the controlled rigid-body inertia:

$$K_b = \frac{I_2}{I_1} \tag{2-1}$$

Examination of the open-loop structural frequency response transfer function provides further insight into the nature of the bending mode gain. For this system, the transfer functions for the bus and solar array attitude response are:

$$\frac{\theta_1(s)}{T_1(s)} = \frac{1}{(I_1+I_2)s^2} + \frac{\dfrac{K_b}{(I_1+I_2)}}{s^2+2\zeta_b\omega_b s+\omega_b{}^2} \tag{2-2}$$

$$\frac{\theta_2(s)}{T_1(s)} = \frac{1}{(I_1+I_2)s^2} - \frac{\dfrac{1}{(I_1+I_2)}}{s^2+2\zeta_b\omega_b s+\omega_b{}^2} \tag{2-3}$$

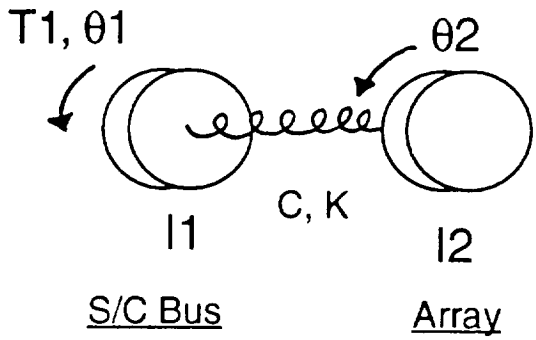

$$\omega_b^2 = \frac{I_1+I_2}{I_1 \cdot I_2} K \qquad 2\zeta_b\omega_b^2 = \frac{I_1+I_2}{I_1 \cdot I_2} C \qquad K_b = \frac{I_2}{I_1} = \frac{\phi^T \phi\, I}{\phi^T M \phi}$$

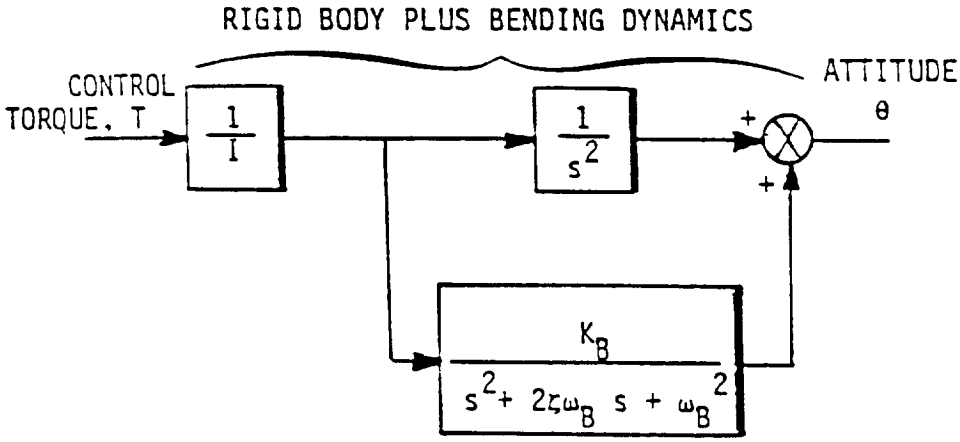

Figure 2-6. Two-Body Model and Block Diagram

The magnitudes of the corresponding open-loop structural frequency responses are plotted in Fig 2-7. At resonance, the transfer function becomes:

$$\left|\frac{\theta_1(s)}{T_1(s)}\right| = \left|\frac{-1}{(I_1+I_2)\omega_b^2}\cdot\left[1+j\frac{K_b}{2\zeta_b}\right]\right| \tag{2-4}$$

$$\left|\frac{\theta_2(s)}{T_1(s)}\right| = \left|\frac{-1}{(I_1+I_2)\omega_b^2}\cdot\left[1+j\frac{-1}{2\zeta_b}\right]\right| \tag{2-5}$$

For lightly-damped modes (small ζ), the complex frequency term is much larger than unity, and the resonant responses can be approximated by

$$\left|\frac{\theta_1(s)}{T_1(s)}\right| \cong \frac{K_b}{2(I_1+I_2)\zeta_b\omega_b^2} \tag{2-6}$$

$$\left|\frac{\theta_2(s)}{T_1(s)}\right| \cong \frac{1}{2(I_1+I_2)\zeta_b\omega_b^2} \tag{2-7}$$

The responses shown in Figure 2-7 and the equations above reveal several characteristics of the system. First, for a free-free system with sensors and actuators collocated on the bus, the resonance in the θ_1/T_1 response is always preceded by a zero, corresponding to the frequency at which the reaction torque due to the flexibility of the array matches the applied torque of the actuator. Second, the gain above the rigid-body line due to the presence of the bending mode is $20\log(K_b/2\zeta)$ dB. Third, the dotted/dashed line in the figure shows how the rigid-body line would continue if the K_b were equal to zero (no appendage). Fourth, at frequencies well after the resonance, the rigid-body line is shifted up by a gain of $20\log(1 + K_b)$ dB. Finally, it should be noted the response of the array (θ_2/T_1) does not depend on the value of K_b, it effectively has a K_b of -1.

The effects of larger and smaller K_b values on the bus open-loop transfer function are shown in Figure 2-8. The heavy dashed line corresponds to a K_b of zero. As can be seen in the figure, larger K_b's correspond to:

(1) Increased magnitude of the flexible-body response.
(2) Increased spacing in frequency between the pole and zero.
(3) Increased upward shift in the rigid-body line after resonance.

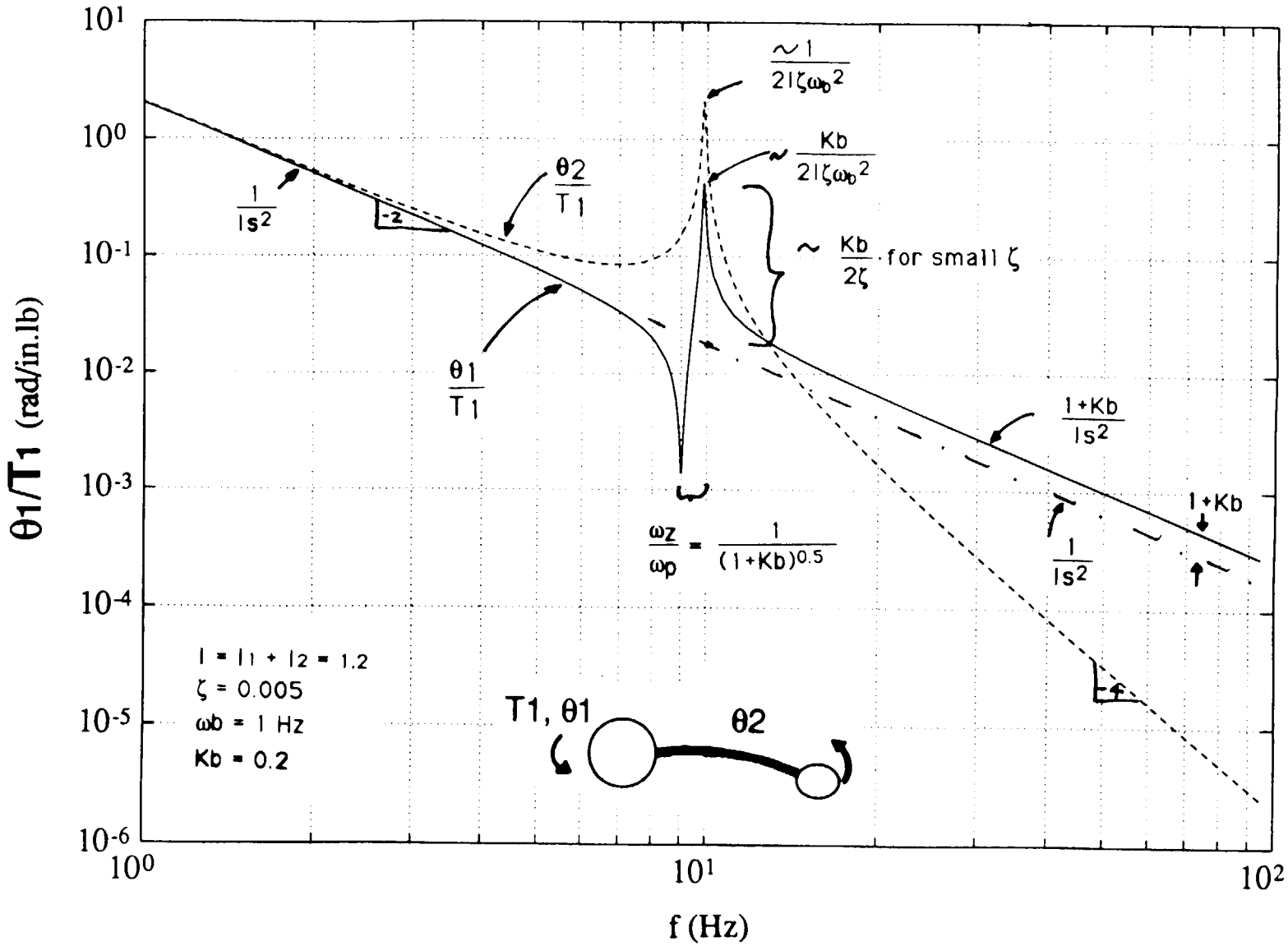

Figure 2-7. Two-Body Model Open-Loop Structural Transfer Function

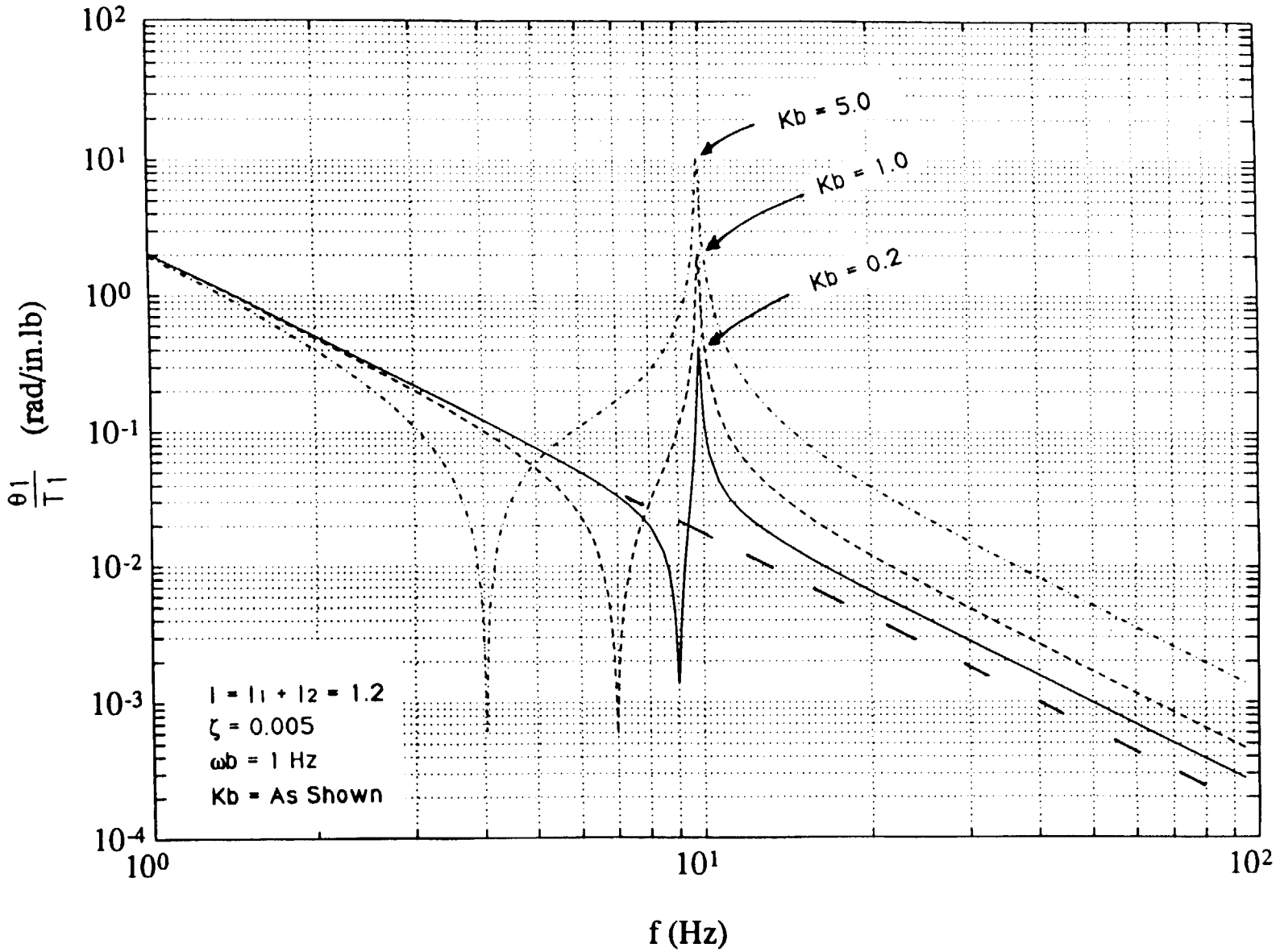

Figure 2-8. Effect of Varying Kb on Open-Loop Structural Transfer Function

Note that for a K_b of 1, the steady-state response at resonance for the solar array and the bus have the same magnitude (as is evident in Figure 2-7 if $K_b = 1$). For values of K_b less than 1, the "rigid-body" response of the bus is greater than that of the array. For K_b values greater than 1, the response of the array is larger than the bus.

A translational analog for the spacecraft pointing Kb problem is provided in Figure 2-9, where M1 is the mass whose position we are attempting to control. It is clear in both of these examples that large Kb's correspond to a potentially difficult control situation where the "tail is wagging the dog".

The values of the terms K_b and $(K_b/2\zeta)$ are closely linked to the stability of the closed-loop system (Figure 2-10). The gain margin of a rigid-body system without a flexible appendage is related to the value of the open-loop magnitude response of the control system at the phase crossover frequency. The amount of gain margin lost due to the addition of an appendage with a frequency ω_b located near the phase crossover frequency of the rigid-body control system is approximately $20\log(K_b/2\zeta)$ dB. As shown in Figure 2-10, the addition of the bending mode has the effect of adding a loop to the gain-phase stability plot, creating an unstable system in this example. Similarly, the much smaller amount of gain margin lost due to an added appendage with its frequency located well below the phase crossover frequency of the rigid-body control system is $20\log(1+K_b)$ dB.

Given the parameters of the rigid-body control design without appendage flexibility, the stability of a spacecraft control system can be evaluated with various attached appendages in terms of the allowable K_b, damping, and frequency for each appendage. Bending mode stability maps can be generated by calculating the value of K_b which causes instability at a particular appendage frequency.

An example for a typical spacecraft is provided in Figure 2-11, using an assumed damping of $\zeta = 0.5\%$ for the appendage modes. Three sets of data are plotted for different solar array gimbal angles. The solid line on the plot (reflecting zero gain or phase margin) has three regions. The region of constant K_b corresponds to the frequencies below the rigid-body crossover frequency. This region is a function of rigid-body gain margin and is virtually unaffected by appendage damping for positive K_b - the limit is when the gain margin of the rigid-body system without flexibility effects is equal to $20\log(1+K_b)$ dB. The second region is the notch in allowable K_b where the appendage resonance adds phase lead and amplification. This region is very sensitive to the modal damping - lighter damping results in a deeper notch with a reduced K_b limit. The third region reflects increasingly allowable K_b where the

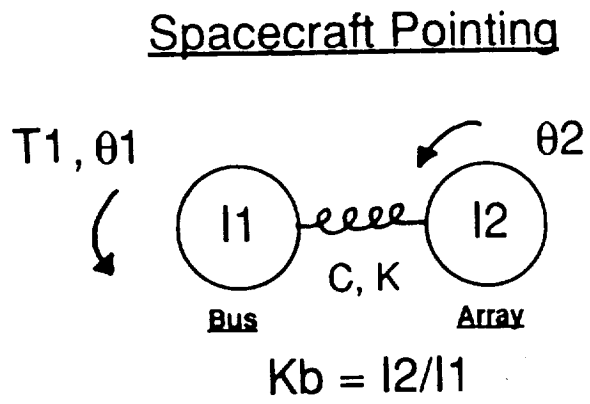

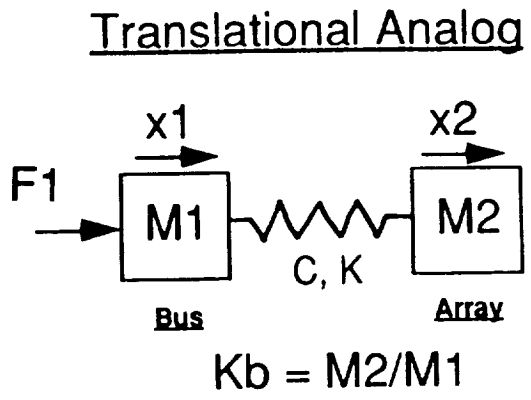

Figure 2-9. Translational Analog to Two-Body Spacecraft Pointing Problem

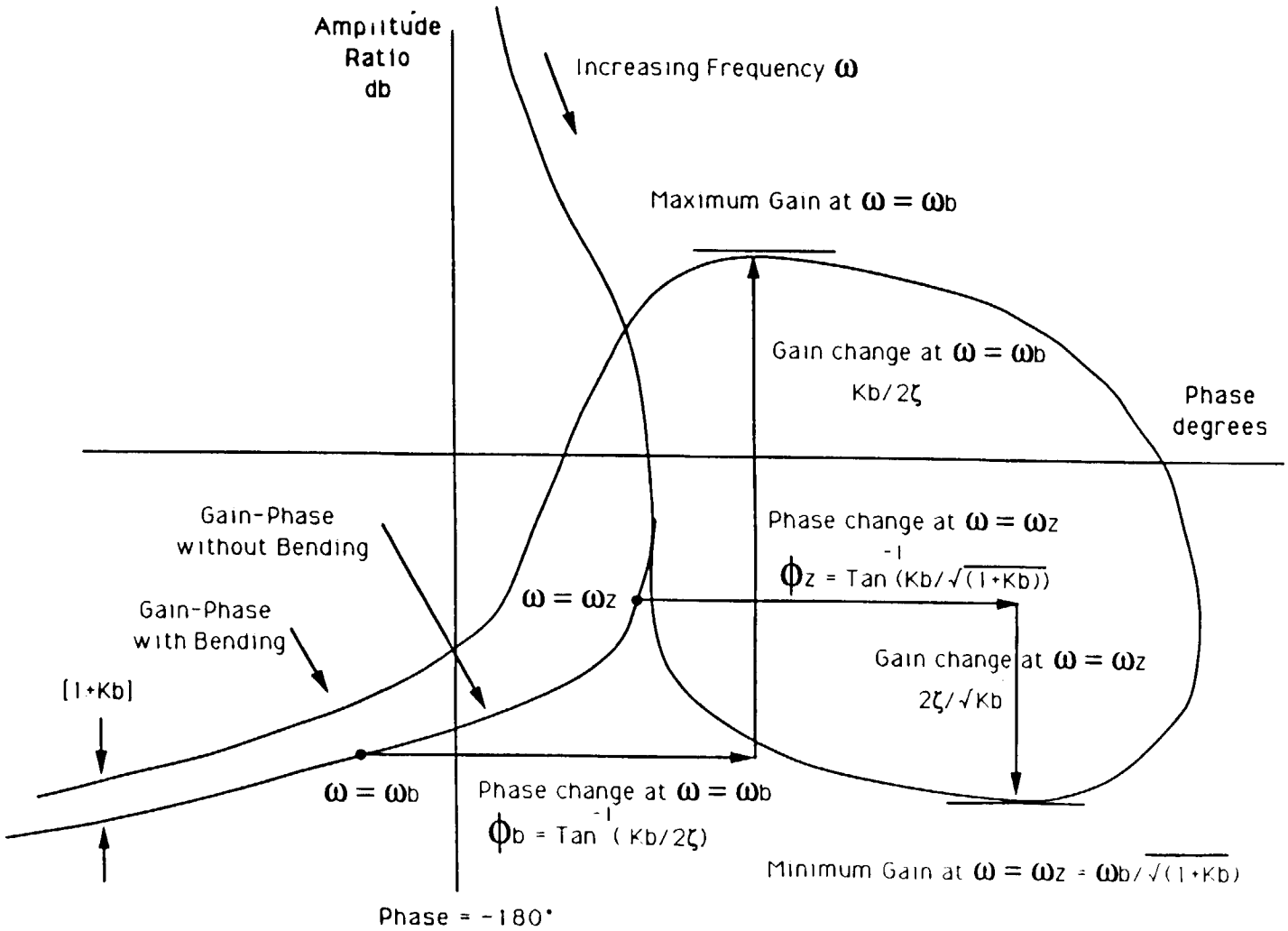

Figure 2-10. Effect of Appendage Mode on Gain-Phase Stability Plot

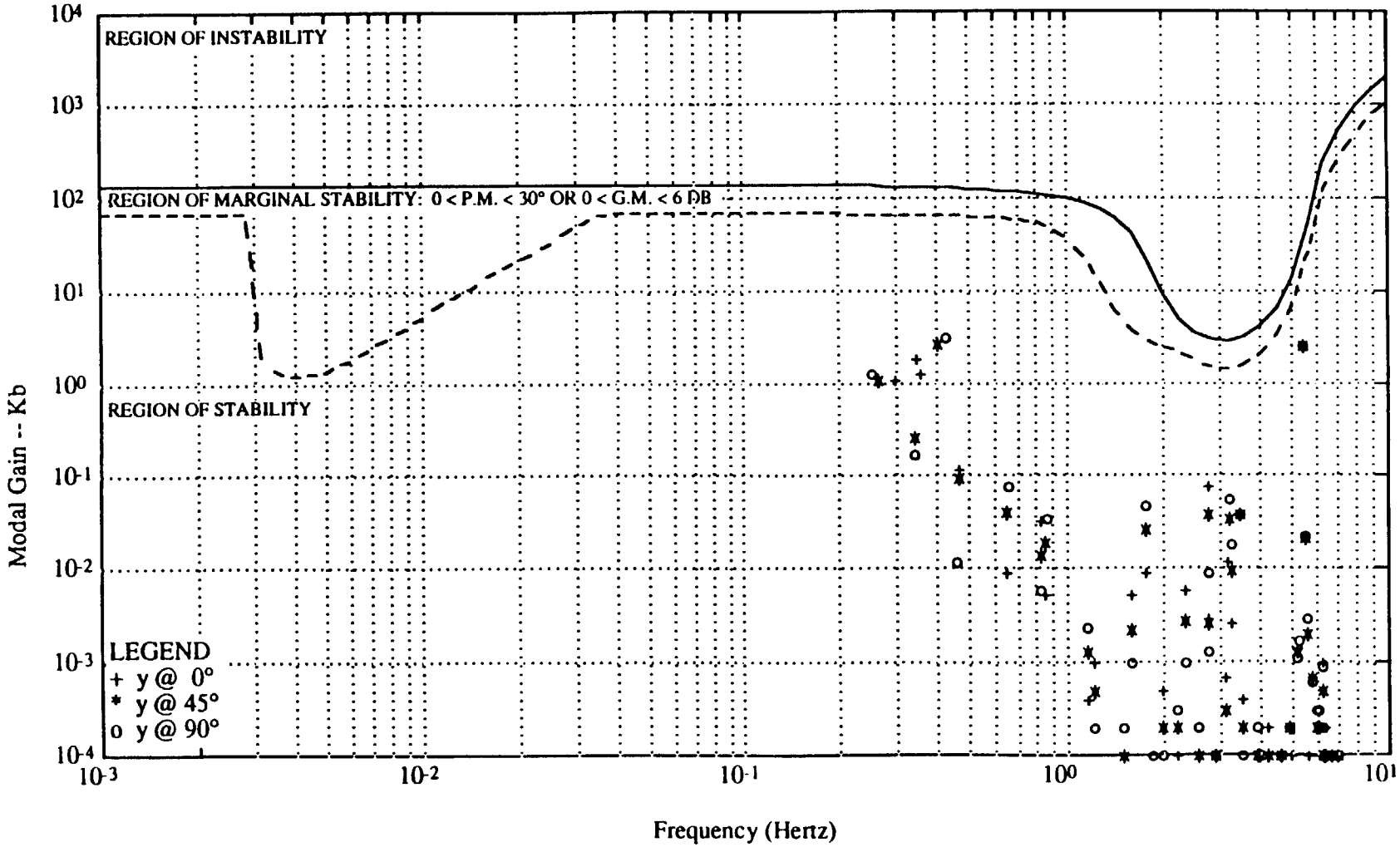

Figure 2-11. Spacecraft Stability Map Example

frequency of the appendage mode is increasingly well-separated from the 0.01 Hz bandwidth of the example control system.

An example of the effect of increasing the control system bandwidth on the stability plot is shown in Figure 2-12. The assumptions used in the analysis are contained in Figure 2-13.

In summary, Equations (2-6) and (2-7), and the annotations in Figure 2-7 indicate that the first order fundamental parameters which describe the structural open-loop frequency response are the bending mode gain (K_b), modal frequency (ω_b), inertia (I), and modal damping (ζ). Given the proposed bandwidth and control system design, these fundamental parameters also provide information about the gain margin and stability of the closed-loop control system.

2.2.2 Generalized Three-Dimensional Modal Gain Matrix

In general, for each flexible mode, the modal gain is a matrix quantity, relating the sensitivities of responses about all three axes due to control inputs about all three axes:

$$K_b = \frac{\underline{\phi}^T \underline{\phi} \underline{I}}{\underline{\phi}^T \underline{M} \underline{\phi}} \qquad (2\text{-}8)$$

If the mode shapes are mass normalized, the denominator of Eq. (2-8) becomes unity, and the K_b matrix for a particular mode can be expressed in terms of the spacecraft inertia matrix and the slopes (angular deflections) at the sensor and actuator locations:

$$K_b = \begin{vmatrix} I_{xx}\phi_x^2 + I_{xy}\phi_x\phi_y + I_{xz}\phi_x\phi_z & I_{xx}\phi_x\phi_y + I_{xy}\phi_y^2 + I_{xz}\phi_y\phi_z & I_{xx}\phi_x\phi_z + I_{xy}\phi_y\phi_z + I_{xz}\phi_z^2 \\ I_{xy}\phi_x^2 + I_{yy}\phi_x\phi_y + I_{yz}\phi_x\phi_z & I_{xy}\phi_x\phi_y + I_{yy}\phi_y^2 + I_{yz}\phi_y\phi_z & I_{xy}\phi_x\phi_z + I_{yy}\phi_y\phi_z + I_{yz}\phi_z^2 \\ I_{xz}\phi_x^2 + I_{yz}\phi_x\phi_y + I_{zz}\phi_x\phi_z & I_{xz}\phi_x\phi_y + I_{yz}\phi_y^2 + I_{zz}\phi_y\phi_z & I_{xz}\phi_x\phi_z + I_{yz}\phi_y\phi_z + I_{zz}\phi_z^2 \end{vmatrix} \qquad (2\text{-}9)$$

For systems with multiple modes, the modal gains for each mode can be described as a matrix using the formulas in Equation 2-9. For the EOS AM-1 spacecraft, the most important K_b's are the diagonal terms associated with the axes of excitation (e.g. roll response at the location of the GN&C sensors due to excitation about roll axis at the location of the reaction wheels). These are indicated on the FRF's in Figures 2-3, 2-4, and 2-5. Examination of the FRF's suggests that the interaction of the four important appendage modes below 1 Hz with the "rigid-body" motion of the spacecraft bus can be characterized as a single 3-body (bus, solar array, and HGA) problem about the roll

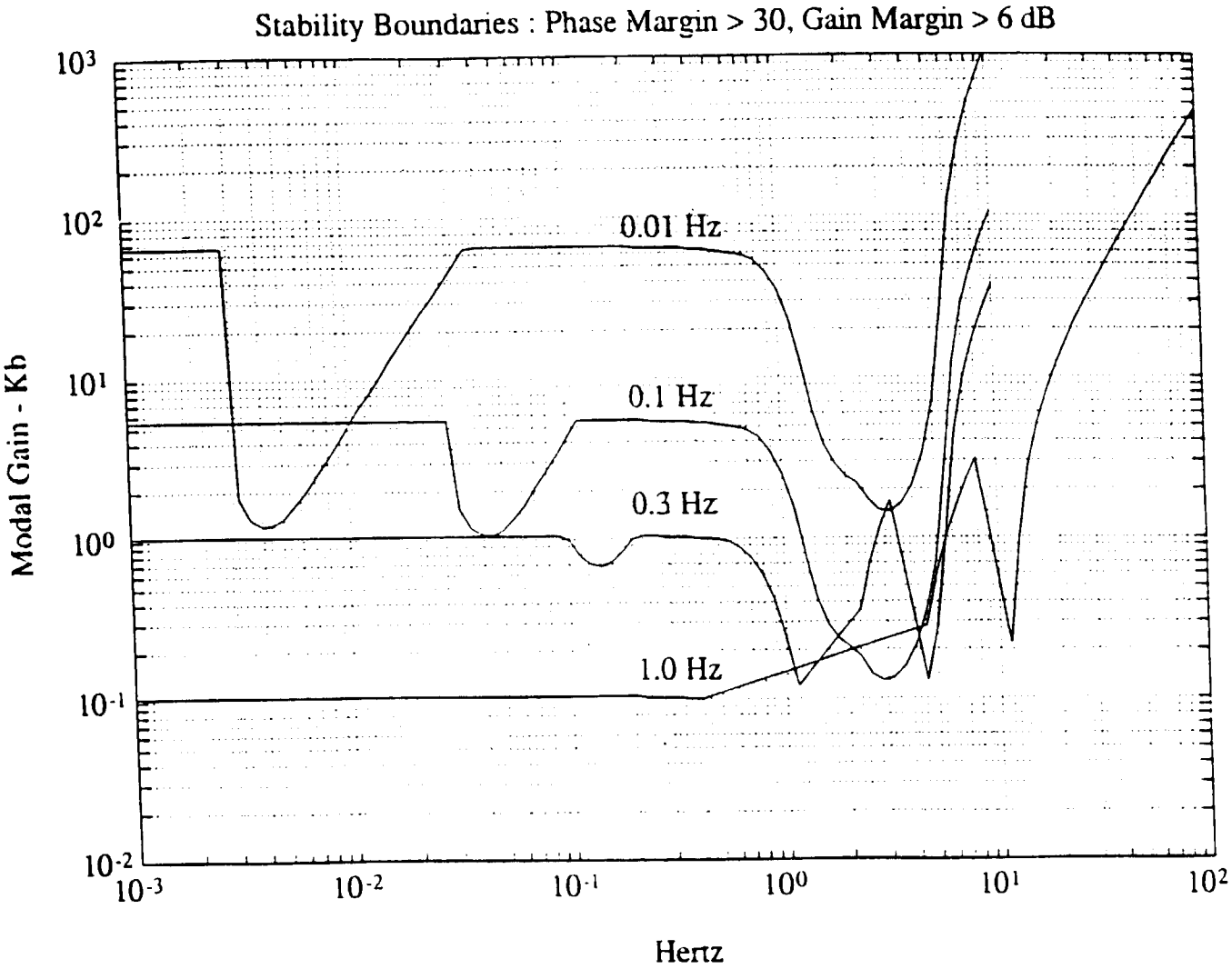

Figure 2-12. Effect of Varying the Bandwidth on Stability Curves

PID Controller

K_r	K_p	K_i
22.5	0.004	0.0
2.25	0.4	0.0
0.75	3.533	0.0
0.225	40.0	0.0

} =>

BW	Damping
0.01 Hz	0.707
0.1 Hz	0.707
0.3 Hz	0.707
1.0 Hz	0.707

- The following are sources of lag

For 0.01, 0.1, 0.3 Hz Systems	For 1.0 Hz System
Gyroscope : 4 Hz BW, 0.5 Damping	Gyroscope : 500 Hz BW, 0.5 Damping
Reaction Wheel : 10 Hz BW, 0.5 Damping	Reaction Wheel : 30 Hz BW, 0.5 Damping

- Computational Delay — 0.025 seconds used
  - * Actual Gyro Read Delay ~ 54 microseconds
  - * Actual Wheel Command Delay ~ 400 microseconds
  - * These delays were calculated as follows:
    - D/A, A/D ~ 100 microseconds per conversion-read/write
    - Serial Reads ~ (2 + number of bits) microseconds/read
- Sampling Rate — 40 Hz

Figure 2-13. Assumptions Used in Stability Map Analysis

axis, and two 2-body problems (bus and solar array or HGA) about the pitch and yaw axes, respectively.

2.2.3 Suspension System Effects

To simulate free-free boundary conditions, the CEM3 testbed will be suspended using long cables (for horizontal isolation) attached to advanced zero-g suspension devices (for vertical isolation). This section investigates the effect of the suspension modes on the simulation of the free-free spacecraft dynamics by comparing the free-free open-loop structural transfer function with the corresponding suspended transfer function. Further detail on suspension system design and potential interactions is provided in References 5, 8, and 9.

The two-body model discussed in Section 2.2.1 can be modified to reflect a suspended test article, as shown in Figure 2-14. The added stiffness and damping of the suspension system are included by attaching a spring (K_1) and a damper (C_1) from the bus to ground. The associated block diagram reflects the fact that there are now two modes, which are assumed not to be closely-spaced, reflecting a good suspension system design. The lower frequency mode is the suspension mode (by design), where the rotations of the bus and array are in phase. The upper frequency mode is the array mode, where the rotations of the bus (θ_1) and the array (θ_2) have opposite sign. The K_b values for these two modes are designated K_{b1} and K_{b2}, respectively, where the values are calculated using equation (2-8) for each mode.

For this system, the open-loop structural frequency response transfer function (θ_1/T_1) is:

$$\frac{\theta_1(s)}{T_1(s)} = \frac{\frac{K_{b1}}{(I_1+I_2)}}{s^2 + 2\zeta_{b1}\omega_{b1}s + \omega_{b1}^2} + \frac{\frac{K_{b2}}{(I_1+I_2)}}{s^2 + 2\zeta_{b2}\omega_{b2}s + \omega_{b2}^2} \qquad (2\text{-}10)$$

Evaluating the transfer function at the array mode frequency ω_{b2} yields:

$$\left|\frac{\theta_1(s)}{T_1(s)}\right| = \left|\frac{-1}{(I_1+I_2)\omega_{b2}^2} \cdot \left[K_{b1} + j\frac{K_{b2}}{2\zeta_{b2}}\right]\right| \qquad (2\text{-}11)$$

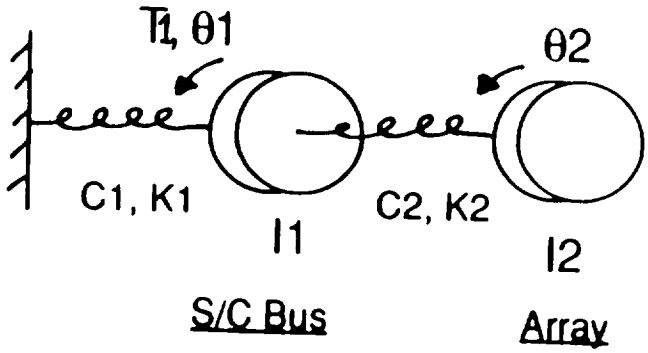

$K1$ = Suspension Stiffness

ω_{b1} = Suspension Roll Mode

ω_{b2} = Solar Array Bending Mode

$$Kb2 \neq \frac{I2}{I1}, \qquad Kb2 = \frac{\phi^T \phi I}{\phi^T M \phi}$$

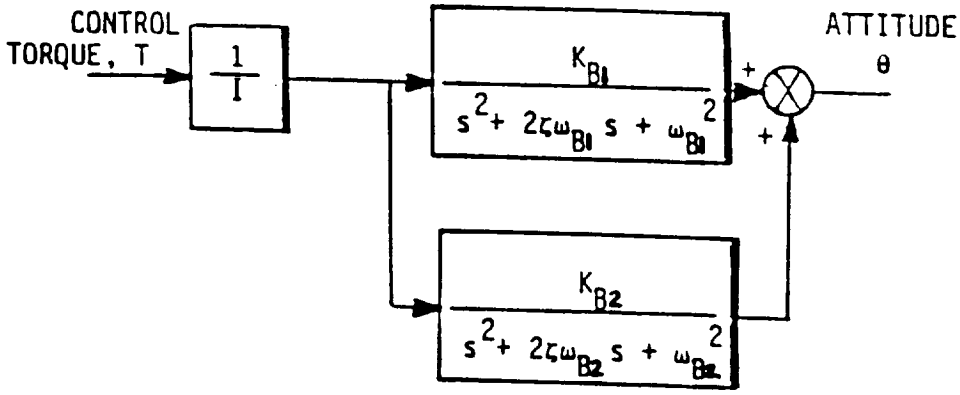

Figure 2-14. Suspended Two-Body Model and Block Diagram

For light damping, the peak resonant response can be approximated by:

$$\left|\frac{\theta_1(s)}{T_1(s)}\right| \cong \frac{K_{b2}}{2(I_1+I_2)\zeta_{b2}\omega_{b2}^2} \qquad (2\text{-}12)$$

Comparing Equations 2-12 and 2-6, it is interesting to note that the peak resonant response of the array mode is dependent only on the K_b and modal parameters of the array mode, and is essentially independent of whether or not the system is free-free or suspended.

Two transfer functions are plotted as dashed lines in Figure 2-15. In both cases the array mode frequency is 1 Hz, while the K_b of both the suspension and array modes is unity. The sole difference between the two dashed-line responses is the suspension frequency, which is 0.10 Hz for the first case and 0.25 Hz for the second case. The corresponding free-free transfer function (Eq. 2-2) for the same K_{b2} and ω_{b2} is plotted as a solid line for reference.

Comparison of the dashed and solid response in Figure 2-15 yields the following observations for suspended as well as multi-mode systems:

(1) For both the free-free and suspended cases, the response of the array mode is identical in the vicinity of the array resonant frequency and at higher frequencies. This is true regardless of the value of K_{b1}.

(2) The difference between the rigid-body line of the free-free system and the mass line of the suspended after the suspension resonance is a gain loss of 20 log(1 - K_b) dB.

(3) A perfect suspension system has a suspension mode with a K_b of unity about the principal axes of inertia, so that 20log(1 - K_b)= 0 dB. This is true for the case plotted in the figure, which is why the mass lines after the array resonance are coincident.

(4) For a suspended system with many modes, the mass line is shifted up or down after the nth mode by the factor $(\Sigma K_{bi})/(\Sigma K_{bi-1})$ for i = 1,2,3 ... n.

(5) The slight shift in the zero location of the array mode for the 0.25 Hz suspension case suggests that this frequency is near the limit of the suspension system interaction. Thus, separation of the suspension modes and the testbed modes by at least a factor of four is desirable.

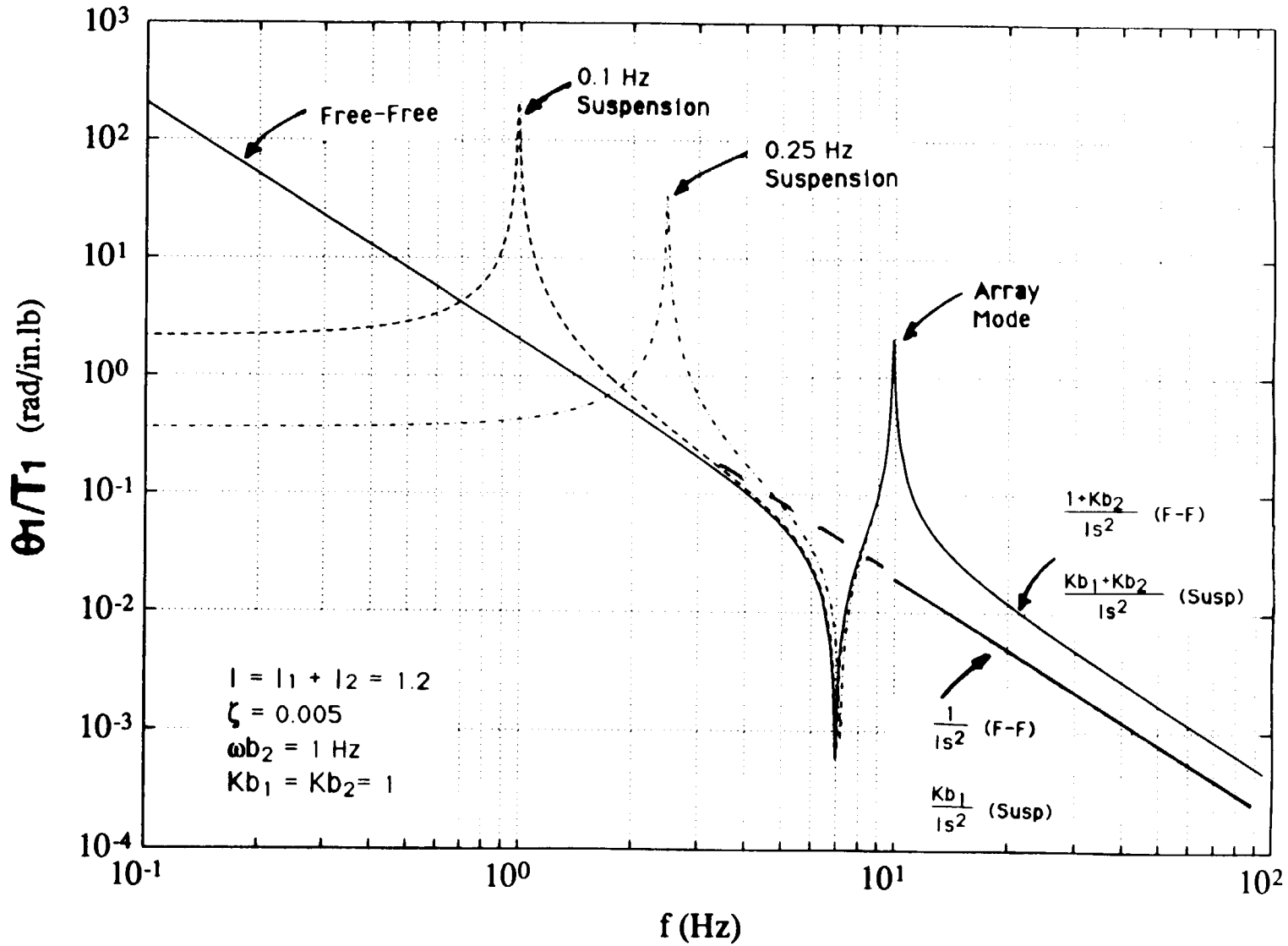

Figure 2-15. Comparison of Free-Free and Suspended Transfer Functions

Note that observation (3) is another way of stating that the perfect suspension system would contain all the elastic energy of the suspension mode within the suspension devices, essentially treating the suspended test article as a rigid body. A K_b of unity for the suspension mode therefore corresponds to making the elastic energy within the suspension devices equal to the kinetic energy of a corresponding free-free rigid-body system. It is also interesting to note that if the suspension and array modes are well-separated, the damping of the suspension system mode has no effect on the quality of the free-free simulation for the array mode.

In summary, a suspended test article can provide an excellent representation of the free-free dynamic interaction of the bus and solar array in the frequency range above the suspension mode, as long as the suspension and array modes are well separated.

2.3 SCALING LAW DEVELOPMENT

The motivation for considering scaling the CEM3 testbed is based on the fact that the weight of the EOS AM-1 spacecraft exceeds the suspension capability of the test facility by a factor of five. A feasibility study was conducted to determine if a scaling method could be implemented to develop a lighter CEM3 testbed with overall dynamic characteristics which are scaled in relation to the EOS AM-1 spacecraft. Recognizing the desire for the CEM3 to be as near full-scale as possible, the goals of the scaling exercise were to develop a scaled design with one-tenth the weight of the EOS AM-1 spacecraft but with full-scale geometry and full-scale dynamics.

In the past, NASA/LaRC has used several structural dynamic scale models and has also participated in the development of new scaling methods[10,11,12]. Reference 13 is an excellent text on the subject. For brevity, the scaling approach is summarized here.

In general, scaling methods can be developed by requiring a simple scalar relationship between the matrix equations governing the dynamic behavior of the CEM3 scale model testbed and the EOS AM-1 spacecraft. Similarity laws are derived by noting that to satisfy this condition, each row and each term in the matrix equations of motion must be multiplied by the same scalar coefficient. Equating the scale factors which make up the coefficient for each term in the equations of motion yields the relevant similarity laws, many of which have an intuitive, physical interpretation (Figure 2-16).

- **Scaling Laws Derived by Requiring a Simple Scalar Relationship Between the Matrix Equations Governing the Scale Model & the EOS AM-1 Spacecraft**
- **Similarity Laws Derived by Noting that Each Row and Each Term in the Matrix Equations Must be Multiplied by the Same Scalar**

$$\underline{M}\ddot{\underline{x}} + \underline{C}\dot{\underline{x}} + \underline{K}\underline{x} = \underline{F} \qquad \ddot{x} + 2\zeta\omega\dot{x} + \omega^2 x = 0$$

$$\lambda_{\underline{M}}\lambda_{\ddot{\underline{x}}} = \lambda_{\underline{C}}\lambda_{\dot{\underline{x}}} = \lambda_{\underline{K}}\lambda_{\underline{x}} = \lambda_{\underline{F}} \qquad \lambda_{\ddot{x}} = 2\lambda_\zeta\lambda_\omega\lambda_{\dot{x}} = \lambda\omega^2\lambda_x = 0$$

Constitutive	Kinematics	Statics	Dynamics
$\lambda_l = \lambda_M\lambda_L^2$	$\lambda_F = \lambda_M\lambda_x/\lambda_t^2$	$\lambda_F = \lambda_{EI}\lambda_x/\lambda_L^3$	$1/\lambda_t^2 = \lambda_{EI}/\lambda_M\lambda_L^3$
$\lambda_{\dot{x}} = \lambda_x/\lambda_t$	$\lambda_T = \lambda_l\lambda_x/\lambda_L\lambda_t^2$	$\lambda_F = \lambda_{EA}\lambda_x/\lambda_L$	$1/\lambda_t^2 = \lambda_{EA}/\lambda_M\lambda_L$
$\lambda_{\ddot{x}} = \lambda_x/\lambda_t^2$	$\lambda_F = \lambda_C\lambda_x/\lambda_t$	$\lambda_T = \lambda_{EI}\lambda_x/\lambda_L^2$	$1/\lambda_t^2 = \lambda_{GJ}/\lambda_l\lambda_L$
$\lambda\varepsilon = \lambda_\theta = \lambda_x/\lambda_L$	⋮	$\lambda_T = \lambda_{GJ}\lambda_x/\lambda_L^2$	$1/\lambda_t^2 = \lambda_{GA}/\lambda_M\lambda_L$
⋮		⋮	⋮

Figure 2-16. Similarity Law Derivation Using Matrix Equations of Motion

Several types of scaling methods can be used which satisfy the similarity laws. These scaling methods involve up to four scale factors which can be independently selected and still satisfy the similarity laws. For this study, two scaling methods were considered. The first is replica scaling, wherein the same materials are used as in the full-scale original and the dimensions on the design drawings are geometrically scaled. A 1/2-scale replica model of the EOS AM-1 spacecraft would weigh less than 2,000 pounds. A scale factor of 1/2 may also be attractive because the existing CEM2 mast is about half the length of the EOS AM-1 solar array. Replica scaling is both the most accurate and costly scaling method, though different levels of fidelity for replica scaling can be used, depending on how much design detail is replicated.

The second method addressed is multiple scaling, where four scale factors are selected. Figure 2-17 summarizes the derivation of a new multiple scaling method specifically developed to meet the objectives of the CEM3 testbed. The method is called 1/10:1 multiple scaling because the mass scale factor (λ_M) is 1/10, while the dimensional (λ_L) scale factor is unity. In this example, the time (λ_t), and deflection response (λ_x) scale factors are also chosen to be unity. This scaling approach is interesting in that setting both λ_t and λ_L to unity creates a situation where the scale factors for all the spatial and temporal derivatives are also equal to unity. Also, since $\lambda_L = 1$, all the powers of λ_L in the stiffness terms are unity, constraining the scale factors for the cross-sectional rigidity properties (λ_{EA}, λ_{EI}, λ_{GA}, λ_{GJ}) to be equal, even though these properties have different units. In a detailed model, this would be accomplished through distortion of the design of the cross-sectional properties, compromising some of the model fidelity (replica scaling involves no such compromises)[10]. However, since the CEM3 testbed is intended to match only the overall characteristics of the EOS AM-1 spacecraft using existing CEM2 hardware, this is a secondary issue.

Three additional variations of the 1/10:1 multiple scaling method were investigated. Scale factors for the four multiple scaling methods and the replica scaling method are compared in Table 2-2.

Multiple scaling method (A) meets the goals of a full-size scale model with full-scale (λ=1) response characteristics $\left(\ddot{\underline{x}}, \dot{\underline{x}}, \underline{x}, \ddot{\underline{\theta}}, \dot{\underline{\theta}}, \underline{\theta}, \varepsilon, \omega\right)$ and 1/10 the mass. This is accomplished by scaling the property characteristics (mass, stiffness, and damping) and the applied forces by 1/10. This is evident in the comparison of the equations of motion for the full-scale system:

$$\underline{M}\ddot{\underline{x}} + \underline{C}\dot{\underline{x}} + \underline{K}\underline{x} = \underline{F} \qquad (2\text{-}13)$$

- **In Multiple Scaling, From 1 to 4 Scale Factors Can be Independently Selected As Long as Similarity Laws Are Met**
- **For CEM3, Choosing $\lambda_M = 0.1$ and $\lambda_L = 1$ Yields Similarity Laws for the Other Scale Factors, Restricting the Number of Subsequent Independent Scale Factor Choices:**

Constitutive	Kinematics	Statics	Dynamics
$\lambda_L = 0.1$	$\lambda_F = 0.1\lambda_x/\lambda_t^2$	$\lambda_F = \lambda_{EI}\lambda_x$	$1/\lambda_t^2 = \lambda_{EI}/0.1$
$\lambda_{\dot{x}} = \lambda_x/\lambda_t$	$\lambda_T = 0.1\lambda_x/\lambda_t^2$	$\lambda_F = \lambda_{EA}\lambda_x$	$1/\lambda_t^2 = \lambda_{EA}/0.1$
$\lambda_{\ddot{x}} = \lambda_x/\lambda_t^2$	$\lambda_F = \lambda_C\lambda_x/\lambda_t$	$\lambda_T = \lambda_{GA}\lambda_x$	$1/\lambda_t^2 = \lambda_{GJ}/0.1$
$\lambda\varepsilon = \lambda_\theta = \lambda_x/\lambda_L$		$\lambda_T = \lambda_{GJ}\lambda_x$	$1/\lambda_t^2 = \lambda_{GA}/0.1$

- **Selecting $\lambda_t = 1$ to Match Frequencies Yields a Scalar Condition Relating Force & Response, Constrains the Rigidity Properties, and Equates the Temporal and Spatial Derivatives in x:**

$$\lambda_F/\lambda_x = 0.1 = \lambda_{EI} = \lambda_{EA} = \lambda_{GJ} = \lambda_{GA}$$

$$\lambda_x = \lambda_{\dot{x}} = \lambda_{\ddot{x}} = \lambda_\varepsilon = \lambda_\theta$$

- **Note that the Strut Cross-Section Properties Must be Distorted in Order to Equate the Scale Factors for EI, EA, GJ, and GA**

Figure 2-17. Derivation of Multiple Scaling Laws

Table 2-2. Comparison of Scaling Options

Parameter	Typical Full-Scale Value(s)	Mult. (A)	Mult. (B)	Mult. (C)	Mult. (D)	Replica 1/2 Scale
Selected Factors						
Mass (Weight), λM	*10,545 lbs*	*0.1*	*0.1*	*0.1*	*0.1*	*0.125*
Length, λL	*20, 6 ft*	*1*	*1*	*1*	*1*	*0.5*
Time (1/freq), λt	*2.5 sec, .4 Hz*	*1*	*1*	*0.5*	*0.5*	*0.5*
Deflection, λx		*1*	*2*	*1*	*0.5*	*0.5*
Derived Factors						
Moment Of Inertia	6.6E7 lb-in^2	0.1	0.1	0.1	0.1	3.13E-03
Static Imbalance		0.1	0.1	0.1	0.1	6.25E-03
Angular Rotation	2.0, 3.5 asec	1	2	1	0.5	1
Velocity		1	2	2	1	1
Angular Velocity		1	2	2	1	2
Acceleration		1	2	4	2	2
Angular Accel		1	2	4	2	4
Disturbance Force	0.33, 0.09 lb	0.1	0.2	0.4	0.2	0.25
Disturbance Torque	195, 5 in-lbs	0.1	0.2	0.4	0.2	0.125
Bending Rigidity, EI	1.16E+08	0.1	0.1	0.4	0.4	6.25E-03
Torsion Rigidity, GJ	2.06E+07	0.1	0.1	0.4	0.4	6.25E-03
Axial Rigidity, EA	9.43E+07	0.1	0.1	0.4	0.4	0.25
Shear Rigidity, GA	8.43E+06	0.1	0.1	0.4	0.4	0.25
Damping Coeff, C		0.1	0.1	0.2	0.2	0.25
Strain		1	2	1	0.5	1
% Crit Damping	0.15, 0.5	1	1	1	1	1
K.E. & S.E.		0.1	0.4	0.4	0.1	0.125
Power		0.1	0.4	0.8	0.2	0.25
BW, Sampling Rate	0.15, 2 Hz	1	1	2	2	2
Effective Density		0.1	0.1	0.1	0.1	1

with the sub-scale system:

$$\left(\frac{\underline{\underline{M}}}{10}\right)\cdot(1\ddot{\underline{x}})+\left(\frac{\underline{\underline{C}}}{10}\right)\cdot(1\dot{\underline{x}})+\left(\frac{\underline{\underline{K}}}{10}\right)\cdot(1\underline{x})=\left(\frac{\underline{F}}{10}\right) \tag{2-14}$$

Multiple scaling method (B) corresponds to the same physical design as (A), except that the applied forces and corresponding responses are scaled by 2 instead of unity:

$$\left(\frac{\underline{\underline{M}}}{10}\right)\cdot(2\ddot{\underline{x}})+\left(\frac{\underline{\underline{C}}}{10}\right)\cdot(2\dot{\underline{x}})+\left(\frac{\underline{\underline{K}}}{10}\right)\cdot(2\underline{x})=\left(\frac{2\underline{F}}{10}\right) \tag{2-15}$$

This has the effect of doubling the strain and quadrupling the power compared to the full-scale spacecraft, but would provide a better signal-to-noise ratio for testing.

Multiple scaling method (C) is the same as (A) with the exception that the frequency has been doubled. The temporal derivatives are no longer unity. Compared to method (A) the bandwidth is doubled, the applied forces are quadrupled, and the power is increased eight-fold. The corresponding equation is:

$$\left(\frac{\underline{\underline{M}}}{10}\right)\cdot(4\ddot{\underline{x}})+\left(2\frac{\underline{\underline{C}}}{10}\right)\cdot(2\dot{\underline{x}})+\left(4\frac{\underline{\underline{K}}}{10}\right)\cdot(1\underline{x})=\left(4\frac{\underline{F}}{10}\right) \tag{2-16}$$

Finally, scaling method (D) is a combined variation of (B) and (C) with reduced power and response:

$$\left(\frac{\underline{\underline{M}}}{10}\right)\cdot(2\ddot{\underline{x}})+\left(2\frac{\underline{\underline{C}}}{10}\right)\cdot(1\dot{\underline{x}})+\left(4\frac{\underline{\underline{K}}}{10}\right)\cdot\left(\frac{\underline{x}}{2}\right)=\left(2\frac{\underline{F}}{10}\right) \tag{2-17}$$

For comparison, the corresponding replica scale factors for a 1/2-scale model are also provided in the last column of Table 2-2. While many of the multiple scaling factors are the same across Table 2-2 for methods (A) through (D), the replica scale factors are nearly all different. Compared to multiple scaling method (A), a replica 1/2-scale model would have half the overall dimensions and deflections, and twice the modal frequencies.

In summary, five scaling approaches have been investigated which may be used in developing the CEM3 testbed. The selection of the most appropriate scaling method to use depends on the particular type of CSI experiment being conducted and the associated key parameters, e.g., strain for a passive damping experiment or

bandwidth for an active control experiment. For multiple scaling methods (A) and (B), the physical testbed structural design is the same, and only the magnitude of the applied forces and responses are changed. In contrast, multiple scaling methods (C) and (D) involve many of the same scale factors, but the testbed structural design (stiffness) is increased to have twice the modal frequencies as EOS AM-1. Finally, a 1/2-scale replica model would also have twice the modal frequencies, but would involve many different scale factors for the other parameters, including the overall size. The final selection of the scaling method is addressed in the next section.

2.4 CONCEPTUAL DESIGN APPROACH

The overall CEM3 testbed conceptual design approach is based on the findings in the previous sections with emphasis placed on the objectives provided by NASA/LaRC. Key drivers which influenced the approach are:

(1) Simulating the overall solar array and HGA flexible appendage dynamic interaction of the EOS AM-1 spacecraft requires the proper scaling of the fundamental parameters which characterize the open-loop structural frequency response.

(2) The weight capability of the existing CEM2 suspension system requires that scaling be used for the CEM3 testbed.

(3) To achieve realistic CSI simulations, the overall size, shape, and dynamics of the CEM3 testbed should be as close to those of the full-scale EOS AM-1 spacecraft as practicable.

(4) Existing CEM2 components should be used to the extent practicable.

(5) To achieve a good simulation of the free-free on-orbit boundary conditions, adequate separation should be provided between the suspension and CEM3 testbed flexible modes.

The fundamental parameters which describe the open-loop frequency response are the bending mode gains, appendage modal frequencies, inertia matrix, modal damping values, and the frequency separation of the low-frequency appendage modes with respect to the spacecraft bus first primary structural mode. In addition, matching the center-of-gravity is a derived requirement to achieve the proper inertias and K_b values for appendage interaction. Note that since the spacecraft is being used

in CSI pointing experiments, the correct scaling of the three diagonal spacecraft rotational inertias is much more important than scaling the mass or the cross products of inertia. The scaling of the actual testbed mass is immaterial and the cross products of inertia need only be very small compared to the diagonal inertias.

The 1/2-scale replica option was eliminated early on in the trade study to select the appropriate scaling method for the CEM3 testbed. The multiple scaling method was selected over the replica scaling method primarily because of the desire to have full-scale size and responses. Also, though the existing CEM2 mast would have the correct length to simulate a 1/2-scale solar array, the testbed primary structure would be only 10 feet long, crowding the attached payloads and equipment.

For the CEM3 testbed, 1/10:1 multiple scaling method (A) was selected as the baseline for the CEM3 testbed primary structure, resulting in the CEM3 testbed having the same overall physical dimensions as the EOS AM-1 spacecraft. The basic approach is to reconfigure the CEM2 testbed truss to the same overall geometry as the EOS AM-1 spacecraft structure. By locating 1/10-scale weights at the appropriate locations to simulate the payloads and attached equipment, the inertias and center-of-gravity can also be matched. This same testbed physical structural design could also be used in different experiments employing 1/10:1 multiple scaling method (B) by simply increasing the magnitude of the applied forces.

The scaling of the solar array and HGA presents a difficult dilemma. Analyses indicate that given that the existing 15-foot CEM2 mast is half the length of the EOS AM-1 array and has a fixed bending rigidity (EI), it is impossible to satisfy both the K_b and frequency requirements associated with scaling method (A). Barring the construction of another 30-foot array simulator (which is a possible option constrained by funding), it was decided to use 1/10:1 multiple scaling method (C) for the low-frequency flexible appendage design. Though scaling method (C) calls for a full 30-foot array length with twice the frequency, design studies indicated that (quite by chance) it is possible to attach a lumped weight to the tip of the CEM2 mast which results in approximately the correct Kb, frequencies, inertias, and center-of-gravity for overall simulation of the appendage interaction. Since the frequency is doubled, this choice also reduces the potential for interaction between the low-frequency CEM3 appendage modes and the suspension system.

In designing the HGA simulator, proper simulation of the flexible 3-body dynamic interaction between the solar array, high gain antenna, and spacecraft bus requires that the HGA frequency also be doubled according to scaling method (C). The result is an open-loop transfer function where the frequencies of the appendages are shifted

up by a factor of two, but with the K_b's, frequency spacing, and full character of the transfer function preserved. Fortunately, the first-order appendage modes are separated from the bus global system modes by nearly two orders of magnitude, so that the bus structure need not be stiffened to increase its frequency correspondingly.

Finally, the approach to simulating the free-free boundary conditions of the on-orbit EOS AM-1 spacecraft is based on suspending the CEM3 testbed in such a way that the suspension modes have a factor of four separation from the relevant testbed flexible modes. Suspension cable attachment points and suspension device stiffness gains are carefully selected to achieve positive structural strength margins and suspension frequencies below 0.2 Hz.

In summary, the approach for reconfiguring the CEM2 testbed is based on designing the suspended CEM3 testbed to match the relevant parameters scaled from the EOS AM-1 spacecraft design shown in Tables 2-3 and 2-4. The most important parameters are shaded in gray. The appendage modal damping is an important parameter that was not included in the tables because it is unknown at this time. A critical damping ratio of 0.5% was assumed. In the conduct of CSI experiments addressing the low-frequency appendage interaction (i.e., below 10 Hz where the bus acts as a rigid body), scaling method (C) should be used in the experiment design (e.g., to calculate the magnitude of the applied forces and the bandwidth of the controller). Scaling method (A) should be used in designing higher-frequency experiments where the flexibility of the bus is important. Until a properly-scaled, 30-foot solar array simulator can be developed, this approach serves as a compromise, allowing the competing objectives of the CEM3 testbed to be met using the existing CEM2 testbed hardware and suspension system.

Table 2-3. Scaled EOS AM-1 Properties - Method A

PROPERTY		EOS AM-1 Full Scale	EOS AM-1 Scaled - (A)
BUS GEOMETRY (In)	L	256	256
	W	68	68
	H	78	78
APPENDAGE GEOMETRY (In)	SA L	351	351
	HGA L	100	100
MASS PROPERTIES (lbf, In, lbf-In^2)	Total Weight	10,500	1,050
	X-CG	157.3	157.3
	Y-CG	-3.1	-3.1
	Z-CG	-8.2	-8.2
	Ixx	4.35E+07	4.35E+06
	Iyy	6.73E+07	6.73E+06
	Izz	8.14E+07	8.14E+06
	Ixy	-1.23E+06	-1.23E+05
	Ixz	1.63E+06	1.63E+05
	Iyz	3.37E+06	3.37E+05
1st System Freq (Hz)	Bus	23	23
	Payload	35	35

Table 2-4. Scaled EOS AM-1 Properties - Method C

Appendage Modes		EOS AM-1 Full Scale	EOS AM-1 Scaled - (C)
SA Yaw	Freq (Hz)	0.295	0.590
	Kb	0.33	0.33
SA Roll	Freq (Hz)	0.380	0.760
	Kb	0.61	0.61
HGA Pitch	Freq (Hz)	0.501	1.002
	Kb	0.07	0.07
HGA Roll	Freq (Hz)	0.660	1.320
	Kb	0.61	0.61

3.0 TESTBED DESIGN AND DEVELOPMENT

Development of the CEM Phase-3 testbed structural configuration was a highly iterative, coupled problem with suspension, scaling, and existing hardware issues to consider during the design process. The final CEM3 testbed design, comprised of truss primary structure, flexible appendages, payload mass simulators, 2-axis pointing gimbals, gas-jet thrusters, and associated electronic boxes is shown in finite element model form in Figures 3-1 and 3-2. The testbed, shown in a free-free configuration, has three 2-axis gimbals mounted on the underside of the structure which simulate the VNIR, MISR, and SWIR science payloads located on the nadir (+Z axis) side of the EOS AM-1 spacecraft. In this orientation, the gimbals are easier to access and have unobstructed fields of view. Lasers mounted on the 2-axis gimbals in conjunction with advanced optical scoring systems located on the lab floor are used to conduct precision pointing experiments. All of the remaining science payloads are modeled as mass simulators which are shown as shaded plates in Figure 3-1. Some of the mass simulators are mounted on payload towers (one or two bays of truss) in order to more accurately match the payload center-of-gravity locations contained in the NASA/LaRC ROM model.

Two flexible appendages are attached to the CEM3 testbed. The deployable mast and variable tip weight originally designed for the CEM Phase-2 testbed are used to simulate the low-frequency dynamics of the single EOS AM-1 solar array. A new CEM3 high gain antenna simulator was designed and fabricated to simulate the low-frequency dynamics of the EOS AM-1 high gain antenna. The horizontal orientation of the cantilevered CEM2 mast requires the use of a zero-g suspension device to off-load its tip weight while the vertically mounted HGA is sufficiently robust and requires no off-loading. Modal tests of both appendages were conducted to characterize their dynamics and update the associated FEM models.

This section addresses the overall design and development testing of the CEM3 testbed components. An overall summary of the CEM Phase-3 testbed structural configuration in terms of Primary Structure (3.1), Attached Payloads (3.2), Appendages (3.3), and Suspension System (3.4) component hardware is provided in the following four sections. Comparisons between the CEM3 and the scaled EOS AM-1 dimensions are provided to demonstrate the geometric similarity between the two models. Test results associated with newly designed CEM hardware components such as the "stock tube" diagonal struts, deployable mast (solar array simulator), and high gain antenna simulator are discussed in the appropriate sections.

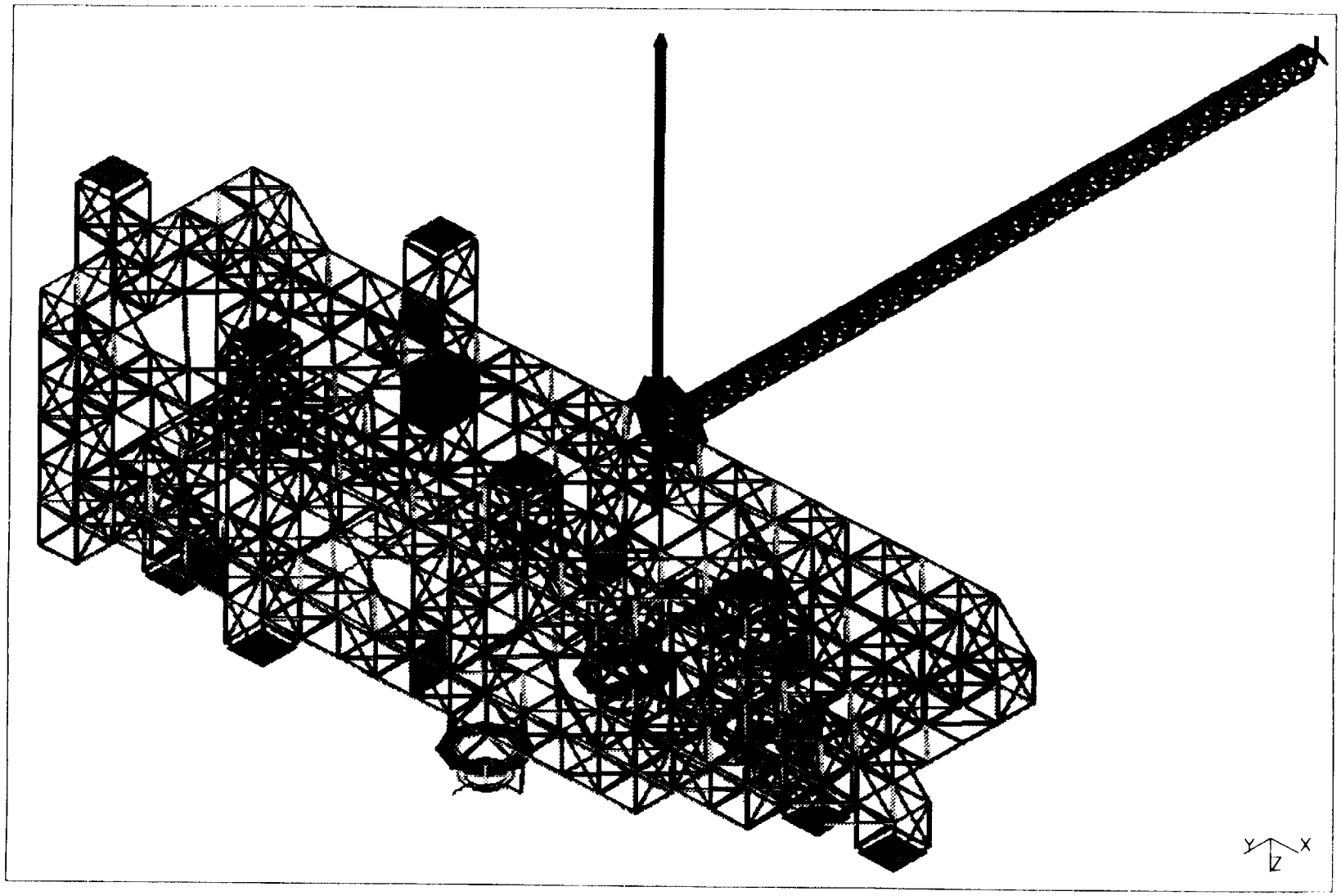

Figure 3-1. CEM3 Baseline Configuration (Isometric View)

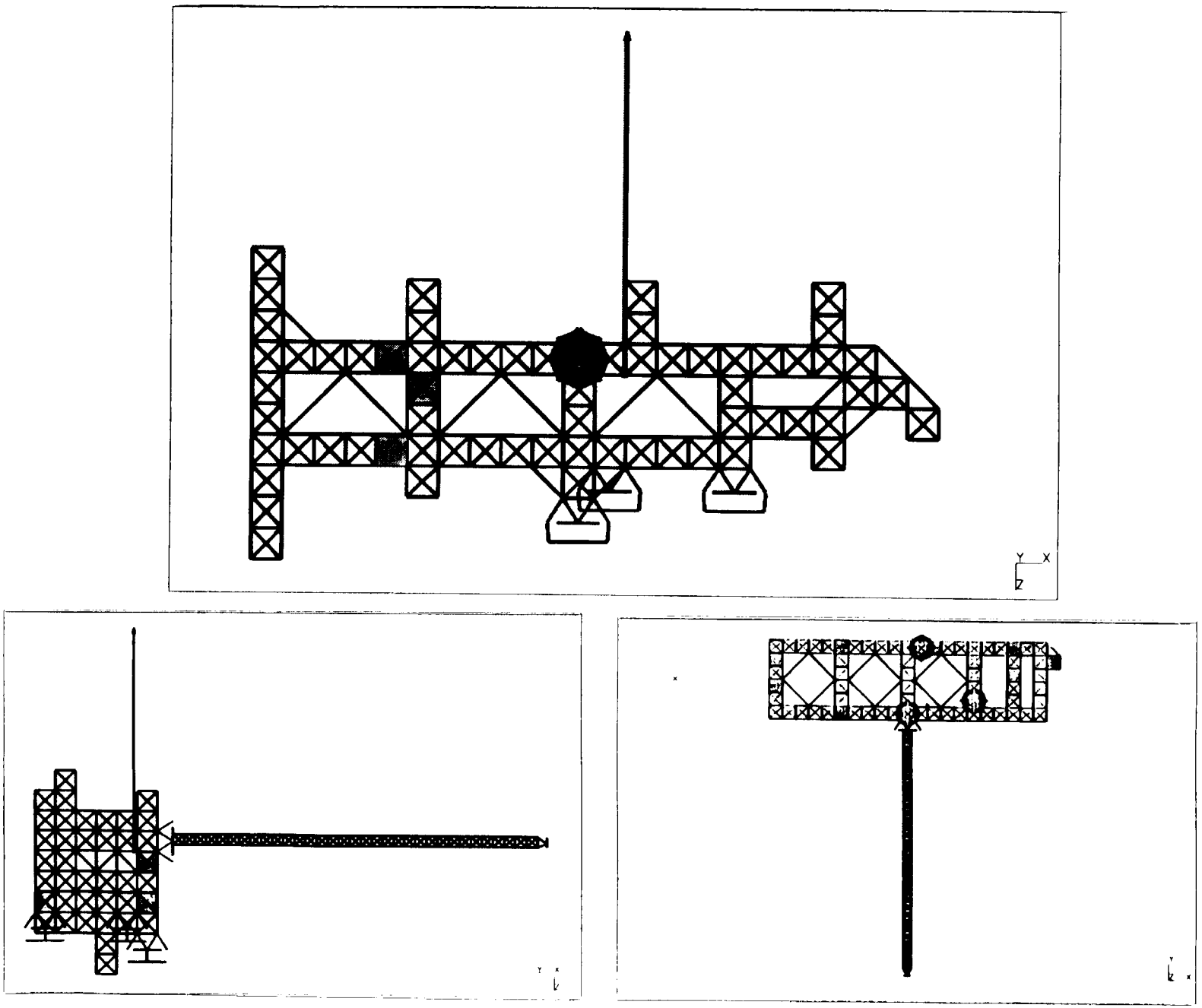

Figure 3-2. CEM3 Baseline Configuration (Orthogonal Views)

3.1 PRIMARY STRUCTURE

Several design iterations were required to arrive at the final CEM3 primary structure configuration which best matches the overall scaled EOS AM-1 bus geometry and stiffness using the existing 10-inch CEM2 truss hardware. The key design drivers for the primary structure in accordance with Tables 2-3 and 2-4 were:

(1) Matching the spacecraft geometry.
(2) Matching the 23 Hz spacecraft first structural mode.
(3) Supporting attached payloads and equipment at the proper c.g. locations in order to match the spacecraft inertia properties.

The design was also strongly influenced by the existing quantity of CEM2 struts.

3.1.1 Truss Design Configuration

The CSI Phase-3 testbed primary structure design shown in Figure 3-3 is based on four truss system longerons (Figure 3-4), six truss bulkheads (Figure 3-5), system diagonals struts, and payload towers. A comparison of the primary structure layouts for the CEM3 and EOS models is shown in Figure 3-6. The length of the CEM3 primary structure is slightly shorter than the EOS AM-1 bus structure (220" vs. 256") while the width (60" vs. 68") and height (80" vs. 78") dimensions of the two structures are fairly close. For a perfectly scaled model, the overall dimensions of both structures should be identical since the length scale factor (λ_L) for 1/10:1 multiple scaling is 1.0. The difference in geometry is primarily attributed to the fact that there are a limited number of CEM2 struts available to build the CEM3 testbed, and that they must be assembled in 10-inch increments. Overall, the scaled geometry and bending stiffness properties of the full-scale EOS AM-1 bus structure are closely approximated by the CEM3 primary structure using the existing CEM2 strut hardware.

In order to achieve primary structure bending stiffness levels sufficient to meet the structural mode frequency requirement, specific longeron types (-1L, -2L, -3L, & -4L) having a range of axial stiffness properties were distributed throughout the structure in a systematic manner. Strategic placement of the stiffer -1L longerons at the outer most location on the system longerons was the key to achieving the desired primary structure overall bending stiffness (Figure 3-4). Judicious placement of the longeron strut types and diagonal struts also served to stiffen local component modes throughout the testbed.

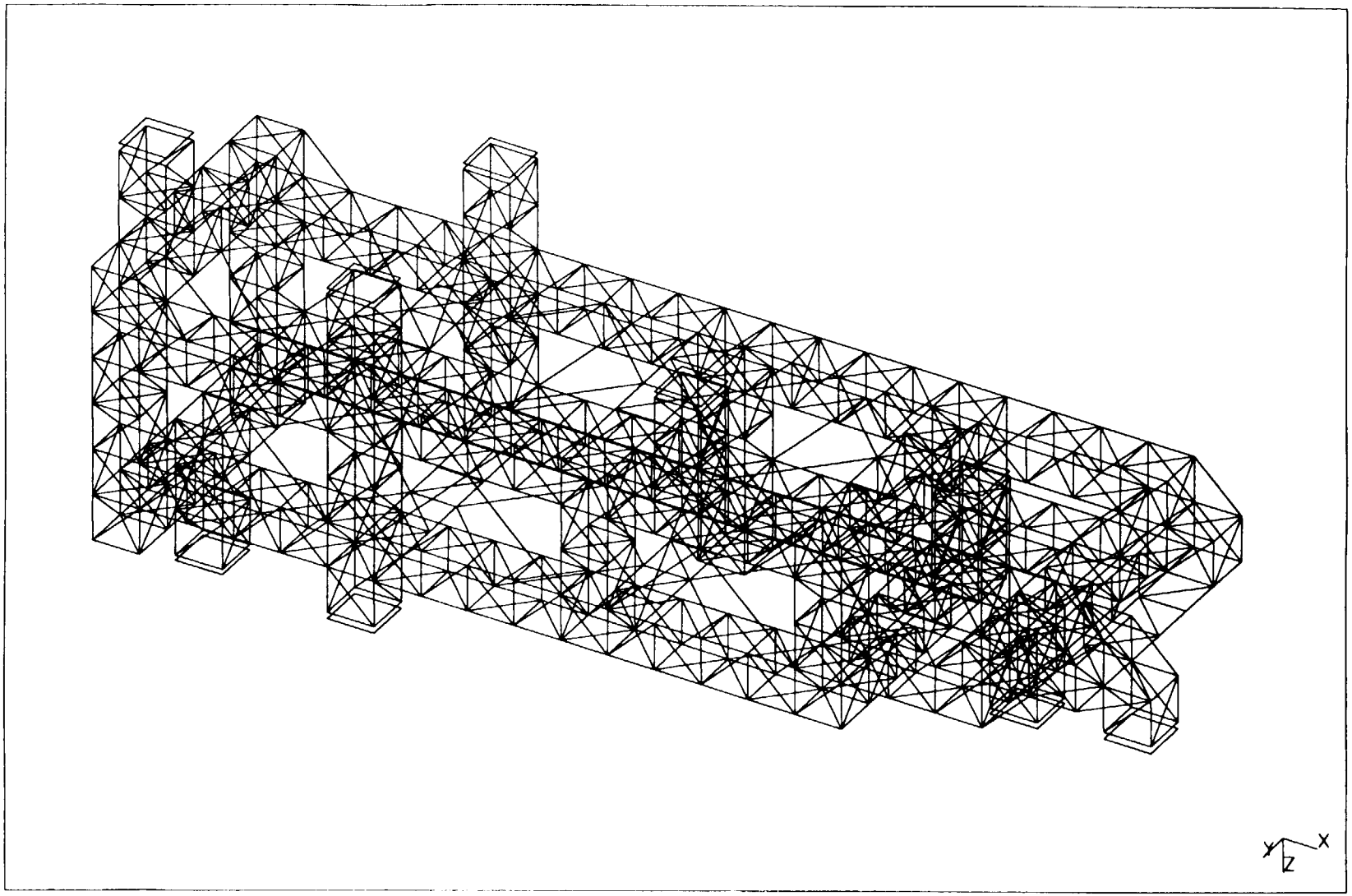

Figure 3-3. CEM3 Primary Structure

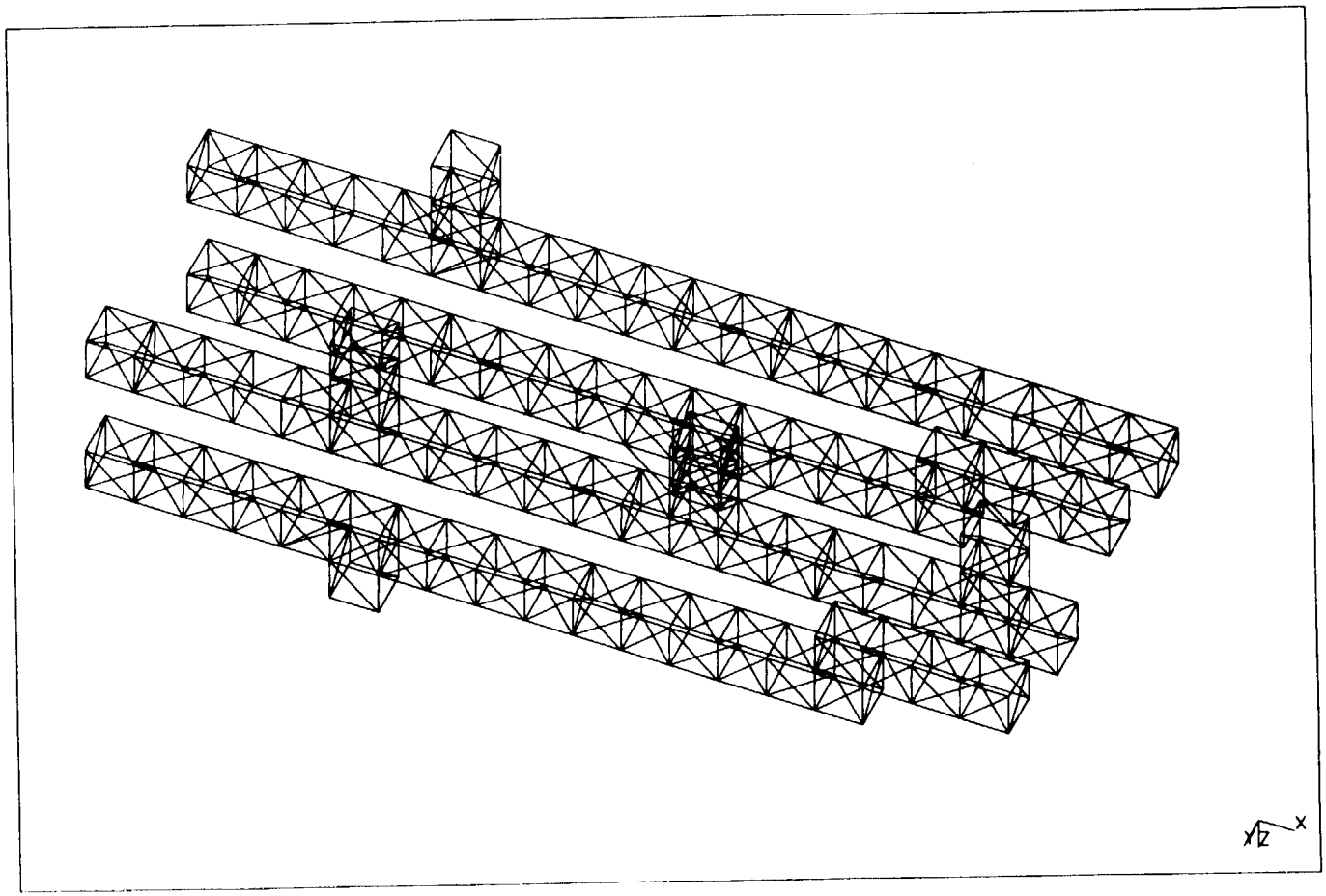

Figure 3-4. CEM3 Primary Structure Longeron Layout

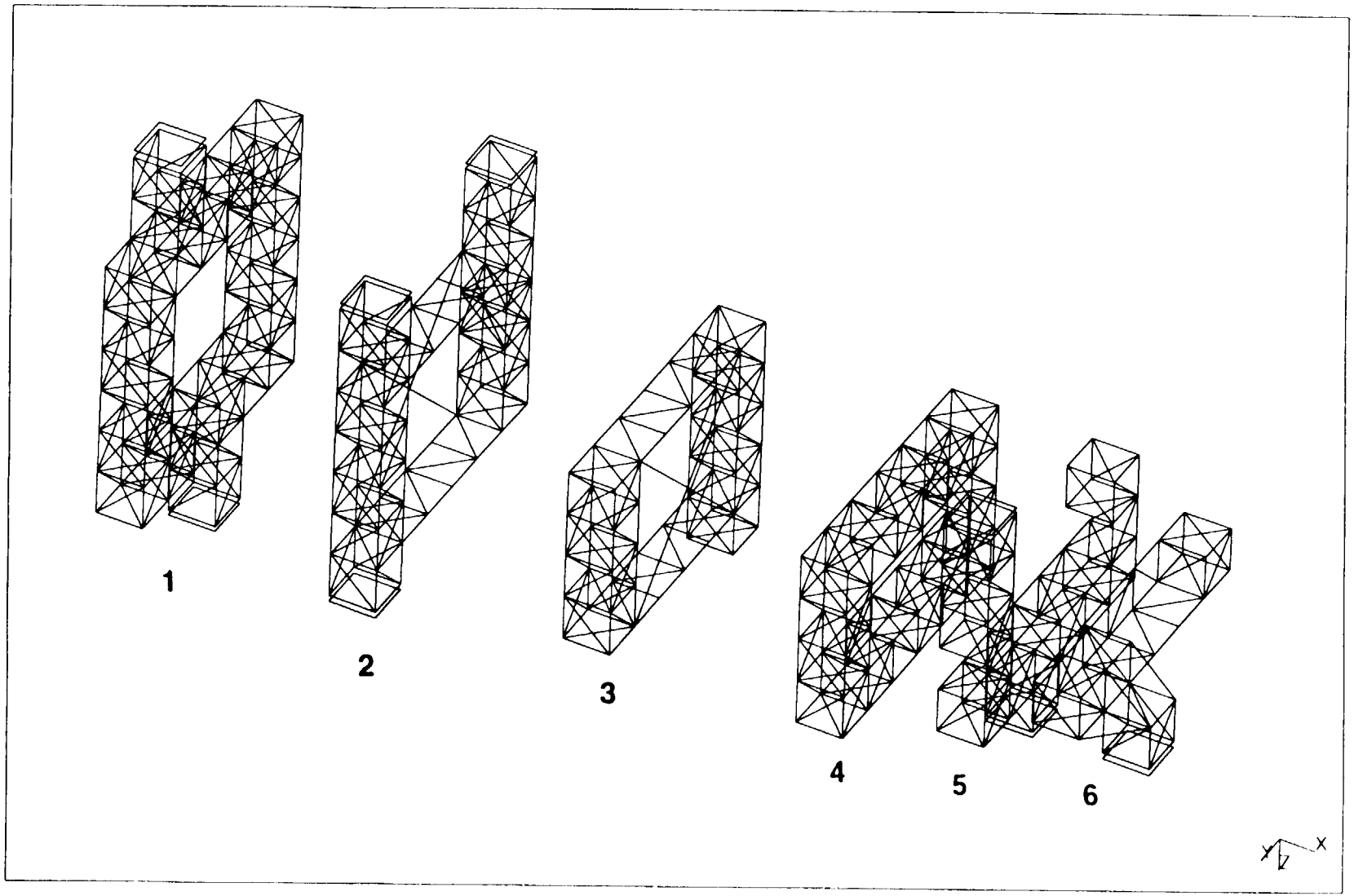

Figure 3-5. CEM3 Primary Structure Bulkhead Layout

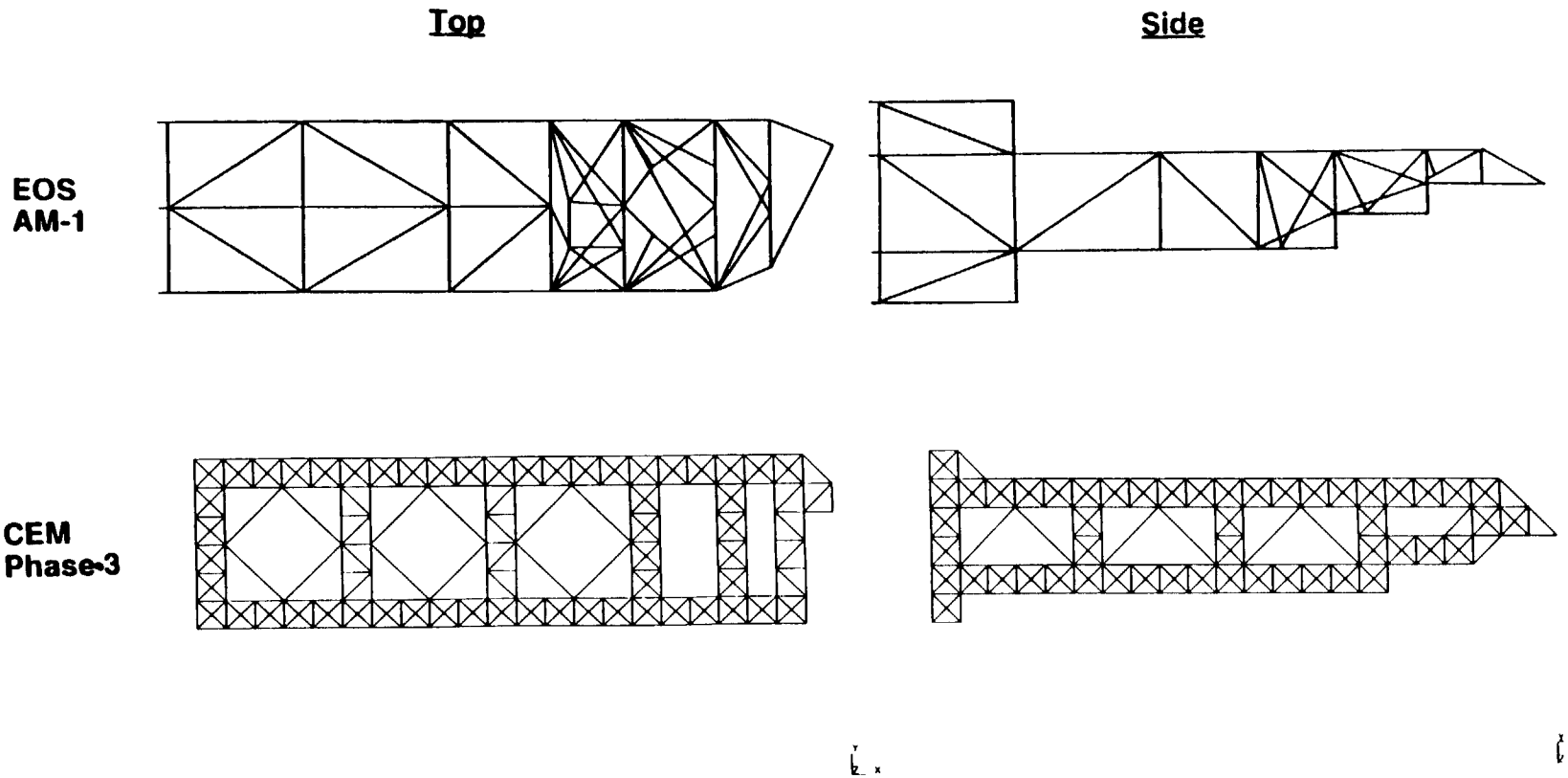

Figure 3-6. CEM3 vs. EOS Primary Structure Comparison

In order to achieve the desired primary structure torsional stiffness required to place the CEM3 first structural mode above 23 Hz, stiffer diagonal struts were needed. Eighty-eight new struts were designed and fabricated with an axial stiffness four times greater than the existing CEM2 diagonal struts. These are designated "stock tube" struts because they are made from a stock tube size, whereas many of the tube sections for the CEM2 struts were turned down on a lathe. Pairs of the stock tube struts were used as system diagonals in the open truss faces between CEM3 bulkheads 1 & 2, 2 & 3, and 3 & 4 and as internal diagonals in bulkheads 2 and 3. The new stock tube diagonal strut is simply a -1L longeron strut (which has a stock tube diameter) whose tube length has been increased from 6.678 inches to 10.820 inches. The design dimensions of the new diagonal strut (-7D) are shown in Figure 3-7. Static tests were performed to quantify the axial stiffness properties of the new strut with the results discussed below in Section 3.1.2. A summary of the effective area, axial stiffness, density, and length properties of each strut type used in the CEM3 model is shown in Table 3-1.

The total quantity of strut hardware required to assemble the CEM3 testbed is summarized in Table 3-2 along with the quantity of strut hardware available at NASA/LaRC. The CEM3 testbed structure was designed using 1915 struts with 94 to spare. A special effort was made to reduce the number of batten frame diagonal struts used in the CEM3 truss which resulted in a surplus of 63 diagonal struts. For the added weight, these struts contribute very little to the stiffness of the testbed and are more effectively used as spare parts.

3.1.2 Stock Tube Diagonal Strut Test

A series of static force-deflection tests was conducted on the stock tube diagonal struts developed for the CEM3 primary truss structure. The objective of the tests was to quantify the equivalent axial stiffness property of the struts for use in the CEM3 finite element model. Five identically prepared stock tube strut assemblies were each tested at least twice in both tension and compression in order to demonstrate repeatability of test results and address experimental uncertainty. Shake-down tests were always conducted prior to performing tests of record in order to remove any preset or slop in the test setup.

Figure 3-8 shows the test setup used during the axial testing. The strut specimen is a complete strut assembly comprised of a "stock tube" strut, two standoffs, two screws, two nuts, and a node ball. The assembly is mounted to the test fixture using the appropriate screws. The stock tube strut was mounted to a diagonal slot on the node ball in order to test the actual node ball/strut orientation which will be used in the

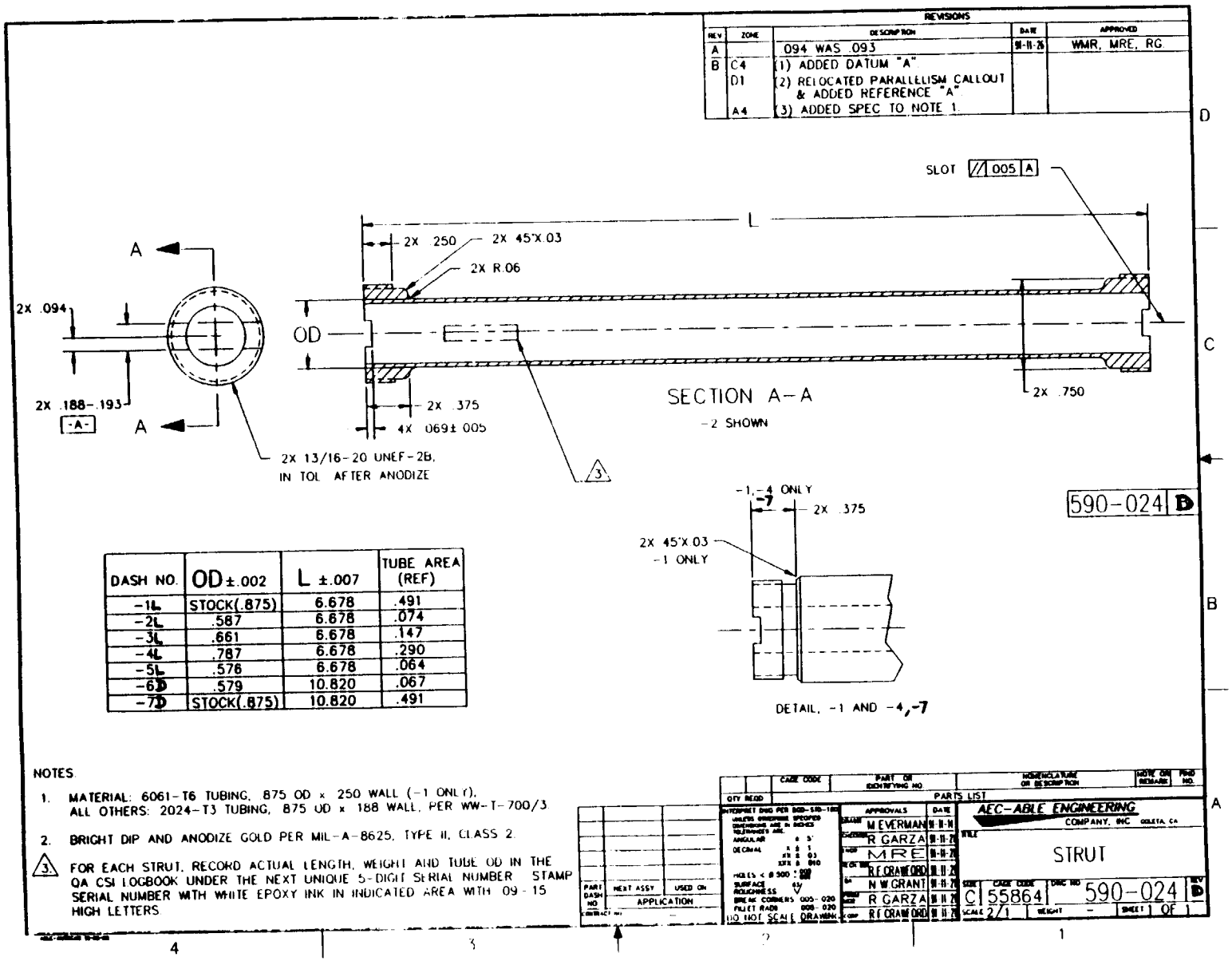

Figure 3-7. CEM Erectable Strut Design

Table 3-1. CEM3 Strut Properties

STRUT TYPE	Length (in)	Effective Area (in^2)	Effective Density (lb-s^2/in^4)	Axial Stiffness (lb/in)
-1L Longeron	10.00	0.3330	3.636E-04	332,549
-2L Longeron	10.00	0.0991	5.821E-04	99,125
-3L Longeron	10.00	0.1750	4.016E-04	174,649
-4L Longeron	10.00	0.2640	3.458E-04	264,236
-5B Batten	10.00	0.0974	5.846E-04	97,359
-6D Diagonal	14.14	0.0831	5.392E-04	58,791
-7D Stock Tube	14.14	0.3454	3.133E-04	244,252

Table 3-2. CEM3 Testbed Strut Count

COMPONENT	LaRC QTY	CEM3 QTY	Δ
-1L Longeron Tube	107	107	0
-2L Longeron Tube	202	202	0
-3L Longeron Tube	66	62	4
-4L Longeron Tube	210	210	0
-5B Batten Tube	605	585	20
-6D Diagonal Tube	724	661	63
-7D Stock Tube Diagonal	95	88	7
Strut Total	*2009*	*1915*	*94*
Stand-offs	3884	3830	54
Nuts	3885	3830	55
Screws	3886	3830	56
Nodes	601	578	23
Half Nodes	24	16	8
45 Deg Nodes	22	16	6

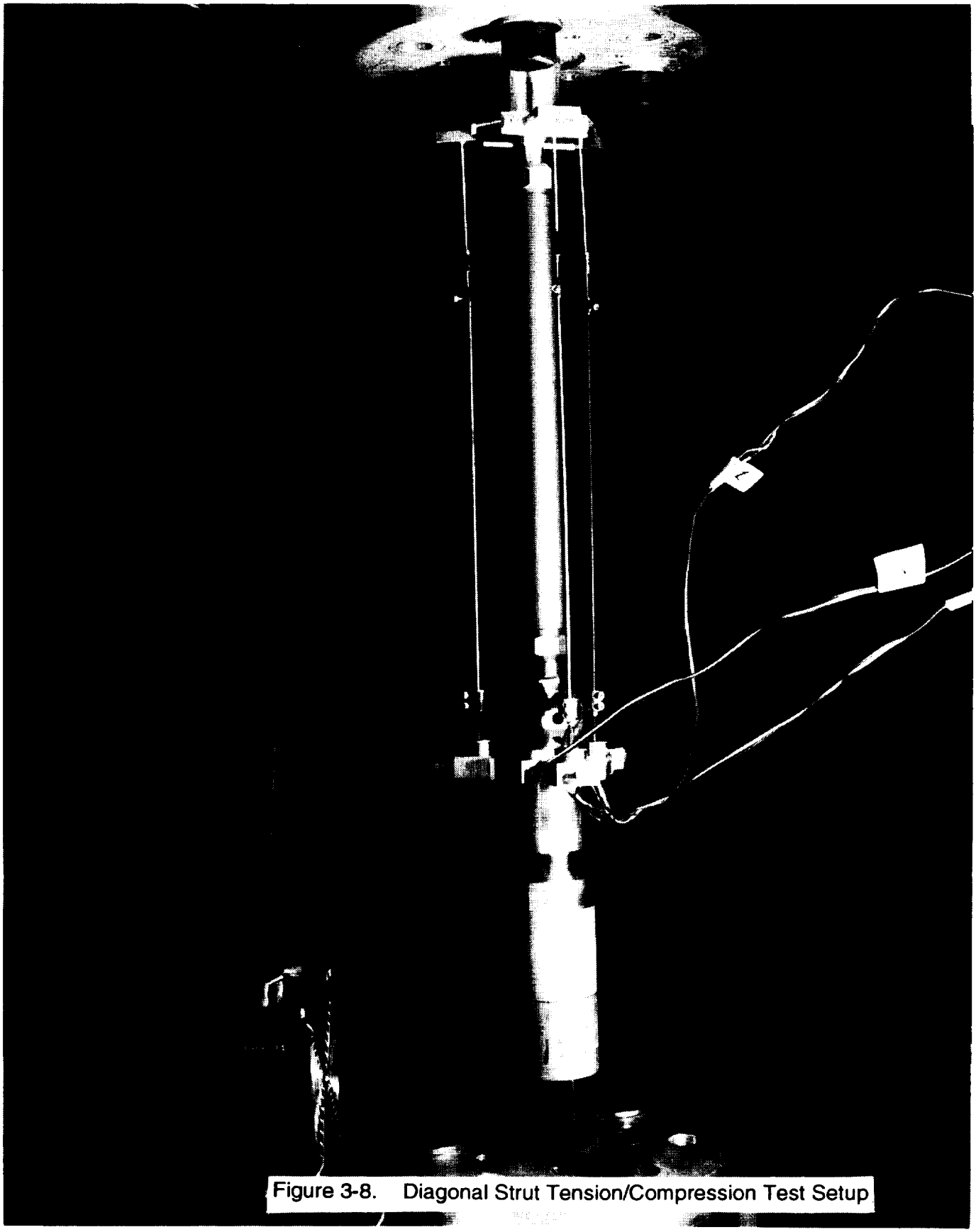

Figure 3-8. Diagonal Strut Tension/Compression Test Setup

CEM3 testbed.

The basic setup and procedure used to test the stock tube strut assemblies is identical to that previously used during the successful testing of the CSI Phase-1 strut hardware[3]. The only exception is performance of a single continuous tension/compression test rather than individual tests. The stock tube strut was first loaded from 0 lbs up to the maximum tensile load, then ramped back through 0 lbs down to the maximum compressive load, and then back again up to the 0 lb starting point. This resulted in a continuous single data record for both the tensile and compressive tests which is extremely useful when evaluating linearity about the origin. The maximum tensile and compressive load values used for all tests were +/- 500 lbs. Torque values of 240 in-lbs for the nuts and 210 in-lbs for the stand-off screws were used to assemble each diagonal strut assembly consistent with the Phase-1 hardware. Only the unique "stock tube" hardware was changed out between each strut test with the node ball and joint components remaining the same for all tests.

The overall results of the 10 axial stiffness tests of record are shown in Table 3-3. Equivalent axial stiffness values were computed for each strut test by performing linear regression on the entire data record which included the combined tension and compression measurements. In performing the linear regression, leading repeated zeros, startup transients, and trailing repeated zeros were manually deleted from the test data to avoid biasing the curve-fit. The average stiffness values computed for each set of test data are extremely close in magnitude with the maximum stiffness value being 246,730 lb/in (XD101_R1) and the minimum stiffness value being 242,130 lb/in (XD102_R1). The difference between the two extreme computed stiffness values is only 1.9% which demonstrates the excellent stiffness repeatability observed during the test series. The overall average strut axial stiffness based on all 10 tests is 244,252 lb/in which is the value used in the CEM3 finite element model. Figure 3-9 shows the quality of the axial load versus displacement data measured during test XD102_R2 which is representative of all the test data. The strut axial behavior is highly linear in both tension and compression.

3.2 ATTACHED PAYLOADS AND EQUIPMENT

The "payloads" (science instruments and subsystem equipment) on the EOS AM-1 spacecraft were modeled on the CEM3 testbed using either a discrete rigid mass or a 2-axis gimbal with an attached mass. The rigid masses simulating the MISR, SWIR, and VNIR science instruments are attached to the three CEM2 2-axis pointing gimbals. Because the primary structure and appendage designs are constrained by

Table 3-3. Stock Tube Diagonal Strut Axial Stiffness Test Results

STRUT ID No.	TEST No.	K (lb/in)
XD101	R1	246,730
XD101	R2	245,280
XD102	R1	242,130
XD102	R2	242,505
XD103	R1	245,875
XD103	R2	245,901
XD104	R1	243,840
XD104	R2	243,606
XD105	R1	243,118
XD105	R2	243,537

K (average) = 244,252 lb/in

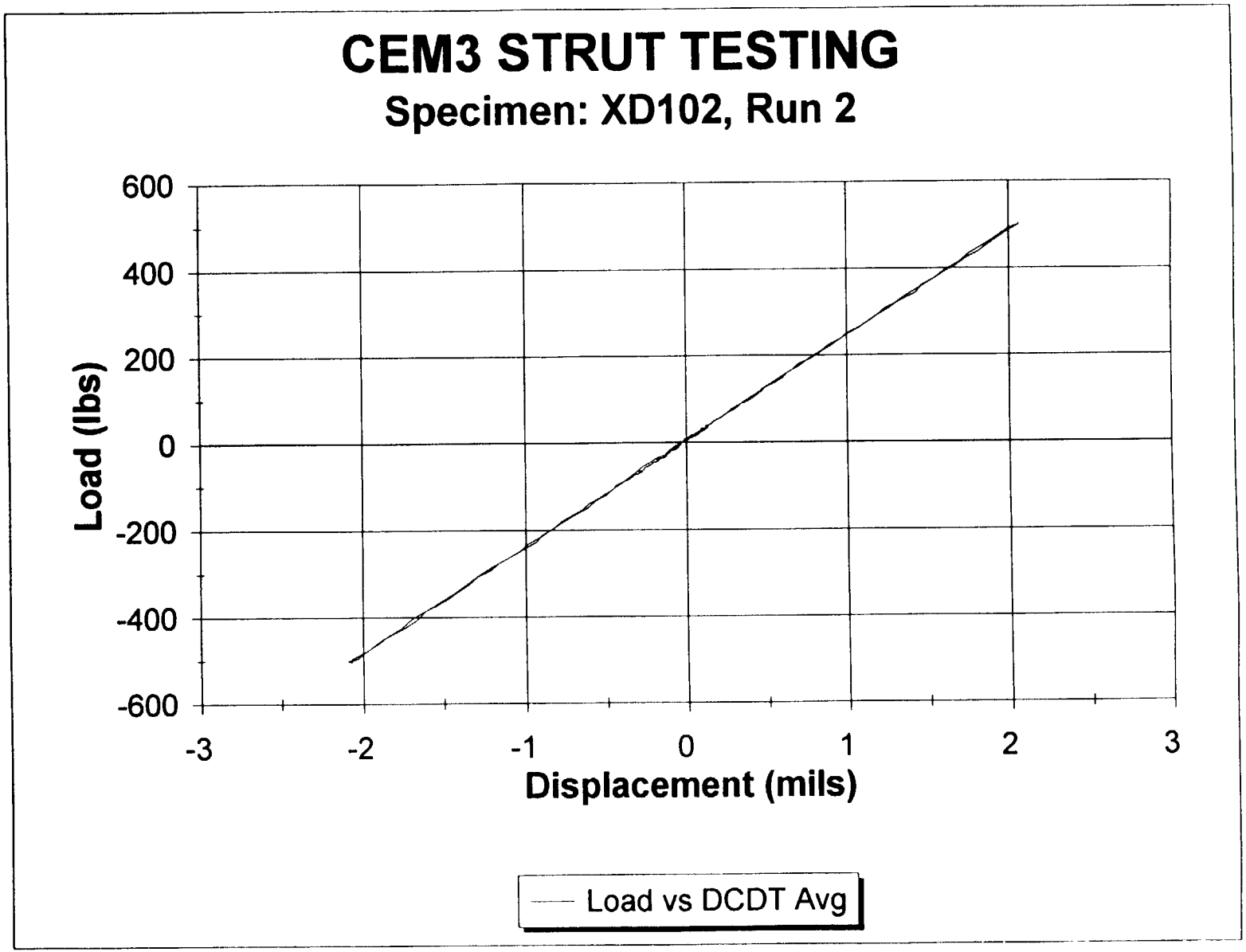

Figure 3-9. Typical Diagonal Strut Force-Displacement Test Results

other variables, the weight and placement of the attached payloads served as the only unconstrained variables that could be adjusted to match the overall spacecraft inertias and c.g. Even the payload weight variables are somewhat constrained because of the "out-of-scale" 90-pound weight of the 2-axis gimbals.

A total of 11 out of the 19 payloads simulated in the EOS AM-1 ROM model were identified as important for the CEM3 model and therefore were included as part of the testbed design. The other 8 payloads were "deleted" to eliminate excess inertia in order to best match the overall EOS AM-1 spacecraft inertia and c.g. properties. Table 3-4 contains a list of the 11 payloads included in the CEM3 model while Table 3-5 shows the 8 deleted payloads. The weight of the deleted payloads is offset by the corresponding weight increase resulting from using the 2-axis gimbals which are significantly heavier than the EOS science instruments they simulate.

The selection of the 8 equipment items to be deleted from the CEM3 testbed was based on several factors. For example, the scaled weights of the SWIR Radiator, TIR Radiator, MOPITT Radiator, and CERES1 equipment were all below 6 lbs and had a negligible effect on the testbed inertia properties. Other payloads with large masses such as the Propulsion Module (PM) and Reaction Wheel Assembly (RWA) were also eliminated. The mass and inertia properties associated with these two payloads are accounted for by the additional weight of the primary structure, gimbals, and control actuator hardware.

Several of the retained payloads are offset from the CEM3 primary structure using payload towers in order to more accurately locate masses at their proper c.g. locations. These towers are simply one or two bays of truss structure. Locating the CEM3 mass simulators as close as possible to their true c.g. coordinates is critical for matching the overall scaled inertia properties of the EOS AM-1 spacecraft. It should be noted that for the CEM3 testbed, the Tape Recorder (TR) payload was divided into two identical mass simulators which have the same effective combined c.g. location. This change was driven by concerns regarding strut count since significantly more truss hardware would be required to position a single TR mass simulator at its true c.g. location.

3.3 APPENDAGES

The design of the appendages was driven by the need to meet the frequency and K_b requirements in Tables 2-3 and 2-4. Correctly matching the appendage mass and c.g. was also important in matching the overall scaled spacecraft inertia.

Table 3-4. Simulated EOS AM-1 Payloads

PAYLOAD DESCRIPTION	SIMULATOR TYPE	SCALED EOS WEIGHT (LBS)
VNIR	Gimbal	40.98
SWIR	Gimbal	29.11
MISR	Gimbal	29.77
CERES2	Rigid Mass	28.47
COMM	Rigid Mass	26.26
GN&C Bench & Shell	Rigid Mass	32.18
MODIS	Rigid Mass	51.87
MOPITT	Rigid Mass	45.52
PMAD	Rigid Mass	69.16
TIR	Rigid Mass	35.94
TR	Rigid Mass	72.30
	Total:	461.56

NOTE: Each CEM3 Gimbal Weighs 90.5 lbs

Table 3-5. Deleted EOS AM-1 Payloads

PAYLOAD DESCRIPTION	SCALED EOS WEIGHT (LBS)
Battery Panel	35.10
CERES1	2.51
DDL Panel	11.11
MOPITT Radiator	5.86
Propulsion Module	89.20
RWA	25.28
SWIR Radiator	4.76
TIR Radiator	4.87
Total:	178.69

The two flexible appendages used on the CEM3 testbed to simulate the EOS AM-1 solar array and high gain antenna are the deployable mast originally designed for the CEM Phase-2 testbed and a newly developed HGA simulator. These two CEM3 appendages approximate the low-frequency dynamics of the EOS appendages and simulate the modal interaction between the appendage and bus structure. The mast is cantilevered horizontally from a 2-axis gimbal stand mounted on the -Y side of the CEM3 testbed while the HGA mounts directly to strut node balls and is cantilevered vertically upward in the CEM3 -Z axis. Both CEM3 appendages have undergone fixed-base modal testing to verify the dynamic properties of the structures, resulting in correlated math models.

3.3.1 Solar Array Simulator Description

A photograph of the actual deployable mast hardware designed and fabricated by AEC-Able Engineering Company, Inc. is shown in Figure 3-10. The aluminum mast is a three longeron, spherical joint design with a deployed length of 180 inches and a diameter of 6.980 inches. To create the CEM3 solar array simulator, a tip weight is added to the mast as shown in Figure 3-11. The weight can be varied from 0 to 50 lbs in 10 lb increments to adjust the mast frequency and resulting modal coupling (K_b) with the testbed. The mast length can also be shortened if necessary by removing individual bays of truss. A detailed description of the CEM2 mast hardware in terms of dimensions, material types, and load carrying capability is provided in Table 3-6.

A comparison of the lengths of the EOS AM-1 solar array and the CEM2 mast (Figure 3-12) shows that the CEM2 mast is approximately one-half the length of the scaled EOS solar array (180" vs. 351"). In terms of width, the EOS blanket measures 196 inches across compared to the mast diameter of only 6.98 inches. Fortunately, even though the mast overall geometry does not closely match EOS, when equipped with a 40-lb tip weight the mast has approximately the same scaled weight and c.g. location as the EOS solar array. This similarity enables the existing CEM2 mast to adequately simulate the scaled dynamic behavior of the EOS solar array.

3.3.2 Solar Array Simulator Modal Test

A modal survey was conducted on the CEM2 deployable mast equipped with a 40-lb tip weight in order to quantify the dynamic characteristics of the solar array simulator and provide the modal parameters needed to correlate the MSC/NASTRAN analytical model. The mast was tested in a vertically cantilevered configuration using a floor-anchored steel fixture (Figure 3-10) rather than in a horizontally mounted configuration similar to what its orientation will be on the CEM3 testbed. Horizontal

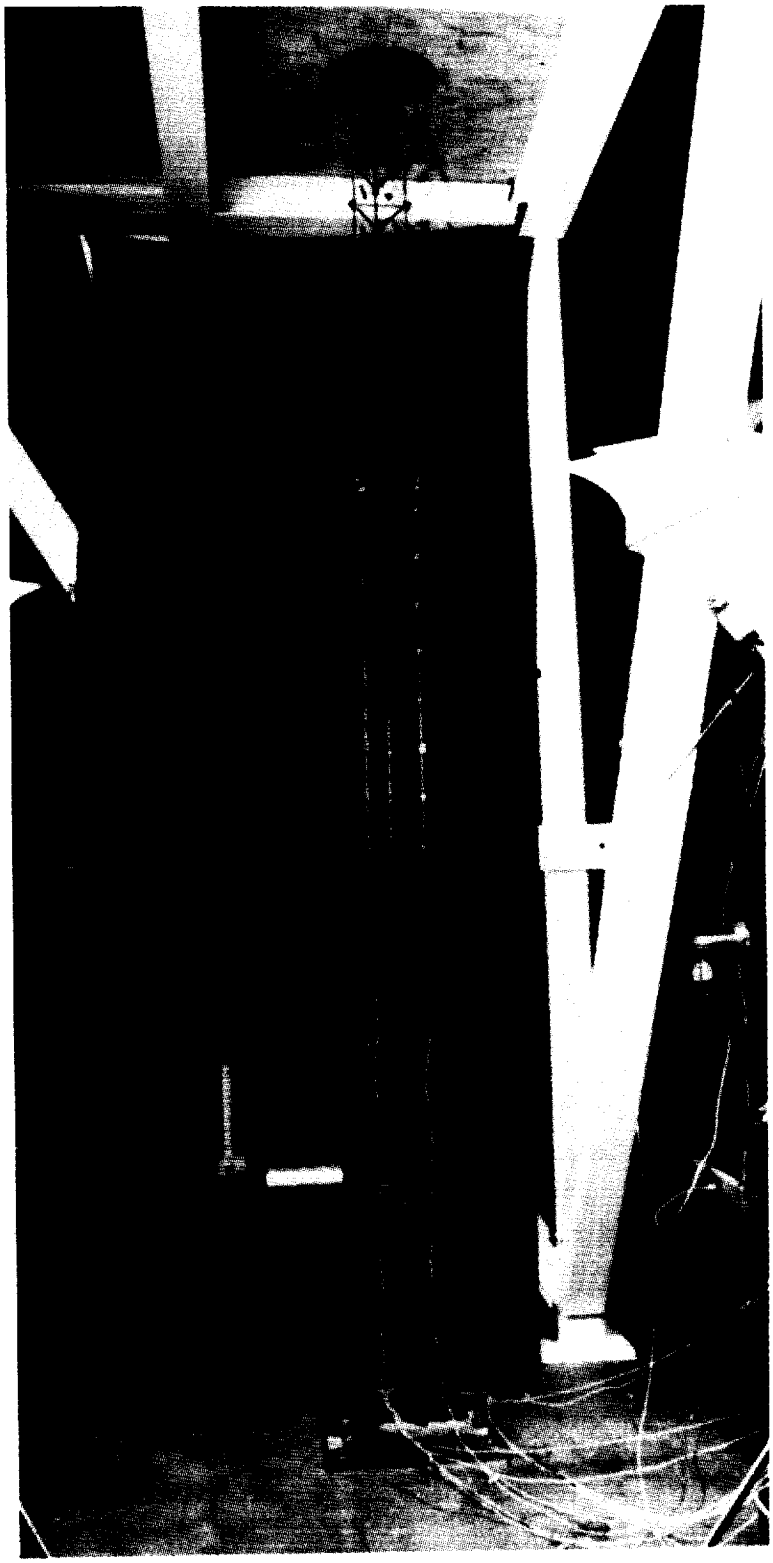

Figure 3-10 AEC-Able Deployable Articulated Mast Hardware

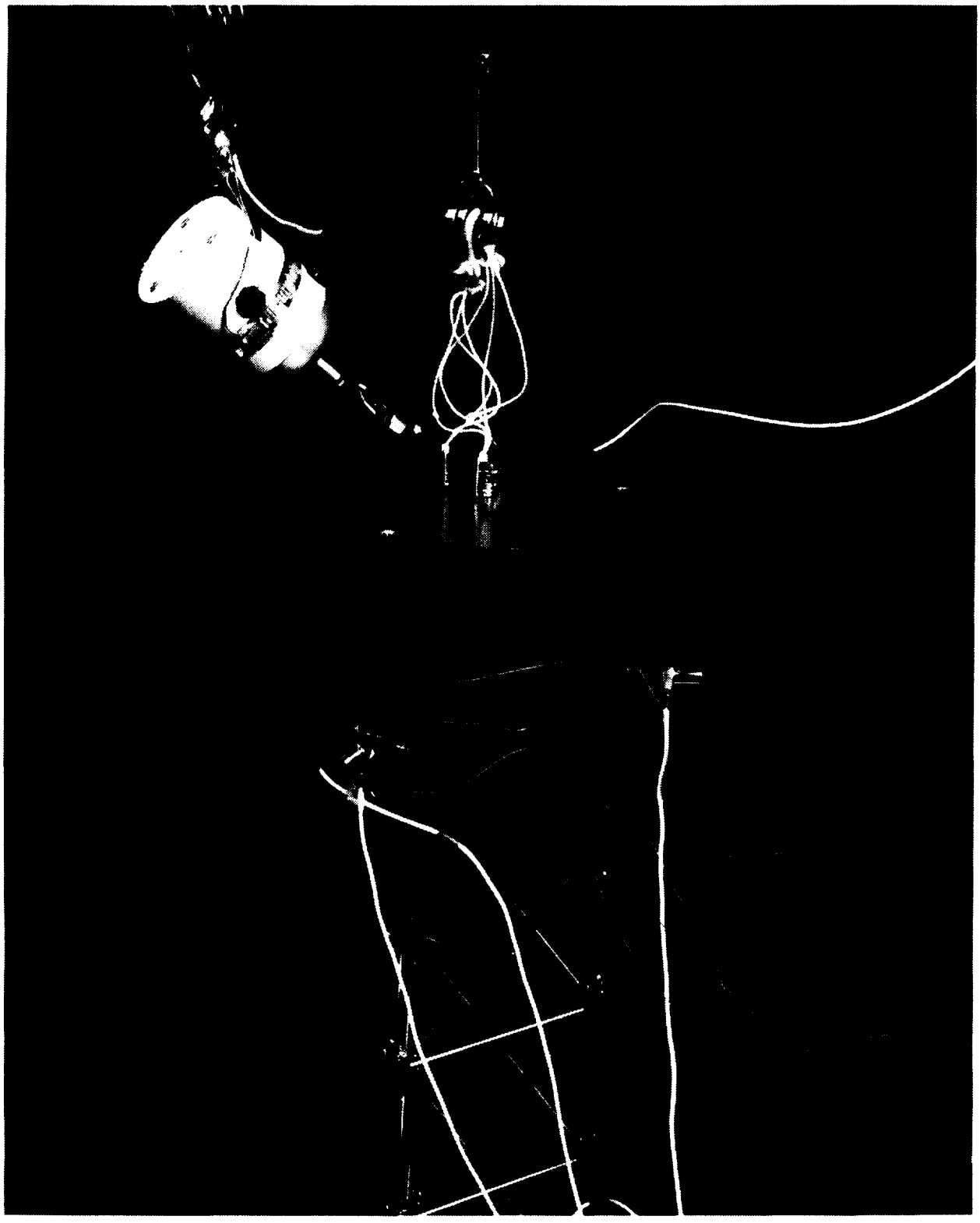

Figure 3-11. AEC-Able Deployable Articulated Mast Tip Weight

Table 3-6. CEM Mast Description

CHARACTERISTIC	VALUE
MAST TYPE	Triangular, Articulated
PRIMARY STRUCTURAL MATERIALS	2024-T4 Aluminum, 303 SS
LONGERON and BATTEN TUBING	0.250 in. OD, 0.020 in. Wall
DIAGONAL CABLE	0.047 in. OD, 7x19 SS
JOINT TYPE	Ball & Socket
MAST DIAMETER	6.980 in.
BAY SIDE	6.045 in.
BAY LENGTH	5.443 in.
ANGLE, BATTEN-TO-DIAGONAL	42.0 deg
NOMINAL MAST LENGTH	180 in.
NOMINAL NUMBER OF BAYS	33
LONGERON BUCKLING LOAD	415 lb
MAST AXIAL BUCKLING LOAD (FIXED/FREE)	236 lb
MINIMUM BENDING STRENGTH	2170 in-lb
SHEAR STRENGTH	28 lb
TORSIONAL STRENGTH	146 in-lb
NOMINAL WEIGHT	10.6 lb

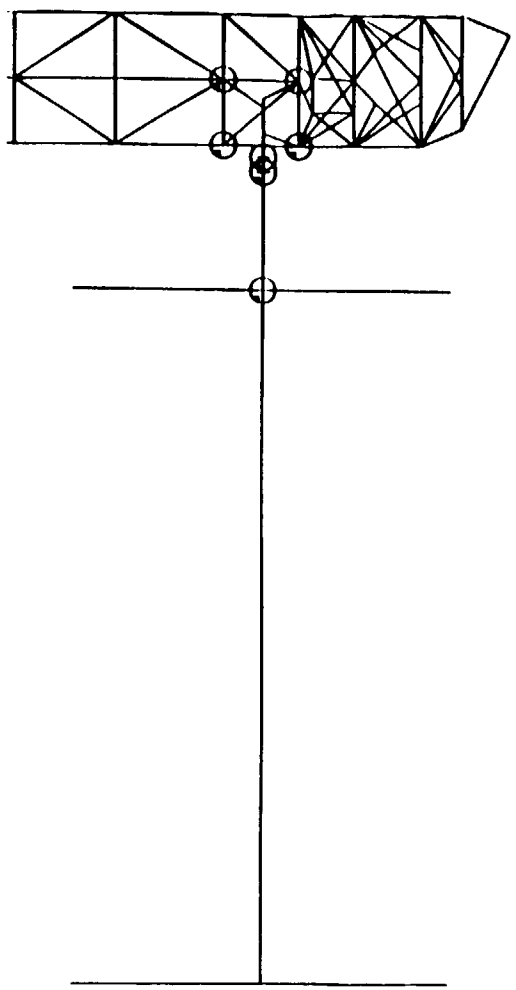

EOS AM-1 (ROM)

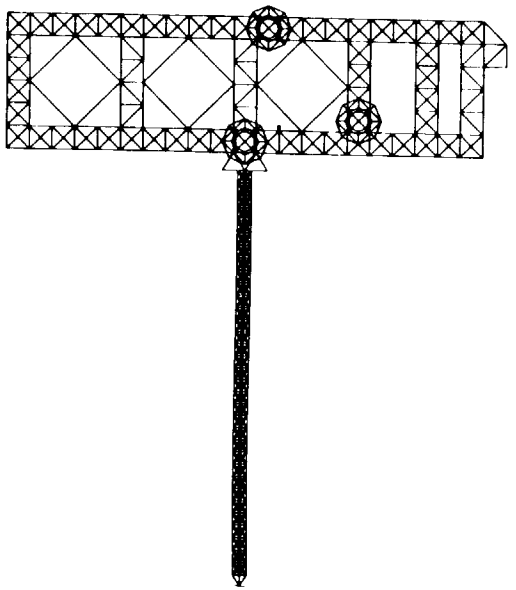

CEM3

Figure 3-12. CEM3 Mast vs. EOS Solar Array Comparison

testing would have required the use of a zero-g suspension system (not readily available at the time of testing) to effectively off-load the 40 lb-tip weight. The geometric stiffness effects on the low-frequency mast modes due to gravity preload along the length of the mast are accounted for in the finite element analysis. Measured frequency, damping, and mode shape data were obtained for fixed-base mast modes up to 55 Hz.

To determine the locations and number of accelerometers needed to adequately describe the dynamic response of the cantilevered mast during a modal survey, pretest Test-Analysis Models (TAM's) were generated using the Guyan static reduction method[14]. A TAM is a reduced order analysis model of the full finite element model whose Degrees-of-Freedom (DOF) are identical to the accelerometer DOF measured during a modal survey. The geometric stiffness effects were included in the TAM model since an updated TAM mass matrix is required to compute post-test cross-orthogonalities between test and analytical modes.

A set of 33 accelerometers were selected for the modal test with the resulting pretest TAM vs. FEM comparison summarized in Table 3-7. Twenty-seven Kistler accelerometers were distributed along the mast length and tip weight along with six piezo-resistive ENDEVCO accelerometers used to accurately capture the low-frequency first bending modes. The accelerometer set measured radial, tangential, and axial motion. Mass associated with instrumentation hardware (2.665 lbs) such as accelerometers, force gauges, and cables was accurately represented in the analytical test model.

The pretest cross-orthogonality and frequency comparisons between the TAM and FEM (Table 3-7) show excellent agreement for the first nine cantilevered modes below 49 Hz. The cross-orthogonality values are all above 0.95 and the frequency errors are less than 1.2% except for the second torsion mode (mode 7) which has a frequency error of 3.2%. The fourth mast bending modes at approximately 50 Hz have diminished cross-orthogonality and frequency comparisons between the TAM and FEM indicating that the sensor set does not adequately capture these modes.

A modal survey on the cantilevered mast structure was performed by subjecting it to a series of burst random excitation tests in both the base-band and zoom modes. A single force shaker was used to excite the fixed-base modes of the cantilevered structure. Two different shaker attachment points were used during testing in order to adequately excite the all the structural modes up to 55 Hz. Figures 3-10 and 3-11 show the two mast shaker excitation points used, one near the base of the mast and the other on the tip weight. Tests were conducted at various excitation levels to assess

Table 3-7. Solar Array Simulator Pretest TAM vs. FEM Cross-Orthogonality

TAM MODE	TAM FREQ (HZ)	XO	FEM MODE	FEM FREQ (HZ)	FREQ ERROR (%)	DESCRIPTION
1	0.541	1.00	1	0.541	0.0	B-1
2	0.541	1.00	2	0.541	0.0	B-1
3	4.292	1.00	3	4.281	0.3	T-1
4	9.099	1.00	4	9.087	0.1	B-2
5	9.099	1.00	5	9.087	0.1	B-2
6	23.929	1.00	6	23.898	0.1	AXIAL
7	26.202	0.96	7	25.392	3.2	T-2
8	26.901	0.97	8	26.585	1.2	B-3
9	26.902	0.97	9	26.585	1.2	B-3
10	51.369	0.82	10	49.265	4.3	B-4
11	51.370	0.82	11	49.265	4.3	B-4

the linearity of the mast dynamic behavior as a function of input amplitude. The higher level excitations resulted in observed tip weight lateral displacements of approximately 1 inch.

Based on the measured mode shape and frequency results obtained from the modal survey, the mast finite element model was correlated using the SDRC CORDS2 Program[15]. The CORDS2 Program uses design sensitivity and optimization methods to identify model updates which minimize frequency differences between test and analysis. Several iterations were required to obtain the final correlated model whose cross-orthogonality and frequency comparisons with measured test data are summarized in Table 3-8. The cross-orthogonality and frequency agreement for the first and second bending mode pairs (modes 1&2 and 4&5), the first and second torsion modes (modes 3 and 7), and the first axial mode (mode 6) are excellent with cross-orthogonalities of 0.98 or better and frequency errors ranging from 0.1% to -3.5%. The higher order mast bending mode pairs (modes 8-11) at approximately 29 Hz (B-3) and 52 Hz (B-4) show excellent frequency agreement (less than 2.3% error) but only marginal cross-orthogonality results (0.79 to 0.86). The marginal cross-orthogonality results associated with the fourth bending mode pair are not unexpected considering the accuracy of the pretest TAM for the higher order modes. The resulting equivalent bending rigidity (EI) corresponding to the correlated mast model is 3.3E+06 lb-in^2 compared to a design value of 3.1E+06 lb-in^2. It should be noted that the TAM mass matrix used for the final cross-orthogonality comparison was based on the correlated full FEM model.

As part of the modal survey, modal damping values were also extracted from the measured data as shown in Table 3-8 where a value of 100% represents a critically damped structure. Nominal damping values (0.0051 g-rms input) ranged from 0.24% to 1.53% with the highest value corresponding to the second torsion mode. The lowest damping values were observed for the low frequency modes (B-1 & T-1). Linearity tests performed by varying input amplitudes (from 0.00051 to 0.0171 g-rms) indicated variations in measured damping levels as a function of input amplitude for the first bending mode pair but not for the first torsion mode whose damping remained constant. Linearity tests were performed for only the first order modes. In terms of frequency linearity, the mast responses for the first order modes were quite linear over the input amplitude range, exhibiting variations of less than 1.5%.

3.3.3 High Gain Antenna Design

A photograph of the CEM3 high gain antenna which is comprised of a flexible boom and a rigid tip weight is shown in Figure 3-13. The boom has a C-channel

Table 3-8. Solar Array Simulator Test vs. Correlated FEM Cross-Orthogonality

TEST MODE	TEST FREQ (HZ)	XO	DAMP (%)	FEM MODE	FEM FREQ (HZ)	FREQ ERROR (%)	DESCRIPTION
1	0.564	1.00	0.41	1	0.574	1.8	B-1
2	0.568	1.00	0.33	2	0.574	1.1	B-1
3	5.164	1.00	0.24	3	5.252	1.7	T-1
4	9.748	0.99	0.52	4	9.427	-3.3	B-2
5	9.767	0.99	0.74	5	9.427	-3.5	B-2
6	27.654	0.98	0.49	6	27.682	0.1	AXIAL
7	28.673	0.98	1.53	7	27.887	-2.7	T-2
8	29.176	0.79	0.69	8	29.154	-0.1	B-3
9	29.285	0.82	1.10	9	29.168	-0.4	B-3
10	52.424	0.85	0.79	10	53.628	2.3	B-4
11	52.619	0.86	0.75	11	53.721	2.1	B-4

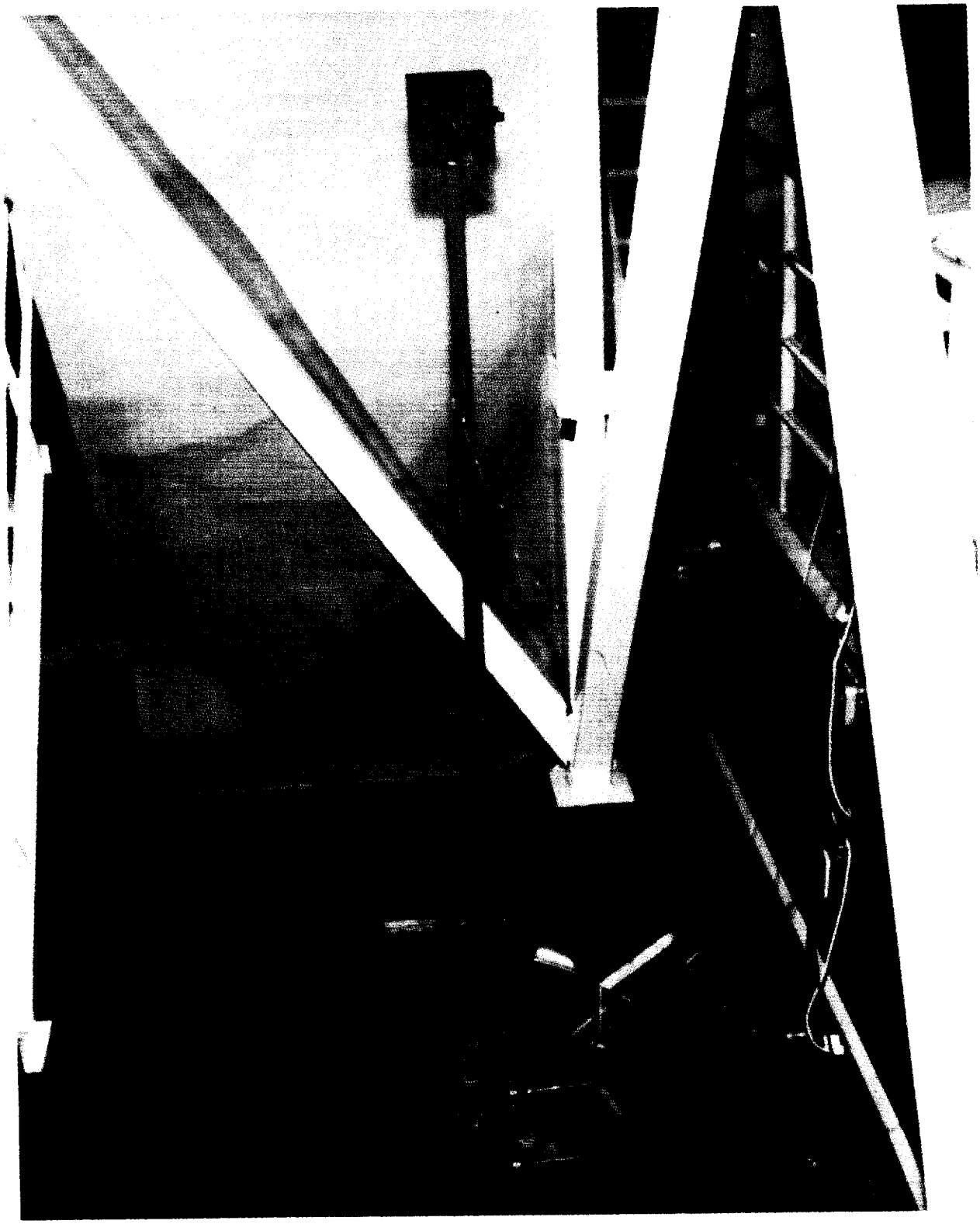

Figure 3-13. CEM3 High Gain Antenna Hardware

cross-section with different bending stiffness properties about each axis. Using an open C-channel rather than a closed rectangular section enabled the desired cross-sectional properties to be obtained using an off-the-shelf piece of hardware. Since the HGA simulator was designed and fabricated especially for the CEM3 testbed, the length and weight dimensions are based on scaled EOS values and therefore are a near perfect match. The cantilevered length from the base of the HGA boom to the c.g. of the 26.5 lb tip weight is 100 inches, identical to EOS.

3.3.4 High Gain Antenna Modal Test

A modal survey was performed on the HGA structure in order to characterize the dynamic behavior of the appendage for use in math model correlation. The antenna was mounted to a single bay of truss in a vertically cantilevered configuration (Figures 3-13 and 3-14) analogous to its configuration on the CEM3 testbed. Even though the geometric stiffness effects on the first HGA bending modes due to gravity preload are relatively minimal, the effects are still accounted for in the finite element analysis. Measured frequency, damping, and mode shape data were obtained for the cantilevered HGA assembly up to 65 Hz.

Identical to the procedure followed during the mast modal survey, a series of TAM's were generated to determine the locations and number of accelerometers needed to adequately describe the few first modes of the cantilevered antenna structure. A set of 16 accelerometers were used with the resulting pretest TAM vs. FEM comparison summarized in Table 3-9. Five bi-axial accelerometer blocks were distributed along the antenna length and 2 tri-axial accelerometer blocks were mounted on the rigid tip weight. Mass associated with instrumentation hardware (0.387 lbs) was accurately represented in the analytical test model.

The pretest cross-orthogonality and frequency comparisons between the TAM and FEM (Table 3-9) show a perfect match for the first bending mode pair (modes 1 and 2) and the first torsion mode (mode 3). The TAM for the second bending mode pair (modes 4 and 5) matches the full FEM quite well with cross-orthogonalities of 0.94 and 0.98 and frequency errors below 2.1%. The third bending modes (modes 6 and 7) which occur above 50 Hz do not compare well, indicating that the sensor set does not adequately capture the higher order bending modes. Since the purpose of the modal survey was to identify the first few modes of the cantilevered HGA in a timely manner, additional effort was not performed to improve the TAM for modes 6 and 7.

In order to accurately model the important shear center offset and neutral axis physical properties associated with the HGA boom C-channel cross-section, the finite element

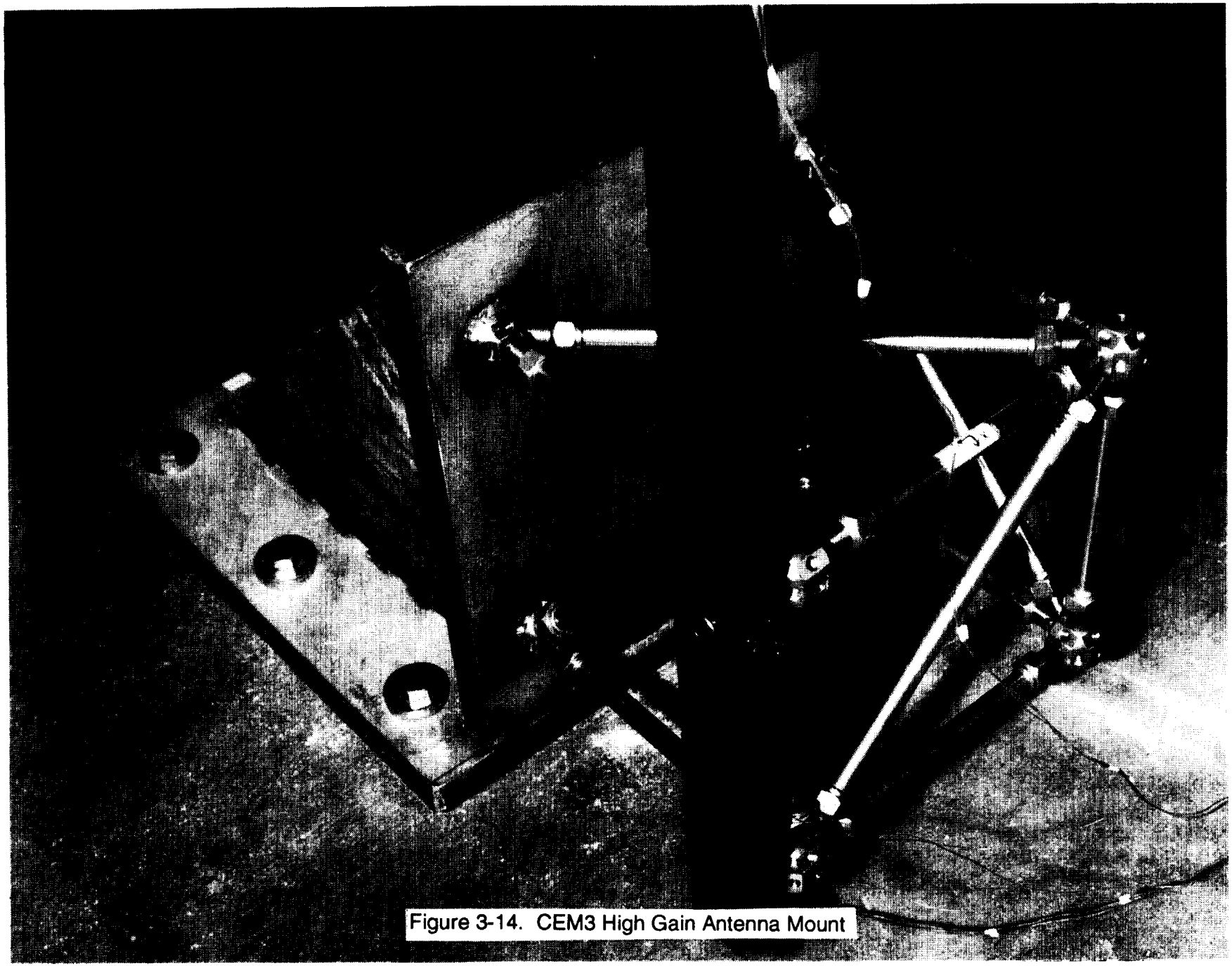

Figure 3-14. CEM3 High Gain Antenna Mount

Table 3-9. HGA Pretest TAM vs. FEM Cross-Orthogonality

TAM MODE	TAM FREQ (HZ)	XO	FEM MODE	FEM FREQ (HZ)	FREQ ERROR (%)	DESCRIPTION
1	1.192	1.00	1	1.192	0.0	B-1-Y
2	1.330	1.00	2	1.330	0.0	B-1-X
3	2.755	1.00	3	2.755	0.0	T-1
4	22.846	0.94	4	22.380	2.1	B-2-Y
5	23.692	0.98	5	23.303	1.7	B-2-X
6	59.741	0.65	6	50.912	17.3	B-3-X
7	69.268	0.83	8	68.247	1.5	B-3-Y

model of the HGA boom was built using plate elements. Beam elements with shear center offsets were not a modeling option since they cannot be used in combination with geometric stiffness in MSC/NASTRAN.

A modal survey of the cantilevered HGA structure was performed by subjecting it to a series of burst random excitation tests in both the base-band and zoom modes. A single force shaker mounted near the base of the HGA boom (Figure 3-13) was used to excite the fixed-base modes of the cantilevered structure up to 65 Hz. Based on the measured mode shape and frequency results obtained from the modal survey, the HGA FEM model was correlated using the CORDS2 Program. Several iterations were required before achieving the final correlated model results summarized in Table 3-10.

The cross-orthogonality and frequency agreement for the first bending mode pair (modes 1 and 2) and the first torsion mode (mode 3) are excellent with cross-orthogonalities of 0.98 or better and frequency errors below 1.5%. The second bending mode pair (modes 4 and 5) at 22 Hz have cross-orthogonality values of 0.90 and 0.92, and frequency errors of -1.6% and 0.9%, respectively. The test results indicate noticeable coupling between these two modes which resulted in the need for linear recombination[16] as part of the correlation effort. The test vs. FEM results for the third bending mode pair are poor which is not unexpected given the accuracy of the pretest TAM for these higher order modes. The TAM mass matrix used for the final cross-orthogonality comparison was based on the correlated full FEM model.

As part of the modal survey, modal damping values were also extracted from the measured data (Table 3-10) where a value of 100% represents a critically damped structure. The results show the antenna assembly to be very lightly damped with damping values ranging from 0.06% to 0.24% for the seven modes extracted in the survey.

3.4 SUSPENSION SYSTEM

Simulating the on-orbit low-frequency dynamic characteristics of the EOS AM-1 spacecraft using the CEM3 testbed in a 1-g laboratory environment can be difficult due to the presence of gravity loads. The advanced suspension devices which off-load gravity and approximate free-free boundary conditions result in six low-frequency testbed rigid-body suspension modes. The interaction between these suspension modes and the testbed flexible body modes must be minimized in order to correctly simulate free-free dynamics and the proper coupling between the bus and appendages which is critical for the low-frequency control experiments.

Table 3-10. HGA Test vs. Correlated FEM Cross-Orthogonality

TEST MODE	TEST FREQ (HZ)	XO	DAMP (%)	FEM MODE	FEM FREQ (HZ)	FREQ ERROR (%)	DESCRIPTION
1	1.165	0.98	0.10	1	1.173	0.7	B-1-Y
2	1.321	0.99	0.08	2	1.304	-1.3	B-1-X
3	2.834	0.99	0.11	3	2.853	0.7	T-1
4	22.024	0.90	0.24	4	21.682	-1.6	B-2-Y
5	22.798	0.92	0.21	5	22.998	0.9	B-2-X
6	54.365	0.73	0.06	6	51.073	-6.1	B-3-X
7	64.128	0.83	0.03	8	67.561	5.4	B-3-Y

The CEM3 testbed is suspended from the NASA/LaRC Building 1293 Space Frame using five CSA zero-g suspension devices originally developed for the Phase-2 testbed[5,8]. The advanced suspension devices provide vertical isolation, while the long cables provide horizontal isolation. These suspension devices have a vertical stroke of +/- 3 inches and an adjustable active stiffness setting ranging from 0.1 lb/in to 2.0 lb/in. Approximately 6 lbs of active mass is associated with the vertical motion of each suspension device, which is negligible compared to the total testbed weight. The CEM3 testbed is hung from the devices using 3/16 inch stainless steel cables. A total of four devices are used to off-load the CEM3 truss primary structure and one device is used to off-load the mast tip weight since the strength of the deployed mast is not sufficient to support a 40-lb tip weight when cantilevered in a horizontal orientation. The locations of the five cable attachment points on the CEM3 testbed are illustrated in Figure 3-15.

The four truss attachment points on the CEM3 primary structure are designed to straddle the testbed center-of-gravity which results in each device equally supporting approximately one-quarter of the testbed weight. These loads are well within the 500 lb capability of each suspension device. Strut axial load calculations performed on the testbed suspended in 1-g with assumed worst case dynamic loads indicate no strut strength or buckling issues for the proposed suspension configuration. The vertical attachment locations of the truss cables to the testbed are approximately 10 inches above the testbed c.g. while the mast cable attachment point is located on the outer radius of the tip weight vertically above its c.g. The cables used to support the truss are 788 inches in length while the mast cable is 783 inches in length.

Suspension stiffness, locations of the cable attachment points relative to the testbed c.g., and cable length are the three key suspension parameters which drive the CEM3 rigid-body suspension mode frequencies. These are the suspension system parameters which can be tuned to meet the desired rigid-body suspension modes frequency requirement of 0.20 Hz or less. All three of the rigid-body rotational mode frequencies (roll, pitch, and yaw) are a function of the cable attachment locations with the roll and pitch frequencies being especially sensitive to the vertical height of the truss attachment points relative to the testbed c.g. In terms of suspension stiffness, the active stiffness settings affect only those modes with vertical testbed motion which are the roll, pitch, and vertical plunge modes. The lateral and fore-aft translational suspension modes are simple pendulum modes whose frequencies are determined by cable length independent of attachment location or device stiffness.

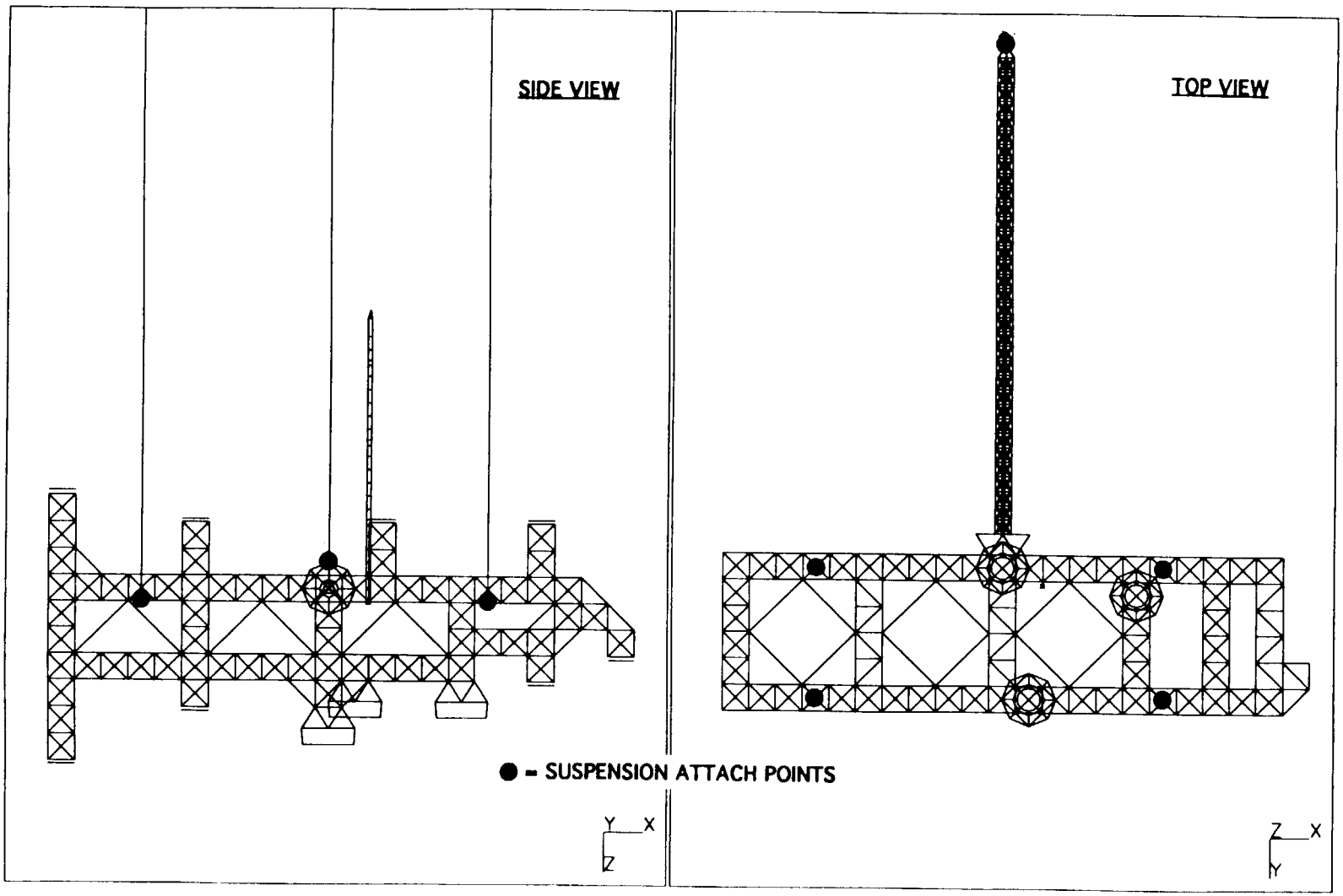

Figure 3-15. CEM3 Suspension System Attachment Locations

4.0 ANALYTICAL PERFORMANCE COMPARISONS

Many intermediate FEM analyses were conducted throughout the iterative CEM3 testbed development in order to evaluate the predicted performance of different designs. In this section the dynamic fidelity of the CEM3 testbed is evaluated by comparing the suspended CEM3 mass property, dynamics, and appendage interaction FEM results with the corresponding scaled on-orbit EOS AM-1 spacecraft FEM results (geometric fidelity was discussed previously in Section 3.0). The CEM3 FEM model used to generate the results described in this section reflects the CEM3 configuration at the time of delivery to NASA/LaRC. It also includes updated component FEM models incorporating the test results for the stock tube diagonal struts, solar array simulator, and HGA hardware described in Section 3.0.

The performance comparisons are divided into four subsections. Section 4.1 compares the overall mass properties of the CEM3 and EOS AM-1 spacecraft. Section 4.2 describes free-free dynamic analyses which were initially used to evaluate the first primary structural modes of the CEM3 testbed design. Section 4.3 describes suspended dynamic analyses which were conducted to evaluate and compare the fidelity of the low-frequency appendage interaction. Additional suspension device stiffness sensitivity analyses that were performed to "tune" the zero-g suspension system are also described. Finally, Section 4.4 provides a summary comparison of all of the key CEM3 testbed characteristics and the corresponding EOS AM-1 parameters.

4.1 MASS PROPERTIES COMPARISON

The system mass properties of the free-free CEM3 model are compared with the scaled EOS AM-1 mass properties in Table 4-1. The CEM3 results are based on the MSC/NASTRAN FEM model representation of the testbed, which includes the control actuators and electronics hardware at truss locations defined by NASA/LaRC. The FEM model does not include weight associated with suspension and instrumentation hardware which may be added for specific experiment configurations.

For the purposes of simulating the on-orbit dynamics of the EOS AM-1 spacecraft, the most important mass properties are the diagonal inertias (I_{xx}, I_{yy}, I_{zz}) and the location of the c.g. Comparison of the diagonal inertias in Table 4-1 indicates excellent agreement between the CEM3 model and the scaled EOS AM-1 spacecraft. Each of the three CEM3 diagonal inertias are within 2% of the EOS target values. Comparison

Table 4-1. Mass Property Comparison

MASS PROPERTY	EOS AM-1 (SCALED)	CEM3 (FREE-FREE)	CEM3/EOS RATIO
Total Weight	1,050	1,425	1.36
Structure Wt.	410	762	1.86
Payload Wt.	640	663	1.04
X-CG	157.33	171.86	-
Y-CG	-3.13	-6.37	-
Z-CG	-8.21	-0.04	-
Ixx	4.35E+06	4.39E+06	1.01
Iyy	6.73E+06	6.84E+06	1.02
Izz	8.14E+06	8.10E+06	1.00
Ixy	-1.23E+05	-1.82E+04	0.15
Ixz	1.63E+05	4.18E+05	2.57
Iyz	3.37E+05	8.04E+04	0.24

of the c.g. locations reveals that the Y and Z c.g. locations agree within a few inches, but the X c.g. location is about 14 inches too far forward. These results are considered acceptable, with the X c.g. difference being due to the fact that the aft end of the CEM3 primary structure was shortened due to the limited supply of CEM2 struts.

Comparison of the total weights in Table 4-1 shows that the CEM3 testbed is 36% heavier than the scaled EOS AM-1 model (1425 lbs vs. 1050 lbs). While the CEM3 payload weights match the EOS payload weights almost exactly, the CEM3 primary structure, appendages, and thruster hardware are 352 lbs heavier than the corresponding EOS components. Much of the difference is attributed to the difficulty of matching the stiffness performance of the graphite/epoxy composite EOS AM-1 primary truss structure using 10-inch bays of aluminum truss. Fortunately, since it is the rotational inertias about the control system axes and not the translational masses which affect pointing performance, the additional mass does not pose a problem for pointing experiments.

Comparison of the cross products of inertia (I_{xy}, I_{xz}, I_{yz}) in Table 4-1 indicates that the CEM3 values differ significantly from the scaled EOS properties. These differences in inertia cross products are driven by the added weight associated with replacing the VNIR, MISR, and SWIR payload masses of 40.98 lbs, 29.77 lbs, and 29.11 lbs, respectively, with 2-axis gimbals weighing 90.5 lbs each. Also, slight differences between the attachment locations of the CEM3 and EOS appendages adversely affect the inertia cross products. Matching the cross products of inertia is of secondary importance as long as they are small compared to the diagonal inertias. Table 4-2 verifies that the off-diagonal inertia ratios are indeed small for both the CEM3 testbed and the EOS AM-1 spacecraft.

For completeness, a mass property spreadsheet documenting the individual weight, c.g., and inertia properties of each hardware component in the CEM3 model is included in Table 4-3. Due to the large strut count associated with the CEM3 truss structure, the individual mass properties of all the strut and node ball hardware are expressed as a single equivalent mass. Future changes in mass properties resulting from modifications to component weights and locations can easily be analyzed using the spreadsheet.

Overall, the most important EOS AM-1 mass properties are matched in the CEM3 testbed. The 1,425-pound testbed weight is well within the 2,000-pound capability of the suspension system, with margin available for added CSI equipment, experiments, and instrumentation.

Table 4-2. Ratio of Cross Products to Diagonal Inertias

RATIO TEMPLATE

	X	Y	Z
X	Ixx/Ixx	Ixy/Ixx & Ixy/Iyy	Ixz/Ixx & Ixz/Izz
Y	Ixy/Ixx & Ixy/Iyy	Iyy/Iyy	Iyz/Iyy & Iyz/Izz
Z	Ixz/Ixx & Ixz/Izz	Iyz/Iyy & Iyz/Izz	Izz/Izz

EOS AM-1 RATIOS

	X	Y	Z
X	1.00	-.03 & -.02	.04 & .02
Y	-.03 & -.02	1.00	.05 & .04
Z	.04 & .02	.05 & .04	1.00

CEM3 RATIOS

	X	Y	Z
X	1.00	-.004 & -.003	.10 & .05
Y	-.004 & -.003	1.00	.01 & .01
Z	.10 & .05	.01 & .01	1.00

Table 4-3. CEM3 Free-Free Mass Properties Spreadsheet

COMPONENT NAME	WEIGHT	CENTER OF GRAVITY			MASS MOM OF INERTIA (LB-IN^2)		
	(LBS)	X (IN)	Y (IN)	Z (IN)	IXX0	IYY0	IZZ0
Truss							
Strut Hardware	615.10	166.90	0.89	-1.69	520300	2728000	2845000
Payloads							
MISR (gimbal)	90.50	176.21	-24.87	42.58	2695	3240	4743
SWIR (gimbal)	90.50	226.21	-14.87	32.58	2695	3240	4743
VNIR (gimbal)	90.50	186.21	24.87	32.58	2695	3240	4743
CERES 2	28.47	76.00	-5.00	51.25	0	0	0
GNC Bench & Shell	32.18	196.00	25.00	-41.32	0	0	0
COMM	26.26	256.00	25.00	-41.21	0	0	0
MODIS	51.87	286.00	15.00	11.67	0	0	0
MOPPIT	45.52	126.00	25.00	31.55	0	0	0
TIR	35.94	256.00	5.00	21.39	0	0	0
TR (+Y)	36.15	126.00	25.00	-41.39	0	0	0
TR (-Y)	36.15	126.00	-25.00	-41.39	0	0	0
PMAD	69.16	76.00	15.00	-51.97	0	0	0
Appendages							
Solar Array Mast	11.01	176	-142.14	-15	0	0	0
Solar Array Tip Weight	40.00	176	-222.0	-15	143.6	278.3	143.6
Gimbal Stand	20.56	176	-37.12	-15	511	882	508
HGA Boom	6.00	191	-18	-65	0	0	0
HGA Tip Weight	26.52	191	-18	-120	0	0	0
Actuators/Electronics							
Thruster	3.70	126	-25	0	0	0	0
Thruster	3.70	126	-20	-5	0	0	0
Thruster	3.70	126	-25	-10	0	0	0
Thruster	3.70	126	-30	-5	0	0	0
Thruster	3.70	121	-25	-5	0	0	0
Thruster	3.70	131	-25	-5	0	0	0
Thruster Electronics	5.00	116	30	15	0	0	0
Air Manifold	15.00	116	-30	-15	0	0	0
Gimbal Electronic Box	10.00	221	-25	15	0	0	0
Gimbal Electronic Box	10.00	171	-25	15	0	0	0
Gimbal Electronic Box	10.00	171	25	15	0	0	0

TOTALS:	WT	XCG	YCG	ZCG	IXXCG	IYYCG	IZZCG
	1424.6	171.86	-6.37	-0.36	4.39E+06	6.84E+06	8.10E+06

4.2 FREE-FREE DYNAMIC ANALYSIS

As an intermediate step in the design process, free-free modal analyses of the CEM3 testbed were conducted to calculate the frequencies of the higher frequency CEM3 primary structure modes which are virtually unaffected by the low-frequency suspension system. While the proper comparison with the EOS AM-1 spacecraft is made using the suspended CEM3 modes, the free-free results are included here for informational purposes since the analyses were an integral part of the design process. They may also be compared with the suspended analysis results provided in the next section.

Table 4-4 lists the first 26 free-free CEM3 modes resulting from the analysis. The first system mode of the testbed occurs at 23.97 Hz (mode 25) and is a torsion mode of the truss primary structure as illustrated in Figure 4-1. This result compares well with the first structural system mode of the EOS AM-1 spacecraft, which is at about 23 Hz. Successfully meeting this frequency goal would not have been possible without the addition of the stock tube diagonal struts to augment the torsional stiffness of the primary structure.

The modes which occur prior to the first CEM3 primary structure system mode are mainly rigid-body modes, appendage modes, and local gimbal payload modes. Figure 4-2 illustrates the local gimbal modes which are rotational and plunge modes of the gimbaled payload mass at 14 and 22 Hz, respectively. Note that the closed-loop control of the 2-axis gimbals should eliminate the rotational payload mode at 14 Hz; therefore, this is not considered a true local payload mode. The first CEM3 payload modes are thus the gimbal plunge modes at 22 Hz. Though the EOS AM-1 design goal is for the payload modes to be above 35 Hz, this result is considered acceptable as the gimbal plunge mode is an artifact of using the existing CEM2 gimbals in the CEM3 testbed.

4.3 SUSPENDED DYNAMIC ANALYSIS

This section evaluates the overall dynamic fidelity of the CEM3 testbed by comparing the final suspended CEM3 FEM modal analysis results with those from the scaled on-orbit EOS AM-1 FEM model. Section 4.3.1 describes the suspension analysis along with the modal results and mode shape plots. Section 4.3.2 specifically addresses the comparison of the appendage interaction characteristics. For informational purposes, Section 4.3.3 summarizes suspension system sensitivity analyses which were used to tune the stiffness gain of the suspension devices.

Table 4-4. CEM3 Free-Free Modal Analysis

MODE No.	FREQ (Hz)	DESCRIPTION
1 - 6	0.00	Rigid Body Modes
7-10	< 2.00	HGA & SA B-1
11	2.87	HGA T-1
12	5.74	SA T-1
13	9.95	SA B-2-Z
14	10.05	SA B-2-X
15-17	13.8 - 14.1	Gimbal Payload Rx
18	21.48	Gimbal Payload Plunge
19	22.00	Gimbal Payload Plunge
20	22.12	HGA B-2-X
21	22.48	Gimbal Payload Plunge
22	23.14	PMAD/HGA Bending
23	23.41	HGA B-2-Y
24	23.50	Towers/PMAD Bending
25	**23.97**	**System 1st Torsion (T-1)**
26	24.88	System Bending/Torsion

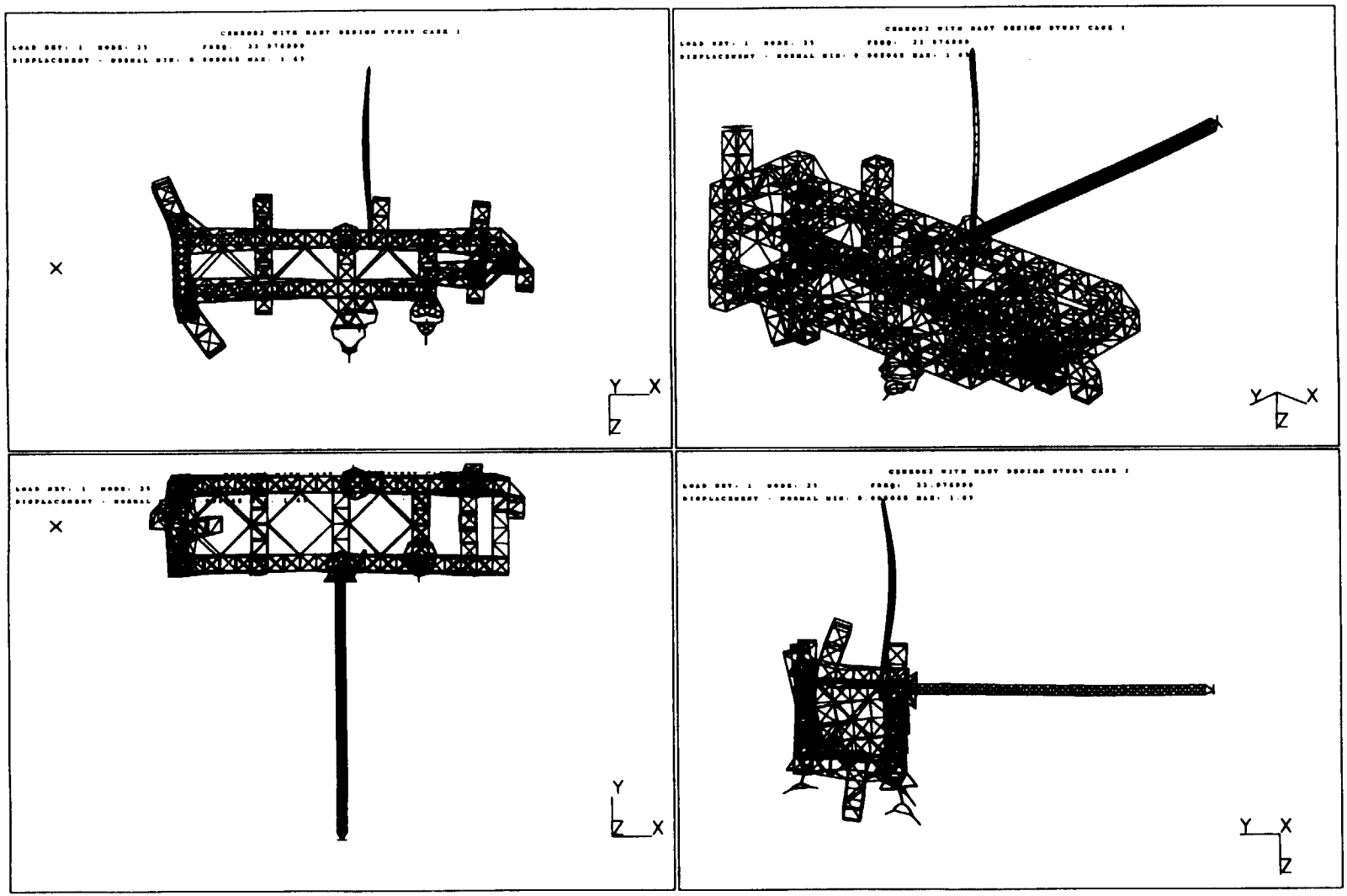

Figure 4-1. CEM3 First Primary Structure Mode Shape

Payload θx @ 14.0 Hz

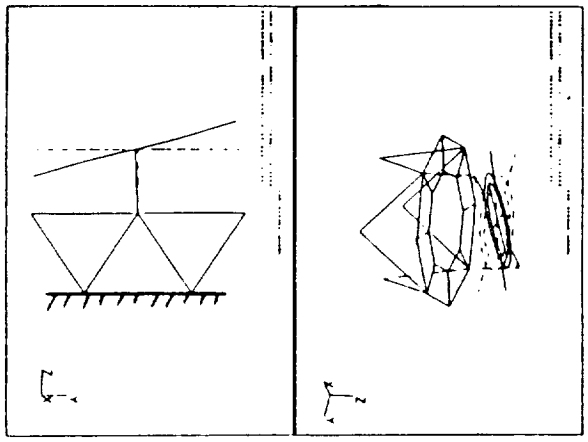

Payload Plunge @ 22.1 Hz

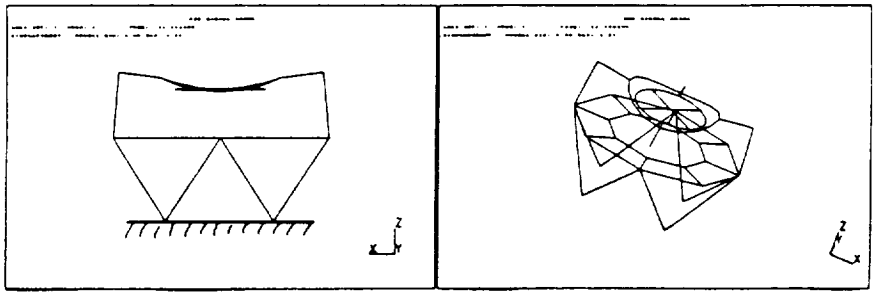

Figure 4-2. Local Gimbal Payload Modes

4.3.1 Suspension Analysis Results

Suspension analyses were conducted with the CEM3 testbed suspended from five zero-g suspension devices as described in Section 3.4. The modal analyses, performed using MSC/NASTRAN Solution 106, included suspension system dynamics and geometric stiffness effects due to gravity preloads. Both parameters have a significant effect on the testbed behavior at low frequencies and therefore must be accurately modeled. At higher frequencies the potential importance of these parameters is significantly reduced, as the gravity-induced effects become negligible and the suspension modes become further separated from the testbed flexible-body modes.

The results of the final eigensolution computed for the baseline CEM3 testbed in its suspended configuration are summarized in Table 4-5. The first 26 modes shown are comprised of rigid-body suspension modes, lower order appendage modes, local gimbal modes, and testbed structural modes. The six rigid-body suspension modes (modes 1 - 6) are all successfully tuned below the 0.20 Hz requirement, using the approach discussed in Section 3.4. In addition, the first system structural mode (mode 25) meets the 23 Hz design goal. A total of 353 modes are predicted up to 200 Hz, excluding local cable modes.

Mode shape plots of the important low-frequency appendage modes which dominate the CEM3 dynamic performance are shown in Figures 4-3 through 4-6. Mode 7 is first bending of the solar array simulator about the testbed yaw axis (B-1-Z) which couples with testbed rigid-body yaw rotation. Modes 8 and 10 are combined first bending of the solar array simulator and HGA appendages about the CEM3 roll axis (B-1-X) which introduces significant testbed rigid-body roll motion. Mode 9 is HGA bending about the CEM3 pitch axis (B-1-Y) and results in very little testbed rigid-body response as shown in Figure 4-5. The testbed rigid-body responses are a result of the testbed inertias reacting the torques generated by motion of the appendage tip weights, the magnitude of which is quantified by the gain K_b. Based on the discussions in Section 2.2, modes 7 and 9 correspond to the 2-body problem while modes 8 and 10 correspond to the three-body problem. The coupling of the HGA and solar array motion in the latter reflects the importance of scaling both appendages consistently.

Note that for the purpose of expediting the suspension analysis, local cable modes and grounding stiffnesses associated with external air lines and wiring attached to the testbed have been ignored. Cable "string" modes which might couple with the structure in the test lab can be de-tuned or replaced with lighter Kevlar cables as

Table 4-5. CEM3 Suspension Analysis Modes

MODE	FREQ (Hz)	DESCRIPTION
1	0.111	RB Pendulum (Lateral)
2	0.111	RB Pendulum (Axial)
3	0.118	RB Plunge
4	0.133	RB Yaw
5	0.190	RB Pitch
6	0.199	RB Roll
7	0.716	SA B-1-Z
8	0.815	SA B-1-X
9	1.258	HGA B-1-Y
10	1.517	HGA B-1-X
11	2.874	HGA T-1
12	5.400	SA T-1
13	9.94	SA B-2-Z
14	10.01	SA B-2-X
15	13.89	Gimbal Payload Rx
16	13.91	Gimbal Payload Rx
17	14.10	Gimbal Payload Rx
18	21.51	Gimbal Payload Plunge
19	22.02	Gimbal Payload Plunge
20	22.19	HGA B-2-X
21	22.46	Gimbal Payload Plunge
22	23.17	PMAD/HGA Bending
23	23.43	HGA B-2-Y
24	23.54	Towers/HGA Bending
25	23.88	System 1st Torsion (T-1)
26	24.73	System Bending/Torsion
53	44.84	Local System Diagonal Strut
353	199.40	-----

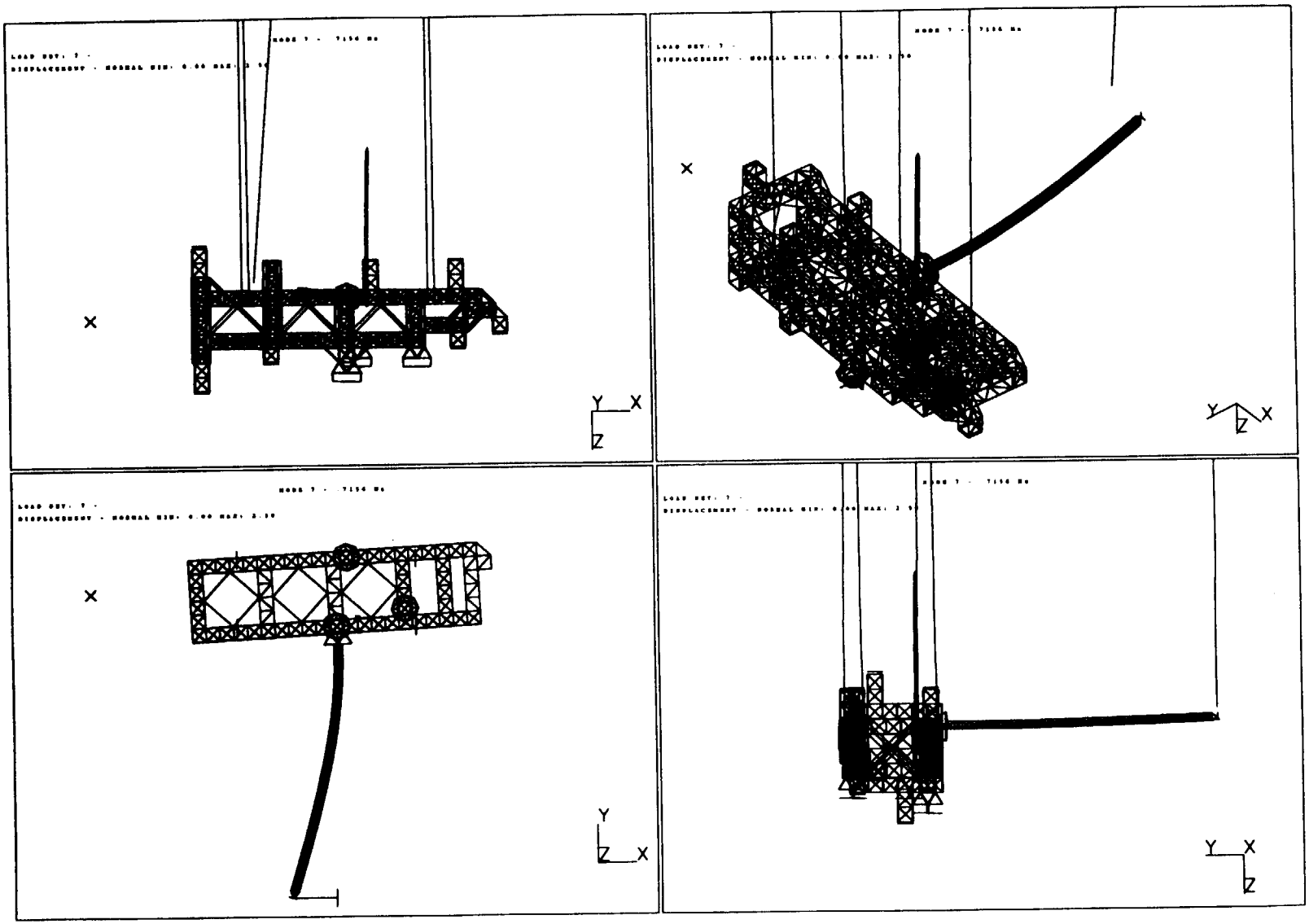

Figure 4-3. CEM3 Suspension Mode #7 (Mast B-1-Z)

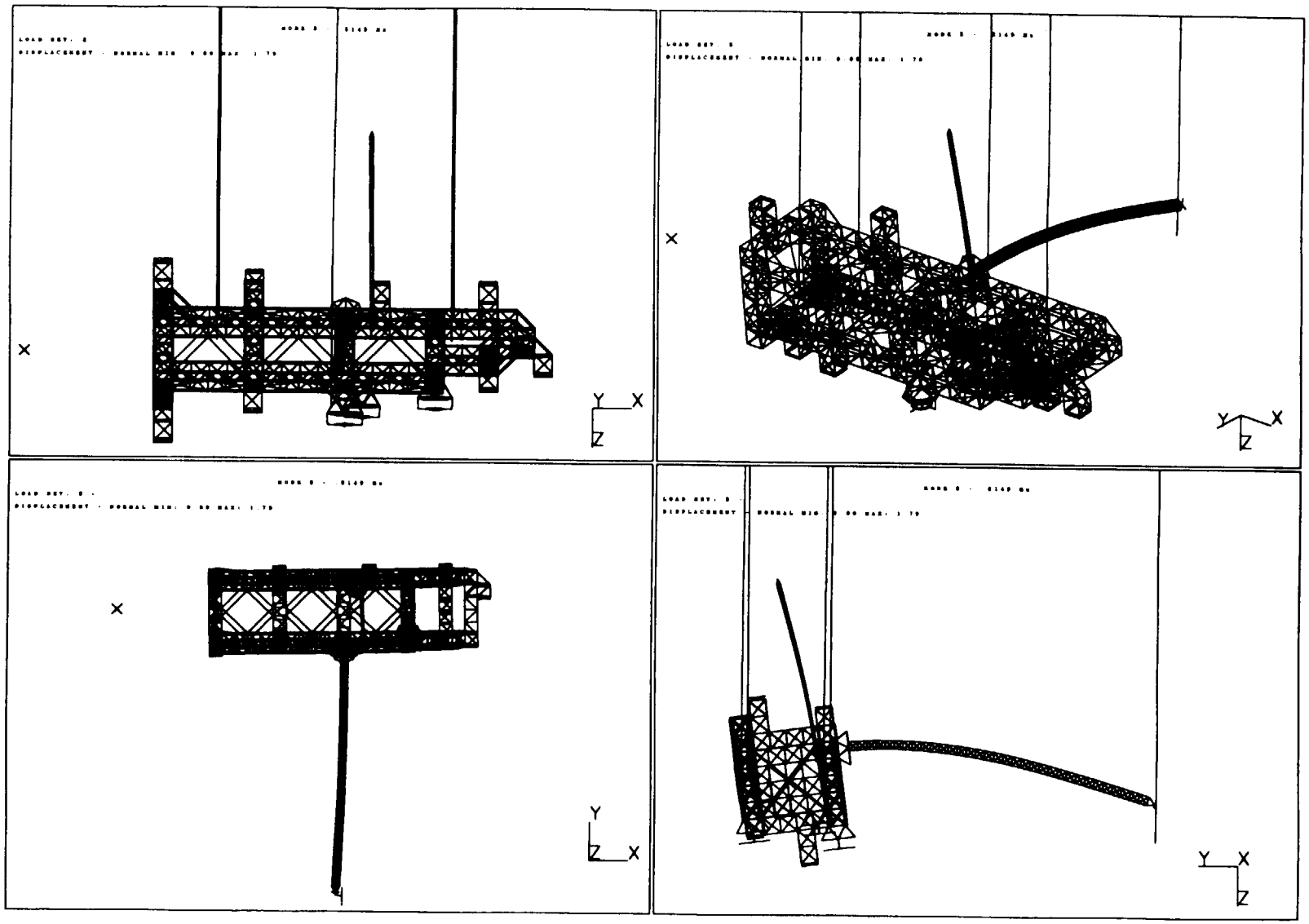

Figure 4-4. CEM3 Suspension Mode #8 (Mast B-1-X)

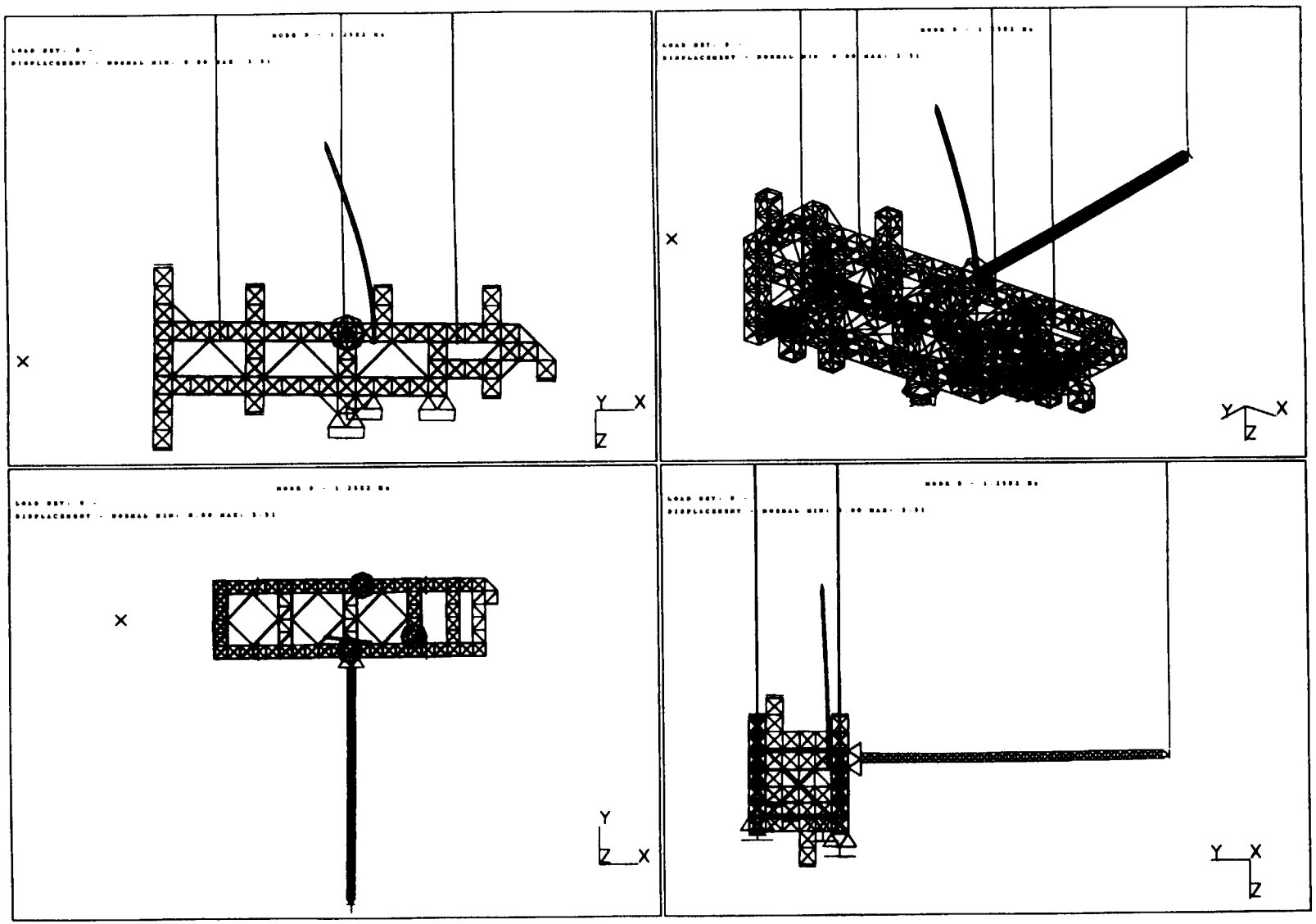

Figure 4-5. CEM3 Suspension Mode #9 (HGA B-1-Y)

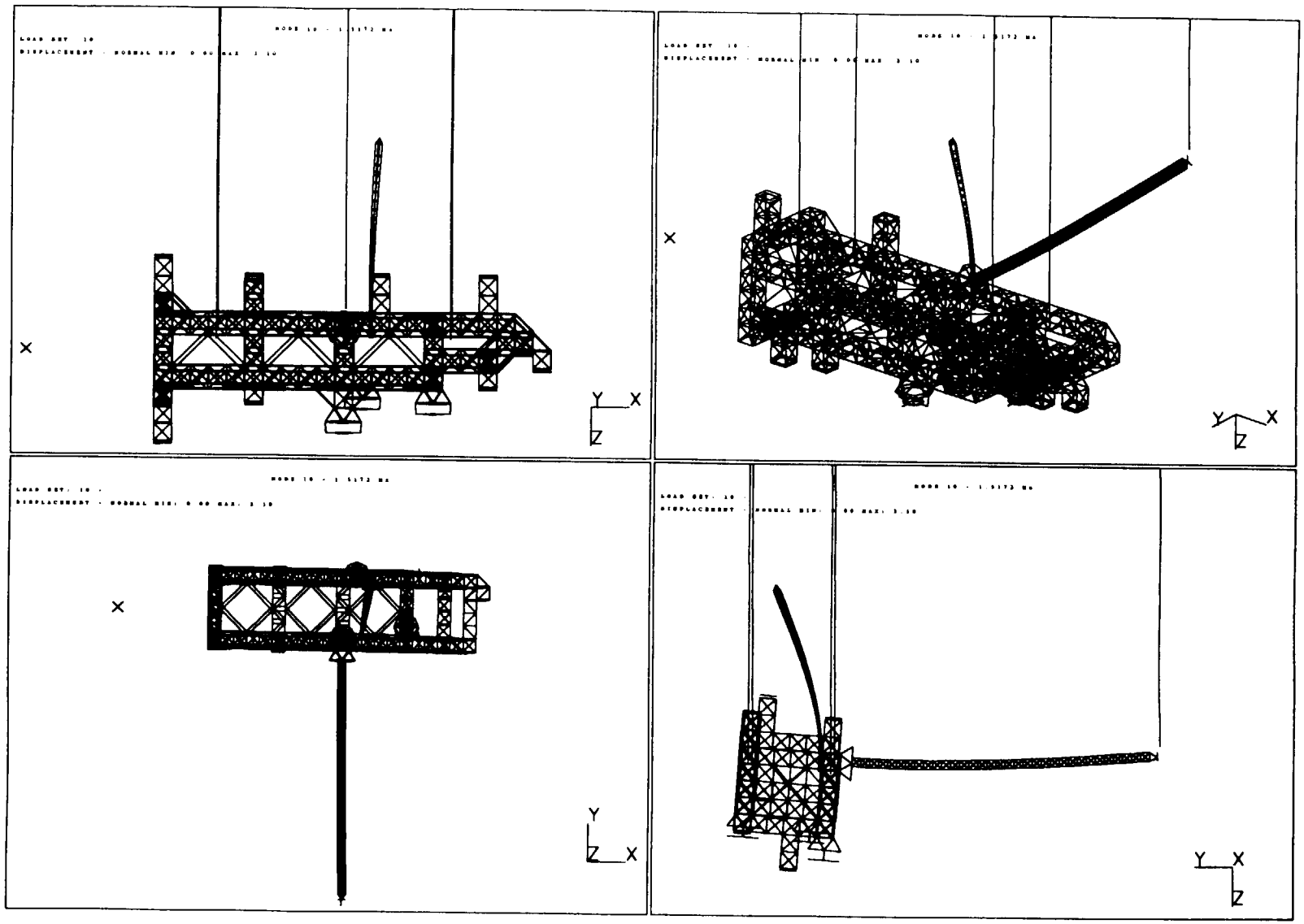

Figure 4-6. CEM3 Suspension Mode #10 (HGA B-1-X)

needed. The external air lines and electrical cables should be added to the FEM model at a later date according to the specifics of each test configuration.

4.3.2 Appendage Mode Interaction Comparison

Using the CEM3 suspended modal data discussed in the previous section, open-loop structural frequency response functions were calculated to evaluate how closely the suspended CEM3 testbed simulates the overall appendage mode dynamic interaction of the on-orbit EOS AM-1 spacecraft. Comparison plots of the magnitude of the open-loop FRF from 0.01 Hz to 200 Hz are shown in Figures 4-7 through 4-9 assuming a constant modal damping value of 0.5%. The sensor DOF's correspond to the GN&C pallet for both models while the actuator DOF's are located on the reaction wheel assembly and the gas-jet thruster plate for the EOS AM-1 and CEM3 testbed, respectively. The magnitude of the EOS AM-1 response has been scaled according to the 1/10:1 multiple scaling method (A) described in Section 2.3. The FRF peaks pertaining to the rigid-body suspension modes and the low-frequency appendage modes are individually labeled on each plot.

In the region below 1 Hz, the CEM3 roll (Figure 4-7), pitch (Figure 4-8), and yaw (Figure 4-9) frequency response functions display the same basic characteristics as the scaled EOS AM-1 FRF's, with two exceptions. First, each CEM3 testbed FRF has a peak associated with a low-frequency suspension mode, as predicted in Section 2.2. Inspection of the CEM3 curves clearly shows that the suspension modes are uncoupled from the appendage modes. Second, as was intended with the approach described in Section 2.4 using scaling method (C), there is a approximately a factor of two difference between the EOS and CEM3 appendage frequencies, while the relative magnitude and frequency spacing are preserved.

The key appendage dynamic interaction parameters for the low-frequency appendage modes (Sections 2.2 and 2.4) were developed from the FRF's using Equation 2-8 and are compared in Tables 4-6 through 4-8. Tables 4-6 and 4-7 show the overall good agreement between the scaled EOS AM-1 and CEM3 appendage frequencies and bending mode gains (K_b's). Table 4-8 shows that the relative frequency separation ratios are consistent for both the HGA and solar array simulator appendages.

Figures 4-7 through 4-9 show that in the region above 1 Hz, the mass lines of the CEM3 and EOS AM-1 are nearly identical in all three FRF's. This reflects the excellent match in the mass inertia properties (I_{xx}, I_{yy}, I_{zz}) mentioned in Section 4.1. Comparisons of the high-frequency responses in the FRF's reveal a high concentration of modes from 23 - 200 Hz in both the CEM3 and EOS AM-1 models.

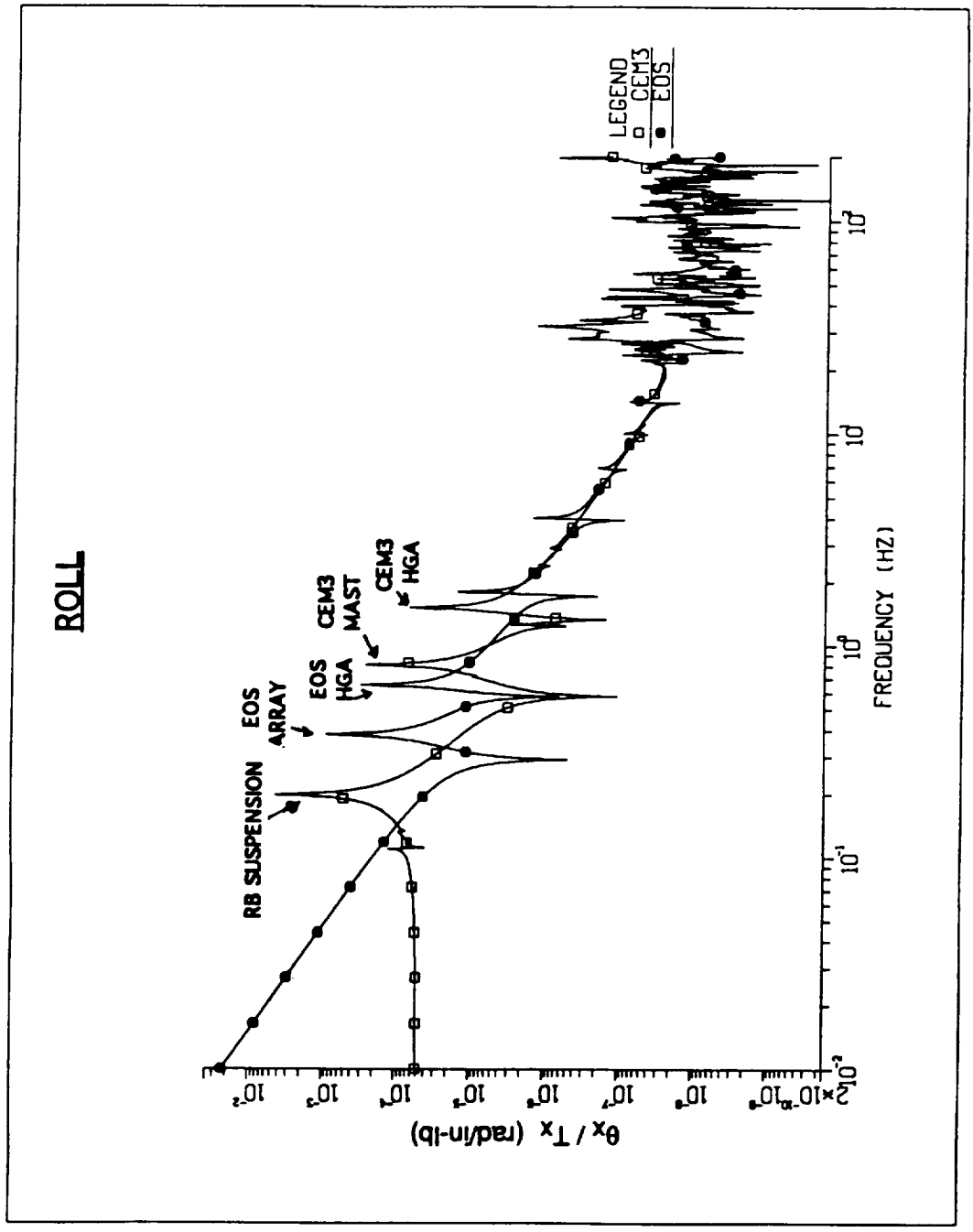

Figure 4-7. Frequency Response Function Comparison - Roll Axis

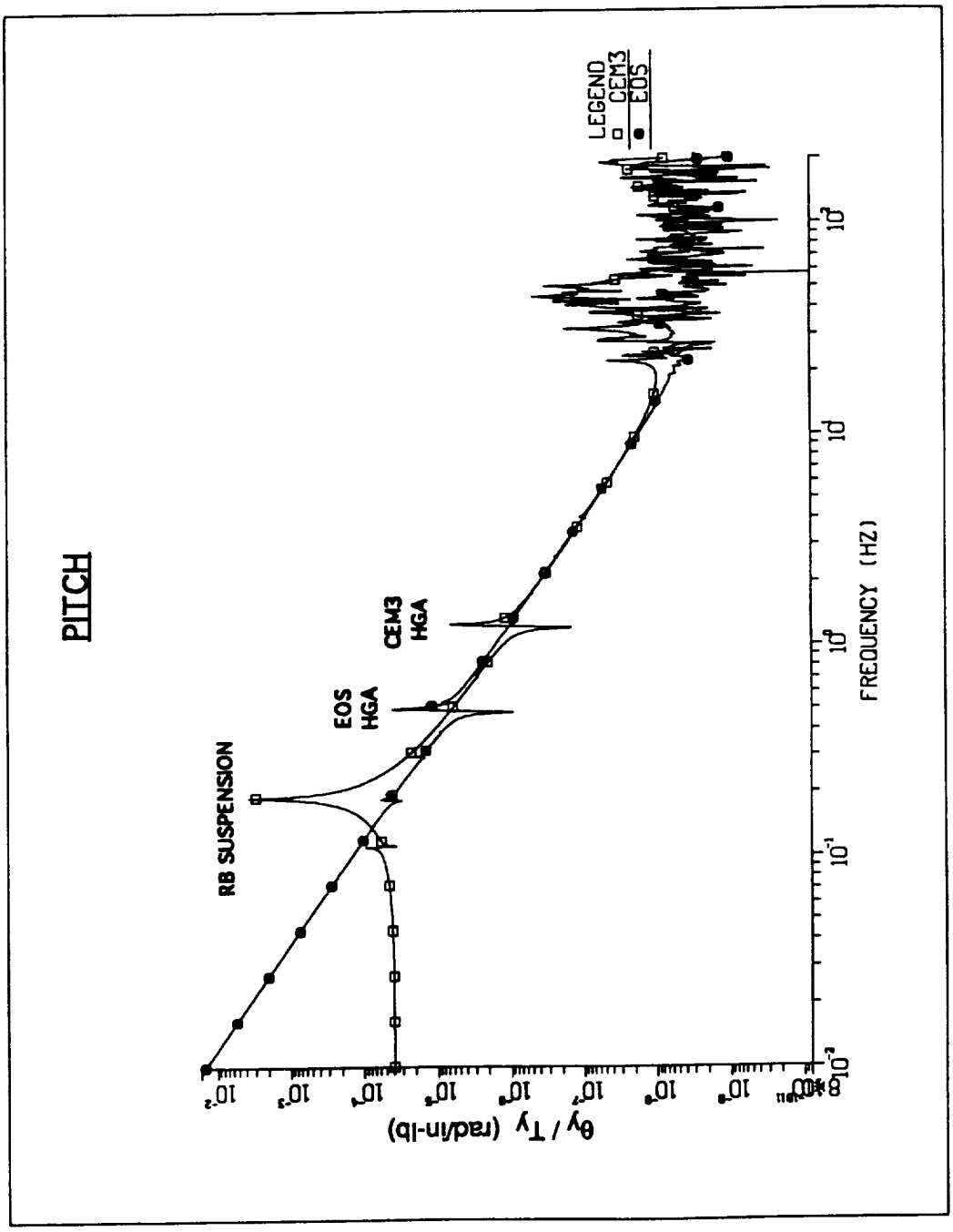

Figure 4-8. Frequency Response Function Comparison - Pitch Axis

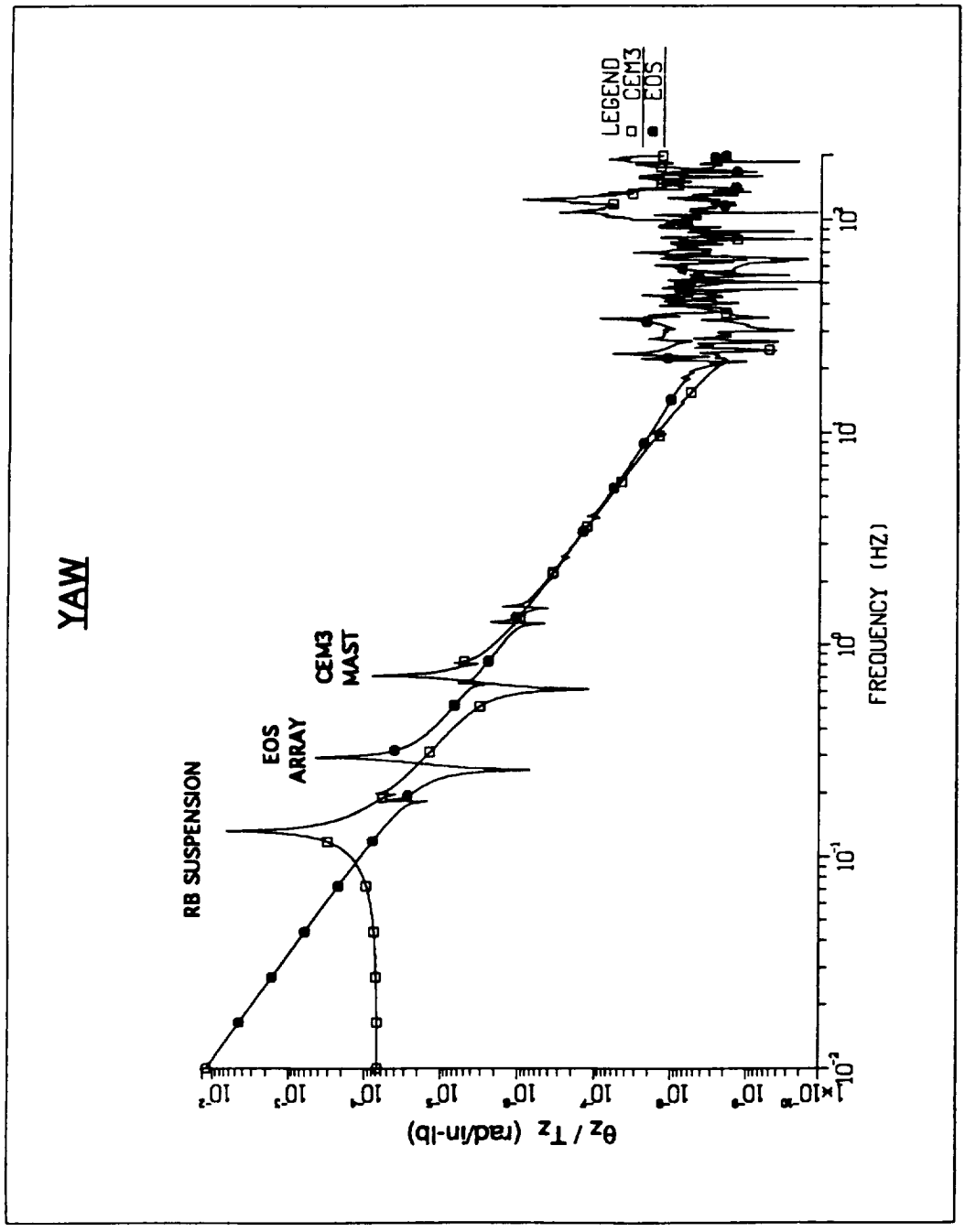

Figure 4-9. Frequency Response Function Comparison - Yaw Axis

Table 4-6. Appendage Interaction Summary

			EOS-AM1 Full Scale	EOS AM-1 Scaled -(C)	CEM3
Roll (B-1-X)	SA	Freq (Hz)	0.380	0.760	0.815
		Kb	0.61	0.61	0.81
	HGA	Freq (Hz)	0.660	1.320	1.517
		Kb	0.61	0.61	0.73
Pitch (B-1-Y)	HGA	Freq (Hz)	0.501	1.002	1.258
		Kb	0.07	0.07	0.07
Yaw (B-1-Z)	SA	Freq (Hz)	0.295	0.590	0.716
		Kb	0.33	0.33	0.35

Table 4-7. CEM3/EOS Frequency and Kb Ratios

		CEM3 / EOS Ratio		
		Frequency		
RB Axis	Appendage	Full Scale	Scaled - (C)	Kb
ROLL	SA	2.14	1.07	1.33
ROLL	HGA	2.30	1.15	1.19
PITCH	HGA	2.51	1.26	1.00
YAW	SA	2.43	1.21	1.06

Table 4-8. Bending Mode Pair Frequency Separation Ratios

SPACECRAFT MODEL	MODE PAIR	
	HGA B-1-X/B-1-Y	SA B-1-X/B-1-Z
EOS AM-1	1.32	1.29
CEM3	1.21	1.14

These correspond to the structural modes and higher order appendage bending modes in the models. Specifically matching these modes was impractical and not part of the current effort. However, the overall modal densities appear similar.

Overall, the dynamic comparison of the open-loop FRF's and the appendage frequencies and K_b's is very good considering that the CEM3 testbed was reconfigured using existing CEM2 hardware. The results presented reflect an iterative effort in the adjustment of the relatively few unconstrained variables in the design equation (i.e. the HGA design and the size of the solar array tip weight) to minimize the differences between the key CEM3 and scaled EOS AM-1 appendage dynamic interaction parameters.

4.3.3 Suspension Mode Sensitivity Study

Parametric studies were conducted to assess the sensitivity of the roll, pitch, and plunge rigid-body suspension mode frequencies to variations in suspension device stiffness, which can be controlled using a gain setting. The pendulum and yaw modes are uncoupled from vertical suspension motion and are therefore insensitive to the suspension device stiffness.

The CEM3 roll mode frequency is significantly more sensitive to the suspension stiffness setting of the device supporting the mast tip weight than to the others due to the long moment arm associated with the mast. Restoring torques about the roll axis are a function of the moment arm squared ($T = Kr^2$). The suspension system effective roll stiffness is dominated by the mast device which has approximately a 220-inch moment arm with respect to the testbed c.g. In comparison, the four suspension devices supporting the truss have only 25-inch moment arms. Figure 4-10 shows a plot of rigid-body roll frequency as a function of mast suspension device stiffness, assuming nominal truss suspension stiffness settings of 0.50 lbs. The figure indicates that the suspension stiffness at the mast tip must be 0.10 lb/in or less in order to achieve a roll frequency below 0.20 Hz.

Additional studies were also performed to understand the sensitivity of the pitch and plunge modes to variations in suspension stiffness. Table 4-9 shows the change in frequency associated with decreasing the four truss suspension device settings from 0.50 lb/in to 0.25 lb/in. The mast device stiffness has only a small effect on the pitch and plunge modes compared to the truss devices, and therefore its stiffness was kept constant at 0.50 lb/in in this analysis. As expected, the results indicate a strong sensitivity of vertical plunge mode frequency to suspension stiffness. The pitch mode frequency is much less sensitive to changes in truss suspension stiffness.

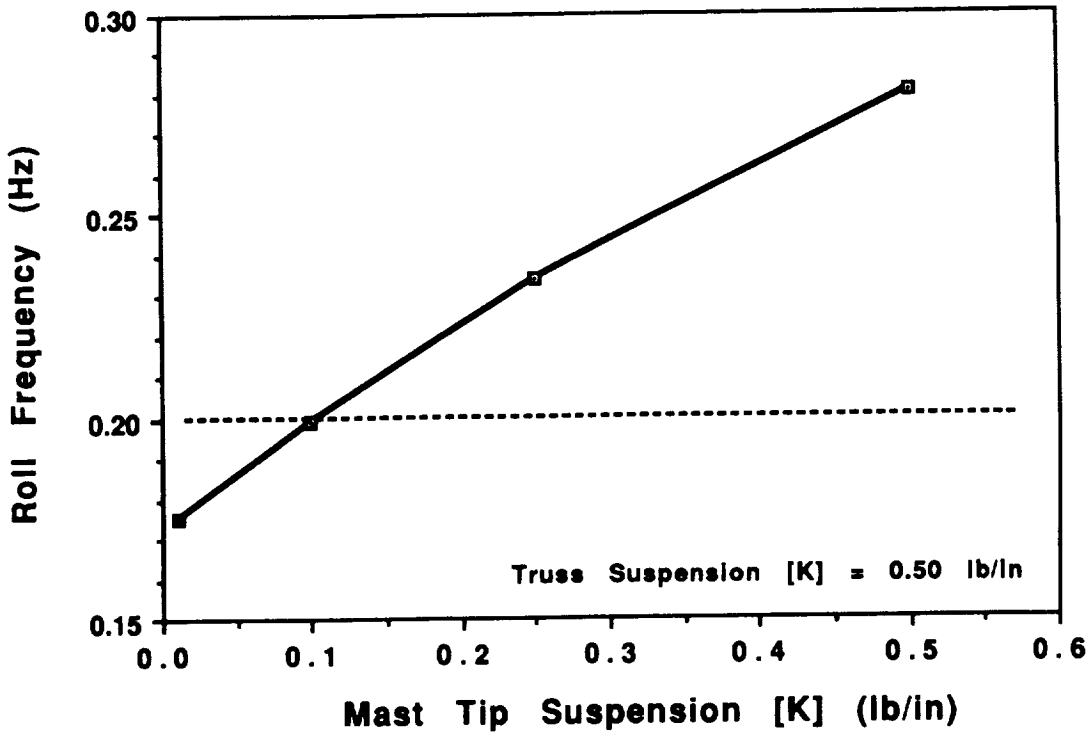

Figure 4-10. Roll Mode Frequency vs. Mast Suspension Stiffness

Table 4-9. Truss Suspension Stiffness Sensitivity

	SUSPENSION MODE (HZ)	
TRUSS [K]	PLUNGE	PITCH
0.50	0.121	0.191
0.25	0.087	0.176

Mast Tip [K] = 0.50 lb/in

More than one unique set of suspension stiffness settings can be selected which result in suspension mode frequencies below 0.20 Hz. For the CEM3 testbed, it was decided to use the supplier-recommended nominal stiffness value of 0.50 lb/in for the truss devices and adjust the mast device stiffness setting as needed to achieve the 0.20 Hz rigid-body suspension frequency requirement. This resulted in the 0.10 lb/in stiffness setting for the suspension device supporting the mast tip weight. In theory, the stiffness setting of this suspension device should be set as low as possible in order to minimize interaction with mast tip motion.

4.4 CEM3 and EOS AM-1 Comparison Summary

An overall comparison of the CEM3 and scaled EOS AM-1 properties is provided in Tables 4-10 and 4-11. The most important parameters are shaded in gray, based on the objectives established by NASA/LaRC.

The results in Table 4-10 show good agreement for the overall bus geometry and the high gain antenna. Because of the requirement to use the existing CEM2 mast, the CEM3 solar array simulator is approximately half of the length desired for the testbed. This difficulty was overcome by using a different scaling method for the appendage design which preserved the important appendage dynamic interaction characteristics, but at twice the frequency.

The total weight of the CEM3 testbed meets the requirement to be below 2,000 lbs, but exceeds the EOS AM-1 target value by 36%. This was a result of using existing aluminum CEM2 struts to simulate the stiffness and frequency characteristics of the graphite/epoxy composite EOS AM-1 primary structure. Fortunately, this has no effect on the pointing performance of the testbed, which involves mainly the diagonal inertias. The results for the center-of-gravity show good agreement for the Y and Z c.g. locations. The X c.g. difference of 14 inches is acceptable, a result of the fact that the aft end of the CEM3 structure was shortened due to the limited supply of CEM2 struts.

Comparison of the diagonal inertias indicates excellent agreement between the CEM3 testbed and the scaled EOS AM-1 spacecraft values. In contrast, the cross products of inertia show poor agreement. This is an acceptable compromise however, as in both the EOS AM-1 spacecraft and the CEM3 testbed the inertia cross products are very small compared to the diagonal inertias.

Table 4-10 also shows that the first system mode frequency of the bus is well-matched, though the first payload mode is not. The latter is an artifact of the requirement to use

Table 4-10. CEM3 Comparison with EOS AM-1 Spacecraft

PROPERTY		EOS AM-1 Full Scale	EOS AM-1 Scaled - (A)	CEM3
BUS GEOMETRY (in)	L	256	256	220
	W	68	68	60
	H	78	78	80
APPENDAGE GEOMETRY (in)	SA L	351	351	180
	HGA L	100	100	100
MASS PROPERTIES (lbf, in, lbf-in^2)	Total Weight	10,500	1,050	1,425
	X-CG	157.3	157.3	171.86
	Y-CG	-3.1	-3.1	-6.37
	Z-CG	-8.2	-8.2	-0.04
	Ixx	4.35E+07	4.35E+06	4.39E+06
	Iyy	6.73E+07	6.73E+06	6.84E+06
	Izz	8.14E+07	8.14E+06	8.10E+06
	Ixy	-1.23E+06	-1.23E+05	-1.82E+04
	Ixz	1.63E+06	1.63E+05	4.18E+05
	Iyz	3.37E+06	3.37E+05	8.04E+04
1st System Freq (Hz)	Bus	23	23	24
	Payload	35	35	22

Table 4-11. CEM3 Comparison with EOS AM-1 Appendage Dynamics

Appendage Modes		EOS AM-1 Full Scale	EOS AM-1 Scaled - (C)	CEM3
SA Yaw	Freq (Hz)	0.295	0.590	0.716
	Kb	0.33	0.33	0.35
SA Roll	Freq (Hz)	0.380	0.760	0.815
	Kb	0.61	0.61	0.81
HGA Pitch	Freq (Hz)	0.501	1.002	1.258
	Kb	0.07	0.07	0.07
HGA Roll	Freq (Hz)	0.660	1.320	1.517
	Kb	0.61	0.61	0.73

the existing CEM2 gimbal design.

Finally, Table 4-11 shows that the important overall character of the appendage dynamic interaction (in terms of frequency spacing, coupling, and modal gain) has been preserved, as further evidenced in the open-loop structural FRF's shown in Figures 4-7 through 4-9. While the appendage modal damping is also an important parameter, these FRF's assume a constant critical modal damping of 0.5%. This assumption should be revisited once modal tests of both the EOS AM-1 spacecraft and the suspended CEM3 testbed have been completed.

Overall, all of the parameters shaded in gray show acceptable, if not good agreement, reflecting a testbed with good fidelity in the important parameters of interest. In conclusion, the CEM2 model hardware has been successfully reconfigured to provide a ground testbed representation of the low-frequency dynamic characteristics of the EOS AM-1 spacecraft. The effort was accomplished within the five-month schedule and at a very minimal cost in new hardware. The resulting CEM3 testbed is now available for use in experiments to develop CSI technology for jitter isolation and suppression and the enhancement of overall spacecraft pointing performance.

5.0 REFERENCES

1. Belvin, W.K., Horta, L.G., and Elliott, K.B., "The LaRC CSI Phase-0 Evolutionary Model Testbed: Design and Experimental Results," 4th NASA/DOD CSI Technology Conference, Orlando, FL, November 1990.

2. Belvin, W.K., Elliott, K.B., and Horta, L.G., "A Synopsis of Test Results and Knowledge Gained from the Phase 0 CSI Evolutionary Model," 5th NASA/DOD CSI Technology Conference, Lake Tahoe, Nevada, March 1992.

3. Gronet, M.J., Davis, D.A., Kintis, D.H., Brillhart, R.D., and Atkins, E.M., "Design, Analysis, and Testing of the Phase 1 CSI Evolutionary Model Erectable Truss," NASA CR-4461, August 1992.

4. Maghami, P.G., Joshi, S.M., Walz, J.E., and Elliott, K.B. "Integrated Design of the CSI Evolutionary Structure: A Verification of the Design Methodology," 5th NASA/DOD CSI Technology Conference, Lake Tahoe, Nevada, March 1992.

5. Kienholz, David A., "Defying Gravity with Active Test Article Suspension Systems," Sound and Vibration, April 1994, pp. 14-21.

6. Belvin, W. K., Maghami, P. G., Tanner, C. and Kenny, S., "Evaluation of CSI Enhancements for Jitter Reduction on the EOS AM-1 Observatory," 9th VPI&SU Symposium on Dynamics and Control of Large Structures, Blacksburg, VA, May 1993.

7. Reed, J., "EOS AM-1 On-Orbit Spacecraft Modal Model, Version 3b," Swales & Associates, Inc. Technical Memo TM-93-062, April 1993.

8. Kienholz, David A., Crawley, Edward F., and Harvey, Jeffrey T., "Very Low Frequency Suspension Systems For Dynamic Testing," AIAA Paper No. 89-1194, 30th AIAA SDM Conference, Mobile, AL, April 1989.

9. Cooley, V.M., and Giunta, A.A., "Laboratory Evaluation of Two Advanced Suspension Systems for Dynamic Testing," 30th AIAA SDM Conference, Mobile, AL, April 1989.

10. Crawley, E.F., Sigler, J.L., van Schoor, M.C., and Gronet, M.J., "Hybrid Scaled Structural Dynamic Models and Their Use in Damping Prediction," Journal of Guidance, Control, and Dynamics, Vol. 13, No. 6, Nov.-Dec. 1990, pp. 1023-1032.

11. Kvaternik, R.G., "Scale Models in Spacecraft Dynamics Research at Langley Research Center - History and Status," Space Station Freedom On-Orbit Structural Verification Workshop, Reston, VA, December 1992.

12. Davis, D.A., Gronet, M.J., Tan, M.K., and Thorne, J., "Conceptual Design and Analysis of a Dynamic Scale Model of the Space Station Freedom," NASA CR-4598, May 1994.

13. Baker, W.E., Westine, P.S., and Dodge, F.T., Similarity Methods in Engineering Dynamics, Hayden, Rochelle Park, NY, 1973.

14. Guyan, R.J., "Reduction of Stiffness and Mass Matrices," AIAA Journal, Vol. 3, Feb. 1965, p380.

15. CORDS2 User's Manual, Version 1.0, Structural Dynamics Research Corporation, San Diego, California, 1988.

16. Hausle, Fred W. and Stroeve, Antonie, "Linear Recombination of Mode Shape Pairs Having Near-Repeated Eigenvalues: Application to CRRES, A Shuttle Payload," Presented at the 6th International Modal Analysis Conference, Kissimmee, Florida, 1988.

REPORT DOCUMENTATION PAGE

Form Approved
OMB No. 0704-0188

1. AGENCY USE ONLY (*Leave blank*)	2. REPORT DATE	3. REPORT TYPE AND DATES COVERED
	October 1994	Contractor Report

4. TITLE AND SUBTITLE
Development of the CSI Phase-3 Evolutionary Model Testbed

5. FUNDING NUMBERS
C NAS1-19241

WU 233-01-01-07

6. AUTHOR(S)
M. J. Gronet, D. A. Davis, and M. K. Tan

7. PERFORMING ORGANIZATION NAME(S) AND ADDRESS(ES)
Lockheed Missiles & Space Company, Inc.
Org. N1 - 01, Bldg. 107
1111 Lockheed Way
Sunnyvale, CA 94089-3504

8. PERFORMING ORGANIZATION REPORT NUMBER
LMSC/P086632

9. SPONSORING / MONITORING AGENCY NAME(S) AND ADDRESS(ES)
National Aeronautics and Space Administration
Langley Research Center
Hampton, VA 23681-0001

10. SPONSORING / MONITORING AGENCY REPORT NUMBER
NASA CR-4630

11. SUPPLEMENTARY NOTES
Langley Technical Monitor: Kenny B. Elliott

12a. DISTRIBUTION / AVAILABILITY STATEMENT
Unclassified - Unlimited
Subject Category 18

12b. DISTRIBUTION CODE

13. ABSTRACT (*Maximum 200 words*)

This report documents the development effort for the reconfiguration of the CSI Evolutionary Model (CEM) Phase-2 testbed into the CEM Phase-3 configuration. This step responds to the need to develop and test CSI technologies associated with typical planned earth science and remote sensing platforms. The primary objective of the CEM Phase-3 ground testbed is to simulate the overall on-orbit dynamic behavior of the EOS AM-1 spacecraft. Key elements of the objective include approximating the low-frequency appendage dynamic interaction of EOS AM-1, allowing for the changeout of components, and simulating the free-free on-orbit environment using an advanced suspension system. The fundamentals of appendage dynamic interaction are reviewed. A new version of the multiple scaling method is used to design the testbed to have the full-scale geometry and dynamics of the EOS AM-1 spacecraft, but at one-tenth the weight. The testbed design is discussed, along with the testing of the solar array, high gain antenna, and strut components. Analytical performance comparisons show that the CEM Phase-3 testbed simulates the EOS AM-1 spacecraft with good fidelity for the important parameters of interest.

14. SUBJECT TERMS
CSI, Control-Structurees Intergration, Scale Models, Suspension Systems, Ground Testing

15. NUMBER OF PAGES
124

16. PRICE CODE
A06

17. SECURITY CLASSIFICATION OF REPORT	18. SECURITY CLASSIFICATION OF THIS PAGE	19. SECURITY CLASSIFICATION OF ABSTRACT	20. LIMITATION OF ABSTRACT
Unclassified	Unclassified	Unclassified	